Assessment of Stormwater Pond Performance through Water Quality Analysis and Hydrodynamic Modeling

Master's Thesis in the Master's Program Infrastructure and Environmental Engineering

FELICIA WALLGREN

SOPHIA WENNING

DEPARTMENT OF ARCHITECTURE AND CIVIL ENGINEERING
DEVISION OF WATER ENVIRONMENT TECHNOLOGY

CHALMERS UNIVERSITY OF TECHNOLOGY
Master's thesis ACEX30
Gothenburg, Sweden 2025

MASTER'S THESIS ACEX30

Assessment of Stormwater Pond Performance through Water Quality Analysis and Hydrodynamic Modeling

Master's Thesis in the Master's Program Infrastructure and Environmental Engineering

FELICIA WALLGREN
SOPHIA WENNING

Department of Architecture and Civil Engineering
Division of Water Environment Technology
CHALMERS UNIVERSITY OF TECHNOLOGY
Gothenburg, Sweden 2025

Assessment of Stormwater Pond Performance through Water Quality Analysis and Hydrodynamic Modeling
Master's Thesis in the Master's Program Infrastructure and Environmental Engineering

FELICIA WALLGREN
SOPHIA WENNING

Examensarbete ACEX30
Institutionen för Arkitektur och Samhällsbyggnadsteknik
Chalmers Tekniska Högskola, 2025

Department of Architecture and Civil Engineering
Division of Water Environment Technology
Chalmers University of Technology
SE-412 96 Göteborg
Sweden
Telephone +46 31 772 1000

Department of Architecture and Civil Engineering
Göteborg, Sweden, 2025

Assessment of Stormwater Pond Performance through Water Quality Analysis and Hydrodynamic Modeling
Master's thesis in the Master's Program Infrastructure and Environmental Engineering

FELICIA WALLGREN & SOPHIA WENNING

Department of Architecture and Civil Engineering
Division of Water Environment Technology
Chalmers University of Technology

ABSTRACT

Traffic-related pollutants in stormwater runoff pose growing risks to aquatic ecosystems and human health. While stormwater ponds are commonly used to retain sediments, their efficiency in capturing emerging pollutants, such as tire wear particles (TWP), is less understood. This thesis combines field sampling and 3D hydrodynamic modeling to investigate pollutant retention and particle transport in a stormwater pond.

For a field sampling campaign at a pond in Sweden, ISCO samplers were used to collect water samples at inlet and outlet. Flow meters which monitored inflow and outflow during rain events were used and connected to the ISCO samplers to trigger sampling at specific water flows. Laboratory analysis included pH, conductivity, suspended solids, nutrients, metals, and organic carbon. Results show that most pollutant loads are reduced through the pond, with outlet concentrations generally below guidelines. However, exceedances of total organic carbon and total nitrogen after long dry periods suggest pollutant build up between events.

To further explore transport mechanisms, a 3D model of the pond was developed in MIKE 3 FM, simulating six scenarios: three with constant flow and three based on observed rain events. Velocity patterns throughout the entire pond were analyzed based on hydrodynamic behavior. Particle tracking of particles with sizes and density of TWP was conducted for three scenarios to assess the behavior of size-defined particle classes under different hydrodynamic conditions. These results however were deemed unreliable as great mass losses were discovered when performing mass balance calculations. Whilst unreliable, the result from the particle tracking does indicated a strong size-dependent settling pattern with larger TWP (100 μm) settling rapidly near the inlet, while finer TWP (10 μm) showed higher mobility, particularly under sustained or high inflow conditions. The results also indicates that rain intensity and wind affects the settling near the inlet.

Overall, the study highlights the ponds' capacity to retain coarse traffic-related particles, but also points to the need for more detailed modeling of finer particles. Recommendations regarding management of pond and further investigation into pond performance include careful vegetation management, and performing modeling that includes antecedent conditions and current vegetation near inlet, and also sensitivity analyses of particle properties to have an even better understanding of transport and sedimentation of emerging pollutants like TWP and microplastics.

Key words: hydrodynamic model, microplastic, MIKE 3 FM, particle tracking, pollution, stormwater pond, tire wear particles, total suspended solids

Bedömning av en dagvattendamms prestation genom vattenkvalitétsanalys och hydrodynamisk modellering.
Examensarbete inom masterprogrammet Infrastruktur och Miljöteknik

FELICIA WALLGREN & SOPHIA WENNING

Institutionen för arkitektur och samhällsbyggnadsteknik
Avdelningen för vatten miljö teknik
Chalmers tekniska högskola

SAMMANFATTNING

Trafikrelaterade föroreningar i dagvattenavrinning utgör ökande risker för vattenekosystem och människors hälsa. Även om dagvattendammar ofta används för att sedimentera partiklar, är dess effiktivitet gällande att fånga framväxande föroreningar, såsom däckslitagepartiklar, mindre utforskad. Denna masteruppsats kombinerar fältprovtagning med 3D hydrodynamisk modellering för att undersöka retention av föroreningar och transport av partiklar i en dagvattendamm.

För en fältprovtagningskampanj vid en damm i Sverige användes ISCO provtagningsenheter som tog vattenprover vid inlopp och utlopp. Flödesmätare som mätte inflöde och utflöde under nederbördstillfällen användes och var anslutna till ISCO provtagningsenheterna för att initiera provtagning vid specifika flöden. Analyser av vattenporver genererade under provtagningskampanjen genomfördes i laboratorium och inkluderade pH, konduktivitet, suspenderade partiklar, näringsämnen, metaller och organiskt kol. Resultaten visade att de flesta föroreningsbelastingar reducerades i dammen och att koncentrationerna i utflödet generellt var inom gränsvärdes omfång/under gränsvärde. Dock, överskreds gränsvärdena för total organiskt kol och total kväve efter en lång torr period vilket tyder på en ansamling av föroreningar mellan regntillfällen.

För att vidare undersöka hur transport sker i dammen, skapades en 3D model av en damm i MIKE 3, och fem scenarion simulerades varav tre hade konstant flöde och två var baserade på observerade regntillfällen. Hastighetsmönster analyserades vid specifika tidssteg för specifika lager för varje scenario. Partikelspårning, av partiklar med storlekar och denistet som däckslitagepartklar, genomfördes också, för tre scenarier, för att undersöka beteendet av storleksdefinierade klasser under olika hydrodynamiska förhållanden. Resultaten bedömdes dock vara opålitliga till följd av stora mass förluster som uppenbarats vid genomförande av massbalans uträkningar. Även om resultaten från partikelspårningen är otillförlitlig, ges ändå en indikation av ett starkt storleksberoende sedimentationsutbredingsmönster, där större däckslitagepartiklar sedimenterar snabbt nära inloppet medans finare däckslitagepartiklar har högre mobilitet, särskilt under ihållande inflöde eller högflödesförhållanden. Resultaten tyder också på att regnintensitet och vind påverkar sedimentationsmönster nära inloppet till dammen.

Övergripande, visar denna studien på den studerade dammens kapacitet att sedimentera trafikrelaterade partiklar men uppenbarar också behovet av mer detaljerad modelering av finare partiklar. Rekommendartioner gällande underhåll och vidare analyser av dammen inkluderar underhåll av vegetation, att genomföra modellering som tar hänsyn till befintliga föroreningsnivåer i dammen före regntillfälle startat och inkluderar den

nuvarande vegetationen, samt att genomföra känslighetsanalys av partikelegenskaper för att få en ännu bättre förståelse för transport och sedimentation av däcklitspartiklar och mikroplaster i dammen.

Nyckelord: dagvattendamm, Däckslitagepartiklar, förorening, hydrodynamisk modell, MIKE 3 FM, mikroplaster, sedimentation, suspenderade partiklar, transport

Contents

Preface

In this study, field sampling at a stormwater pond and water quality analysis of collected samples have been conducted. The sampling campaign laboratory work have been carried out from April to June 2025. The work is part of a project concerning transport and behavior of TWP in stormwater ponds.

The project is carried out at the Department of Architecture and Civil Engineering, Chalmers University of Technology, Sweden. This project has been carried out with Mia Bondelind as examiner and consultant and Elly Lucia Gaggini as a supervisor.

All field sampling has been carried out at Kryddvägen pond, Angered, which is owned and managed by Kretslopp och vatten, Göteborgs Stad. The engineers Sofia Polo Ruiz de Arechavaleta and Salwan Zaynal, are highly valued for providing information and advice throughout the project. Also, the sampling campaign couldn't have been done without the help and experience of engineer Anders Dahl from DHI Sverige AB.

All analysis have been carried out in the Water & Environmental Engineering Laboratory, which is part of the Department of Architecture and Civil Engineering. Research Specialist Amir Saeid Mohammadi is highly appreciated for his consultation and help with planning and conducting the experiments.

Gothenburg, June 2025
Felicia Wallgren and Sophia Wenning

1 Introduction

Stormwater management has become an increasingly significant environmental concern in urban and suburban areas. As precipitation flows over impervious surfaces such as roads, parking lots, and rooftops, it accumulates a variety of pollutants, including heavy metals, hydrocarbons, nutrients, microplastics, and tire wear particles (TWP) (Barałkiewicz et al., 2014; Fletcher et al., 2013). These contaminants are then transported into surface water bodies, soil, and groundwater, posing risks to aquatic ecosystems and human health (Järlskog et al., 2021).

Recognizing the potential environmental and human health hazards associated with stormwater pollution, policymakers in the European Union and worldwide have increased their efforts to mitigate its impact. Regulatory frameworks such as the EU Water Framework Directive 2000/60/EC (European Union, 2000) emphasize the need for sustainable stormwater management practices to reduce pollutant loads in receiving waters and improve water quality.

United Nations (2015) lists Sustainable Development Goals (SDGs) and the research regarding stormwater treatment solutions such as stormwater pond, which is investigated in this report, aligns with several of them (SDG 6, 11, 12, 14 & 15) as well. To ensure protection of human health and the environment, especially as urbanization is increasing, there is a need and want to further develop and research stormwater treatment solutions, including stormwater ponds (Scholz, 2023).

stormwater pond are widely used as a mitigation measure to control pollutant transport and improve water quality in urban runoff. These ponds function by slowing water flow, allowing particles to settle and reducing the pollutant load in discharged water (Ferguson, 1998).Research on stormwater pond has largely focused on understanding particle transport, pollutant retention and sedimentation processes (Öborn et al., 2024; Pettersson, 1999; Scholz, 2023). However, as new pollutants of concern, such as microplastics and TWP, have gained attention, their behavior in stormwater pond remains less well understood.

While stormwater pond are effective in trapping larger particles and certain contaminants, their ability to retain microplastics and TWP is less explored. Moreover, stormwater pond design challenges include optimizing hydraulic efficiency, minimizing resuspension of settled pollutants, and adapting to varying storm intensities. All while no two catchment areas and external conditions are the same and are therefore not always comparable, when designing a pond (Davis, 2020). Assessing pond performance is also complex, as it requires detailed field measurements and comprehensive modeling approaches to accurately estimate pollutant retention and transport (Center for Watershed Protection, n.d.; Scholz, 2023).

Assessing stormwater pond performance, i.e. how well it removes pollutants from the water through settling of particles, requires doing field sampling and subsequent analysis. Typically, the analysis consists of comparing samples at inlet to samples taken at outlet. Methods commonly used in field sampling include ISCO sampling at pond inlets and outlets to quantify retention efficiency, and water and sediment grab sampling to monitor sedimentation processes - the primary function of stormwater pond (Gillis, 2017; Nayeb Yazdi et al., 2021; Pettersson, 1999). Another common feature of the

named studies is the performance of water quality analysis through sample analysis in laboratory, and/or water quality monitoring on site. Additionally, some studies have combined field sampling with numerical modeling to improve assessments of stormwater pond effectiveness and develop validation datasets for predictive models (EPA, 2024; Gao & Li, 2014; Pettersson, 1999).

Despite advances in stormwater pond assessment, most modeling studies have relied on 2D approaches, with few studies applying 3D models to stormwater ponds. MIKE 3, a three-dimensional hydrodynamic model, has mainly been used to model coastal areas and rivers (Bondelind et al., 2018; Moharir et al., 2014), but it has also been used to investigate pollutant transport in wet detention ponds (Bentzen, 2010). More recently, Rama (2023) applied MIKE 3 to model a specific part of a stormwater pond—the forebay—to gain insights into its hydraulic properties and design optimization. However, validation of MIKE 3 models using real field data remains limited, underscoring the need for further research.

This study builds on previous research by applying MIKE 3 FM to model pollutant transport in an entire stormwater pond, rather than just specific sections. A key strength of this study is the integration of extensive field sampling with advanced numerical modeling, providing a 3D hydrodynamic model based on real-world data. Water quality parameters are analyzed in the laboratory using samples collected via an ISCO sampling campaign during monitored rainfall events. By incorporating multiple rainfall scenarios, this study assesses how rain intensity and duration influence pollutant retention.

Through this approach, this study not only evaluates overall pond effectiveness under different conditions but also provides insights into pollutant transport pathways. These findings can support the design of more efficient stormwater treatment systems, supporting efforts to mitigate urban runoff pollution. Furthermore, this research contributes to broader regulatory and environmental management strategies aimed at reducing microplastics pollution and protecting aquatic ecosystems (EPA, 2023; Lundy et al., 2021; Rasmussen et al., 2024).

1.1 Aim

This study aimed to evaluate the performance of a stormwater pond during rain events by integrating water quality monitoring with hydrodynamic modeling, with a focus on pollutant retention efficiency and the transport behavior of traffic-related contaminants, including TWP.

By analyzing water quality parameters from samples taken from the ponds' inlet and outlet, the efficiency of the pond in terms of reducing pollutants emitted during rain events was determined.

Based on these findings, a hydrodynamic model using MIKE was created and set up for simulation of flow and particle transport in the pond Kryddvägen. The model was used to simulate various flow conditions caused by different rain characteristics such as duration, rainfall depth and intensity, to understand how varying conditions affect the retention and subsequently the discharge pollution load into receiving waters.

Understanding these processes contributes to improved stormwater management strategies and provide insight into the performance of stormwater ponds in mitigating pollution under variable environmental conditions.

The objectives were to:

- Build a hydrodynamic model of a stormwater pond
- Carry out a sampling campaign targeting traffic-related pollutants in runoff
- Validate the model with measurements of flow, rain intensity and water quality parameters
- Investigate pollutant loads and transport of particles during rain events

1.2 Limitations

This study is subject to several limitations due to the scope of the thesis, time constraints, and budget. A significant limitation is that the research focuses on a single stormwater pond, meaning the findings may not be directly generalizable to other ponds with different designs, sizes, catchment area, or environmental conditions.

Another significant limitation is the dependency on weather conditions for data collection. The quality and quantity of stormwater sampling rely on the occurrence of sufficiently intense rain events. Since only a few rainfall events could be captured within the study period, the results may not fully reflect the pond's performance under a wide range of hydrological conditions.

Furthermore, variations in pollutant loading, seasonal influences, and external environmental factors that could impact the stormwater treatment efficiency are not comprehensively considered. The sampling campaign was restricted solely to the spring season, offering no seasonal variance in the validation data.

An additional limitation lies in unknown effects of in-pond processes on analyzed outlet samples. The observed concentration of pollutants in the samples from the outlet of the pond may differ from what is to be expected based on the inflow concentration due to in-pond processes during ascended dry days before the rain event on the sampling day.

The presence of TWP could only be implied according to literature via TSS analysis, but not directly proven in the course of sampling and laboratory work. While correlations has been found between TSS and TWP (r=0.87) (Gaggini et al., 2024), the actual correlation in this specific pond is unknown and therefore assumed to match correlation in literature.

Another modeling limitation is that only three size classes of TWP were modeled, and that the shape of the particles were assumed to be round. The three size classes modeled lies within literature size ranges but not all classes existent in literature are represented.

Simplifications of the in- and outlet in the mesh used in the MIKE 3 flow model were made. The inlet and outlet positions are set approximately at the water level. The boundaries are also at this height, as it is not possible to model pipes in MIKE 3. An additional simplification of the mesh was that the land boundary at the outline of pond was set to standing water level and thus the remaining pond geometry was cut off affecting the hydrodynamics when water level rises.

A limitation with the model created is that it does not consider the present vegetation, especially existent at the inlet, within the pond, where it likely influences flow dynamics, sedimentation and nutrient retention processes. Additionally, wind forcing is applied using data from local weather station. However, the surrounding conditions differ

between station and pond, so local wind conditions may differ from those recorded and affect surface mixing and circulation patterns.

Moreover, due to software limitations, hydrodynamic decoupling between different vertical layers takes place and density stratification effects (e.g. due to temperature differences) cannot be implemented, which could limit the models ability to accurately represent stratification and vertical transport processes.

The MIKE 3 Particle Tracking Module also has some limitations. The particles behave independently of each other, there are no interactions such as collisions, aggregation or break-up and no transformation through biological or chemical processes. Additionally, the method is very computationally intensive when simulating a large number of particles. For practical reasons, real particle concentrations - such as the total suspended solids content - have to be downscaled, often to a representative sample (e.g. one million particles per class), instead of modeling them at full number.

2 Literature review

This literature review gives an overview of what stormwater is, the purpose of having a stormwater pond, and how ponds function. The review is also done to increase the awareness of traffic related pollution, especially tire wear particles, in stormwater and the pollutants' potential impact on environmental and human health. Methodology of studies conducting automated stormwater sampling and sediment sampling in water bodies is presented. Finally, an overview of the different modeling approaches used to model pollutant transport in water bodies is given, with more focus on 3D hydrodynamic modeling used in present work.

2.1 Stormwater as urban issue

Stormwater is the runoff generated by rainfall that flows over land surfaces and enters ditches, streams, or storm sewers, typically without a significant base-flow component. It is primarily influenced by land use and climate, with urban areas experiencing higher runoff due to impervious surfaces (Betson, 1964; Overton & Meadows, 1976).

In urban and suburban environments, stormwater runoff has become a growing environmental concern. As rainfall or snowmelt flows over impervious surfaces such as roads, parking lots, and rooftops, it accumulates pollutants, including oil, grease, heavy metals, sediments, debris, and microplastics. This contaminated runoff is then either infiltrated into the soil or discharged into surface waters, posing risks to aquatic ecosystems and human health (Barałkiewicz et al., 2014). The total amount of contaminants transported by stormwater at a given time is referred to as *pollutant load*, which describes the quantity of polluting material carried by a transporting agent, such as water, wind or ice, according to the European Environment Agency glossary (EEA, n.d.). In the context of stormwater, pollutant load varies depending on factors such as land use, rainfall intensity, and the presence of stormwater treatment measures.

Urbanization significantly alters the natural water cycle by increasing stormwater runoff and reducing infiltration into the soil. The replacement of natural vegetation with impervious surfaces leads to higher peak flows, increased erosion, and greater risks of flooding. In addition to hydrological changes, urban stormwater runoff acts as a major transport pathway for pollutants, affecting water quality and ecosystem health (Fletcher et al., 2013). Climate change is expected to further intensify these stormwater-related challenges. Rising global temperatures and increasing rainfall variability contribute to more frequent and severe extreme weather events, exacerbating both urban flooding and pollutant loads in stormwater runoff (IPCC, 2021).

To mitigate these impacts, stormwater management strategies emphasize Best Management Practices (BMP), including nature-based solutions such as green roofs, permeable pavements, rain gardens, and stormwater ponds. These approaches help improve water quality by enhancing pollutant removal processes while also reducing runoff volume and peak flows. Stormwater ponds, for example, play a crucial role in retaining water, promoting sedimentation, and allowing pollutants to settle before being discharged into receiving water bodies. The integration of such sustainable drainage solutions is essential for urban resilience and long-term environmental protection (Scholz, 2023).

2.2 Purpose and function of stormwater ponds

To mitigate the adverse environmental effects from stormwater pollution, stormwater ponds are utilized. These systems are engineered to serve multiple purposes, including attenuating peak flow rates, reducing downstream flooding, ecological and aesthetic values and improving water quality. While ponds differ in form and size due to non-identical catchment areas and operational conditions (e.g. Pettersson, 1999; Öborn et al., 2024; Koutnik et al., 2022), these ponds typically consist of forebays, main ponds, and outlet structures that work together to retain water and promote sedimentation. Despite their widespread use, the effectiveness of stormwater ponds in capturing emerging pollutants like TWP and other particulate matter remains poorly understood, particularly during high-flow events such as heavy rainstorms (Koutnik et al., 2022; Scholz, 2023).

2.2.1 Key components of a stormwater pond

The key components of a stormwater pond have the following functions:

Inlet structures are where stormwater enters the pond, often equipped with energy dissipation features to reduce erosion. Forebays are areas around inlets where the heaviest sediments settle. Outlet structures control the flow of the water out of the pond and are often equipped with an overflow mechanism to manage excess water during heavy rainfall events. The pond itself consists of an excavated basin with a certain volume. Part of it constantly retains a certain volume of water and is known as the clarifier. The space above it is the intermediate storage tank, which fills and empties with every rain event (Ferguson, 1998; Scholz, 2023).

Flood protection is practiced by retaining rainwater ponds to prevent flooding and minimize erosion. The basin is designed to fill with water during the rain event and the water flows out through the outlet structure with a similar flow velocity as before the catchment area was urbanized. To capture the runoff, each stormwater retention basin must have some unfilled capacity that can fill up with water during a rain event. During extreme storm events, stormwater ponds can reach capacity. The overflow structure or emergency spillway prevents overtopping by safely directing excess water downstream, reducing the risk of flooding (Ferguson, 1998).

2.2.2 Water treatment mechanisms

Stormwater ponds improve water quality by capturing and settling suspended solids and associated pollutants through several key mechanisms. The following guideline values are sought to be reached before discharge into Gothenburgs stormwater networks and recipients (Table 2.1). The guideline values for metals, metalloids and half-metals are listed as total concentration. Dissolved form of As, Cd, Hg, Ni and Pb is assumed to be approximately 50% of the total concentration listed in Table 2.1 (Vorne & Waara, 2021).

Table 2.1: Limit values for discharges to the city of Gothenburg to stormwater networks and recipients (Göteborgs stad, 2020; Vorne & Waara, 2021).

Parameter	Guideline Value
Routine parameters	
pH	6.5–9
Suspended Solids (mg/L)	25
Organic sum parameters	
Total Organic Carbon (TOC) (mg/L)	12
Eutrophying substances	
Total phosphorus (TP) (mg/L)	0.050
Total nitrogen (TN) (µg/L)	1250
Half-metals, metals and metalloids (µg/L)	
As (Arsenic)	16
Cd (Cadmium and its compounds)	0.9
Cr (Chromium)	7
Cu (Copper)	10
Hg (Mercury)	0.07
Ni (Nickel and its compounds)	68
Pb (Lead)	28
Zn (Zinc)	30

As stormwater enters the pond, the reduced flow velocity allows heavier particles, such as sediment, TWP, and other debris, to settle in the forebay before reaching the main pond. This sedimentation process is one of the primary methods by which pollutants are removed, as many contaminants, including heavy metals, hydrocarbons, and nutrients, are often attached to particulate matter (Ferguson, 1998).

Additionally, biological and chemical processes within the pond can contribute to pollutant removal. Vegetation and microbial activity help break down organic pollutants, while adsorption, oxidation and precipitation processes aid in removing dissolved contaminants such as phosphorus and certain heavy metals. Biofouling and aggregation can further influence particle dynamics, enhancing sedimentation and contaminant capture by increasing particle density and particle surface (Kooi et al., 2017).

The permanent water volume, or clarifier, enhances pollutant removal by promoting longer detention times, which increases sedimentation efficiency and allows for biological uptake of nutrients (Burton et al., 2013). The permanent water volume, or clarifier, further enhances pollutant removal by promoting longer detention times, which increases sedimentation efficiency and allows for biological uptake of nutrients (Burton

et al., 2013).

Furthermore, stormwater ponds act as a buffer against thermal pollution by reducing temperature fluctuations in runoff, which can otherwise negatively impact aquatic ecosystems. By integrating these physical, chemical, and biological treatment processes, stormwater ponds play a crucial role in improving water quality before the treated water is discharged into downstream surface water bodies (Scholz, 2023).

2.2.3 Design criteria

The design of stormwater ponds is influenced by several factors that affect their efficiency in managing runoff and enabling the water treatment mechanisms as mentioned before. Key considerations include residence time, length-to-width ratio, and desired flow conditions. Maintenance is then carried out to preserve this functionality and efficiency.

The retention time determines how long the rainwater remains in the pond before it flows out through the outlet structure. Longer retention times improve sedimentation and the removal of pollutants, as suspended matter has more time to settle. The optimum retention time depends on the pond volume, the inflow rate and the water quality objectives. For wet detention basins, at least 50% of the water quality volume should be stored in the permanent basin (Burton et al., 2013; Davis, 2020).

Different design features can also target particles of varying size and density. For instance, deep forebays are effective at trapping coarse, heavy particles such as sand and grit near the inlet (Scholz, 2023), while shallow vegetated zones (e.g., constructed wetlands) are better suited for capturing finer, lighter particles and promoting biological uptake (USEPA, 2004).

The flow conditions in the pond should be designed in such a way that effective sedimentation and water treatment is possible. A laminar flow facilitates the settling of particles, while a turbulent flow can lead to the resuspension of sediments. Features such as baffles or berms help to evenly distribute the flow, maintain low flow velocities and create calm conditions that improve sedimentation and biological treatment (Center for Watershed Protection, n.d.; Ferguson, 1998).

In addition to engineered features, natural vegetative areas, including riparian zones around drainage channels, can play an important role in stormwater pond design by slowing flow and promoting sedimentation. Here, stormwater often travels through small, concentrated flow paths shaped by natural topography or formed by deposition deltas at the edge of vegetated zones. These flow channels help distribute incoming water more evenly and reduce erosion. The vegetation in these areas may range from grasses to shrubs or trees with ground litter, all of which contribute to pollutant filtering and flow attenuation (USEPA, 2004).

However, creating dead zones, i. e. areas with little or no flow, should be avoided. This can reduce the overall efficiency of the treatment as oxygen exchange and sediment transport are restricted. In turn, recirculation zones can cause localized mixing, which leads to resuspension of particles. Both of these effects can lead to a reduction in the effective pond volume. Dead zones also reduce hydraulic efficiency by shortening flow paths and allowing untreated water to bypass active treatment zones. Designing long flow paths and irregular pond shapes and incorporating flow directing structures can

help minimize inefficiencies and secure consistent treatment performance (Kadlec & Wallace, 2009).

The length-to-width ratio influences the flow patterns and sedimentation efficiency. An elongated pond shape favors a plug flow, which prolongs water circulation and promotes sediment deposition. Ponds with a low length to width ratio are more prone to mixing, which can reduce efficiency. Design guidelines usually recommend a minimum length to width ratio of 3:1 to 5:1 to optimize pollutant removal and minimize sediment resuspension (Davis, 2020).

Regular maintenance is essential to ensure that stormwater ponds remain functional and effective. The forebay should be dredged every 5 to 7 years or once 50% of its storage capacity is lost. Sediments from ponds that do not receive runoff from known contamination sources are generally non-hazardous and can be disposed of through land application or in landfills. However, testing may be required if the pond collects runoff from potentially polluted areas. Maintenance access should be designed to support inspection and equipment, with stable routes that allow entry to key features such as the forebay, safety bench, riser, and outlet with adequate space for vehicle maneuvering (Center for Watershed Protection, n.d.).

2.3 Analysis of water quality parameters

As mentioned, there is a large variation of pollutants in stormwater, such as oil, grease, heavy metals, sediments, debris, and microplastics. In this section, properties, occurrence, environmental hazards and remediation efficiency in stormwater ponds are given for the pollutants addressed in this study: suspended solids, microplastics, tire wear particles, nutrients, organics and metals.

2.3.1 TSS/VSS

Total suspended solids and volatile suspended solids (VSS) represent particulate matter in stormwater runoff, including soil, organic debris, and pollutants adsorbed to sediment (EBS, 2011; McKetta Jr, 1998). These particles can degrade water quality, harm aquatic life, and transport nutrients or toxic substances downstream (Kirshen, 1972). Stormwater ponds are effective at removing TSS through sedimentation, as heavier particles settle out in the still water. While ponds excel at capturing coarse solids, their efficiency can vary for finer or more buoyant particles, including some VSS, which may require additional treatment for optimal removal (MOE, 1994; Yang et al., 2023).

2.3.2 Microplastics

Microplastics are an emerging contaminant, whose large emission (Järlskog et al., 2024; Thompson et al., 2024) and detection in human organs (Nihart et al., 2025) and in fish (Barboza et al., 2020) indicate a need to prevent them spreading into the environment.

Microplastics can be divided into primary and secondary microplastics (GESAMP, 2015). Primary microplastics are described as plastic particles designed to be of the size of microplastics, such as micro-beads in cosmetics, or plastic powders for molding, or plastic pellets used as raw material in manufacturing of plastic items. Secondary microplastics on the other hand are plastic particles that are of the microplastics size due to the breakdown of larger plastic items through fragmentation and weathering. Secondary microplastics are created during utilization and wearing of plastic products such

as tires, paints, and textiles but also through the exposure of plastic items in nature to the environment, especially solar UV radiation, over time.

There are no international definition for size limits on microplastics (Magnusson et al., 2016), but the upper boundary is usually set to 5 mm (Arthur Courtney et al., 2009; GESAMP, 2015; Magnusson et al., 2016) and the lower boundary between 1 nm (Magnusson et al., 2016) and 1 µm micrometer(GESAMP, 2015). For this study, microplastics are defined as plastic particles within the size range of 1 µm to 5 mm.

Cho et al. (2023) found in their study that 99% of the microplastics load was discharged into a receiving stream trough stormwater runoff and that only 1% of the microplastics load came from waste water treatment plant (WWTP), highlighting that stormwater is a key pathway for microplastics to reach the aquatic environment. Reviewing microplastics concentrations in literature, it is clear that there is a large variety of concentrations globally, as microplastic concentration varies from 0 to 197 000 items per liter (Shafi et al., 2024; Sewwandi et al., 2024; Wang et al., 2022). Sewwandi et al. (2024) studied literature on stormwater runoff reviewed several reports with studies from Sweden, and deduced that the average mean concentration of microplastics in Sweden is 1327.17 ± 840.54 items per liter.

Regarding the typical characteristics of microplastics in stormwater, the most common size were 20–100 µm and 100–200 µm in stormwater runoff, which had industrial and residential catchment, investigated by Cho et al. (2023). Regarding the shape of microplastics, Cho et al. (2023) states that the most common one, in their study, was the shape of a fragment, followed by the shape of a fiber. Between the different studied catchment areas (industrial and residential), 60% of the polymers in the stormwater runoff were polypropylene (PP) and polyethylene (PE). PP and PE, together with polyvinyl chloride (PVC), polyester and polystyrene (PS) were found to be the most common polymers, when combining the results from seven ponds with various catchment areas (industrial, commercial, highway and residential) (F. Liu et al., 2019).

The microplastics found in stormwater can either be lighter-than-water of heavier-than-water (Rasmussen et al., 2024). Rasmussen et al. (2024) found that while lighter-than-water microplastics were retained rather efficiently with a removal rate of 77–95% in four studied ponds, heavier-than-water microplastics had a higher removal rate of 97–99%.

The composition of microplastics in stormwater can be affected by several factors, one of which being the land use of the catchment area (Cho et al., 2023; F. Liu et al., 2019). F. Liu et al. (2019) stated that the catchment type in itself cannot describe the polymer composition, however Cho et al. (2023) explains that there was some more variation in polymer type in runoff from the industrial area compared to the one with residential area. F. Liu et al. (2019) explains that the size of microplastics could be seen as more describable by the catchments area. F. Liu et al. (2019) explains that the largest size of microplastics normally could be found in the pond with highway catchment, and the smallest in the ponds with commercial and industrial catchments. There was a great variability with respect to the size and composition of microplastics for industrial and commercial ponds when comparing ponds with the same catchment type with each other. However, regarding the three studied residential ponds, it was found that they between each other had comparable microplastics size and composition.

Other factors affecting the concentrations and properties of microplastics in stormwater

are the number of antecedent dry days (ADD) and the rainfall characteristics. More antecedent days and higher total rainfall depth were both found to yield higher concentrations of microplastics in stormwater (Cho et al., 2023). Also, the time since the start of runoff affected the size distribution of microplastics. The majority of the microplastics were transported within the first 40% of the total runoff time, but the proportion of heavier and coarser microplastics, increased in the later runoff period (Cho et al., 2023).

2.3.3 Tire wear particles

Tire wear particles are an emerging pollutant gaining increasing attention due to their ubiquity and potential environmental impacts (European Commission, 2023). TWP are a significant category of microplastics pollution, often classified as secondary microplastics because they are generated through mechanical abrasion rather than being intentionally produced in microscopic form. While TWP share characteristics with other microplastics, they differ in composition. They particles consist of a complex mixture of synthetic rubber, fillers, and various chemical additives (EMEP/EEA, 2016). TWP are also important because they make up the majority of microplastics in the environment: Their estimated levels are almost fifty times higher than those of other microplastics (European Commission, 2023).

TWP are generated by friction between tires and road surfaces, resulting in an elongated cylindrical shape with lengths ranging from 10 to 200 μm and widths below 20 μm. There is also a wide range of particle sizes, from visible debris to nanoscale fragments (0.5–600 μm) (Järlskog et al., 2022; Knight et al., 2020; Sommer et al., 2018). These particles typically feature a central rubber core derived from tire tread abrasion, often encrusted with smaller particles originating from brake wear, road wear, and various road dust components such as soil or concrete. Through this, TWP reach a relatively high density of 1.7 to 2.1 g/cm^3 (Vogelsang et al., 2020).

Particle encrustation significantly affects the physical properties of TWP. While pure rubber particles are relatively light, the encrustation with minerals of the TWP particle increases their overall density and mass (Järlskog et al., 2020; Klöckner et al., 2019). These changes can influence the transport behavior and settling properties of TWP in an aqueous environment. This also produces a chemically heterogeneous surface on the particles, which can carry additional pollutants such as metals or hydrocarbons, depending on the road and environmental conditions (Sommer et al., 2018).

The composition of TWP is influenced by factors such as the type of tire (e.g., car vs. truck, summer vs. winter), manufacturing differences, and the degree of accumulated wear. Table 2.2 shows typical tire tread compositions found in the literature, indicating a high proportion of fillers, softeners, and various additives.

Component	Proportion (mass%)	Composition
Basic material	40—50	Natural rubber (Polyisoprene, C_5H_8), synthetic rubber
Filler	30—35	Carbon black (C), silica (SiO_2), chalk ($CaCO_3$)
Softener	15	Oil, resin
Vulcanization agents	2—5	Sulfur (S), zinc oxide (ZnO)
Additives	5—10	Various (composition unknown)

Table 2.2: General components of tire treads (Camatini et al., 2001; Gunawardana et al., 2012; G. Wu, 2017).

Moreover, as TWP accumulate material through road and brake wear, their elemental composition changes. Table 2.3 outlines how this transformation alters the particle surface, increasing the presence of metals and inorganic elements (Sommer et al., 2018).

Diagnostic Features	Elements
Partly covered with road- and brake wear.	C, S, Zn; Si, Al, Na, Ca, K, Mg; Fe, Cu
Completely covered with road and brake wear.	Si, Al, Ca, Na, K, Mg; Fe, Cu, Zn, Ti, Mo, Mn, Ba, Sn, W

Table 2.3: Characteristics and Composition of TWP (Sommer et al., 2018).

Due to their complex and evolving composition, TWP are not only chemically diverse but also act as carriers for other pollutants such as PAHs, metals, and even microplastics (Sommer et al., 2018). Beyond their chemical complexity, TWP are highly persistent and mobile in the environment. Their durability allows them to travel long distances with minimal degradation, facilitating the widespread distribution of both the particles themselves and the harmful substances they carry (Öborn et al., 2024; Zhong et al., 2024).

Studies indicate that a substantial proportion of emitted TWP are extremely small. For instance, Zhong et al. (2024) found that 94.80% of TWP mass generated in controlled laboratory settings were below 100 nm.

Other research further supports the prevalence of nanoscale TWP. Sommer et al. (2018) identified particle sizes predominantly between 0.5 and 12 μm, averaging 1.5 μm, while Knight et al. (2020) reported a maximum size of 600 μm. Similarly, Järlskog et al. (2022) measured TWP in the size ranges of 2–20 μm and 20–125 μm. Gaggini et al. (2024) found that TWP between 1.6 and 20 μm accounted for 20–60% of collected samples. This range of sizes, especially the smaller particles indicate potential bioavailability of TWP.

TWP has been detected in considerable concentrations within stormwater and stormwater systems, showing their widespread presence and persistence in the environment. A study by Gaggini et al. (2024) investigating TWP along a highway stormwater system reporting concentrations ranging from 0.15 to 17 mg/L in water samples and 1.0 to 40 mg/g in sediments, indicating both high mobility in water and substantial accumulation in sediments. Similarly, Rødland et al. (2022) found even higher TWP concentrations

in stormwater runoff, ranging from 14.5 to 47.8 mg/L in water and 4.75 to 53.1 mg/g in sediment samples. Other studies have confirmed the presence of TWP in urban runoff, such as Dröge and Tromp (2019) who measured 51 to 59 mg/L in water, and Klöckner et al. (2020) reporting 0.95 to 11 mg/g in sediments. Overall, the studies emphasizes the role of TWP as a widespread and long-residency pollutant contributing to water pollution and sediment enrichment, making improved mitigation strategies necessary.

Several studies are suggesting that TWP concentrations are closely linked to TSS and VSS (Gaggini et al., 2024; Rødland et al., 2022). Strong correlations have been found between TWP and TSS (r = 0.87) and organic content via loss on ignition (LOI, r = 0.72) (Gaggini et al., 2024). The strong correlations indicate that TWP behave similarly to other suspended solids and organic.

Once released into the environment, TWP undergo weathering processes such as oxidation and interaction with road dust, altering their composition and properties before they reach water bodies (Baensch-Baltruschat et al., 2020; Jan Kole et al., 2017). These transformations influence their fate and potential ecological impacts, highlighting the need for further research on their transport and degradation mechanisms.

Toxicological studies on TWP mainly focus on aquatic organisms, where oxidative stress, inflammation, and endocrine disruption are the main damage mechanisms (J. Liu et al., 2023). While TWP particles can be harmful, much of the toxicity stems from their leachates, containing compounds such as PAHs, zinc and additives such as 6PPD quinone (Jaeger et al., 2024; Tian et al., 2022). Identifying specific toxic compounds remains difficult due to the leachates complex composition (J. Liu et al., 2023). Additionally, sunlight can increase toxicity by triggering photochemical reactions on TWP surfaces, forming more stable and reactive pollutants (K. Li et al., 2022).

2.3.4 Nutrients and organics

Nutrients in urban runoff primarily originate from atmospheric deposition and traffic (as key sources), fertilizers, organic matter and pet waste, which contribute to elevated nitrogen and phosphorous levels in stormwater (Ejhed et al., 2018; J. Wu & Malmström, 2015).

Estimates by Ejhed et al. (2018) suggests that stormwater is a relatively minor contributor to overall nutrient loads in water recipients in Sweden (1% of nitrogen load and 4% of phosphorus load), but it is also pointed out by Ejhed et al. (2018) that there is a significant variability across different water bodies. In some areas, stormwater accounts for more than 50% of the total nitrogen or phosphorous load, emphasizing the potential local impact.

An important factor regarding nutrients in urban runoff is, that when comparing runoff from different land use areas it is found that around 80% of the total dissolved nitrogen from urban and suburban runoff is bioavailable whilst only 20–60% is bioavailable in runoff from forest and pastures (Seitzinger et al., 2002). Given that there are potential local impacts for certain water bodies and that there is a variance in bio-availability of nutrients depending on catchment area, neglecting nutrient removal from stormwater may pose a risk to water quality in sensitive areas in Sweden.

When considering nutrient and organic matter removal in stormwater ponds, there are multiple factors to consider. Stormwater ponds has been described as active biochemi-

cal processing hotspots and identified multiple aspects influencing nutrient and organic matter removal (Lusk et al., 2025).

Firstly, sedimentation alone is not a reliable indicator for nutrient removal, as nitrogen, phosphorous and carbon are not permanently retained through assimilation and sedimentation (Lusk et al., 2025). Second, outflow concentrations of N, P and C are regulated by more than just the inflow characteristics and concentrations. Internal pond processes, such as mineralization of material in the sediment can alter nutrient levels, resulting in outflow concentrations that do not align with what is expected based on the inflow conditions from recent storm events. The outflows in the ponds then reflect the internal biochemical activity rather than the input from outside. Third, they state the importance of monitoring both inorganic and organic nutrient forms to fully understand internal cycling within a stormwater pond. While these ponds often harbor diverse biological communities that may play a role in nutrient removal, the extent of this influence remains under-researched. Furthermore, despite similarities to natural water bodies, stormwater ponds exhibit unique biogeochemical conditions due to higher contamination levels from urban pollutants, including heavy metals and microplastics. This distinction means that assumptions about nutrient behavior in natural systems may not always apply to stormwater ponds.

Additionally, Lusk et al. (2025) explain that optimizing for removal of P may hinder removal of N and vice versa. Finally, nutrient management in stormwater ponds may also conflict with strategies aiming at reducing green house gas emissions from stormwater ponds.

There are various ponds in existence, and when comparing ponds with each other, there has been discussion about how the pond itself affects the removal rate of nutrients and organic matter. Sønderup et al. (2016) has found that the age of the pond, the size of the pond, and the type of pond affect the removal rate. They studied 66 ponds located in the southern part of Denmark. Out of the 66 ponds, 46 are wet ponds, seven are wet ponds combined with vegetated sand filter within the pond before the outlet, five are ditches, five are grooves with overflow possibilities to a detention area and one is a dry pond. Regarding the type of pond, it is explained that the most optimal type in a moist country like Denmark would be a wet pond with a vegetated sand filter (which had between 40 to 80% retention efficiency of particulate fractions) or to only have a wet pond (which had between 10 to 20% retention efficiency of particulate fractions). Sønderup et al. (2016) suggest, when it comes to size, that the minimum distance between inlet and outlet should be 50 m but preferably above 80 meters and that the ratio between the volume of the pond and the area of the impermeable part of the catchment area should be above 0.025 m^3/m^2. The reason being that those measurements would lead to a long retention time and a use of the entire water body. It is stated that many ponds have poor retention due to their design, where the first flush of a heavy rain event is passing through smaller ponds into receiving water causing negative effects there. Regarding age and how it affects the retention of pollutants, it is explained that the age for the pond since either construction or renovation should not be more than 5 years to achieve optimal retention. This is due to ponds less than 5 years having a retention efficiency of around 40–50% of particulate fractions of organic matter, phosphorus and nitrogen, while ponds older, between 5–10 years, has around 0–30% and even older has barely any. They state that there is a need to consider management and maintenance for ponds older than 5 years.

2.3.5 Metal concentration

Metals are the main contributors to eco-toxicity impacts from stormwater, especially copper and zinc which according to Brudler et al. (2019) literature review, contributed to over 90% of the total ecotoxicty impacts when compared to nutrients, 18 additional metals and nearly 300 organic compounds.

Traffic can be a source of metals in stormwater. Hwang et al. (2016) concluded in their literature review that urban road dust has high amount of trace metals including copper (Cu), zinc (Zn), lead (Pb) and platinum group elements (PGEs), which are mainly released from vehicles. For the four mentioned types of metals, it has been found that the concentration of those in the road dust is up to 100 times as much as the background level concentrations. The primary source for Cu and Zn constitutes of wear of both brake pads and tires, while PGEs are released form the catalytic converters. The concentration of the Cu, Zn and PGEs has increased in many urban areas due to more urban sprawl, more vehicles and more distance traveled. The concentration of lead has decreased greatly since the outphasing of leaded gasoline and will be decreasing even more because of a resent ban prohibiting the use of lead wheel balancing weight in some of the states of the USA, as well as in Europe.

The concentration of metals in stormwater runoff varies with catchment area (Joshi and Balasubramanian, 2010; Egemose et al., 2015). Joshi and Balasubramanian (2010) studied and compared runoff from industrial and residential areas in Singapore. They studied trace elements of twelve metals and one metalloid and found that Fe followed by Al, Zn and Ti had the highest concentration in residential area. Fe, Zn and Al were also abundant in the dissolved fraction which is described as the fraction that is of immediate risk to the aquatic ecosystem. The concentrations of most of the studied elements were below discharge limits but some of them temporarily exceeded it, foremost during first flush periods. The elements noted as exhibiting first flush behavior are Co, Ti, Ni, V, and Zn. Additionally, they studied potential sources for the elements in the runoff from the two catchment types and found that the main sources for the elements in residential runoff was paints from building walls, crustal leaching, and atmospheric deposition.

Egemose et al. (2015) on the other hand studied 37 ponds, in Denmark, with various catchment areas: uncultivated, rural with mostly villages in agricultural areas, urban and industrial. The metals studied were copper (Cu), chromium (Cr), cadmium (Cd), lead (Pb), nickel (Ni) and zinc (Zn). They state that the concentration of metals varied between different catchment types, and that the average concentrations in the stormwater runoff generally were the highest in industrial areas followed by urban, uncultivated, and lastly rural areas. Egemose et al. (2015) states that while the catchment type can not influence the retention within the ponds directly, it may impact it through differences in dissolved versus particulate forms of metals in the inflow to the ponds between the catchment types and varying grain size distribution between catchment types. Egemose et al. (2015) explains how the removal efficiency varies depending on if the metals are in dissolved versus particulate phase and concludes that stormwater ponds have the ability to effectively remove metals in particulate forms through the sedimentation process but that it is more difficult to remove dissolved fractions. The removal of the metals Pb, Ni and Zn was more efficient than for the others due to higher particulate fraction of those metals. The samples taken from the outlets of the ponds revealed that heavy metals exiting the ponds mainly were dissolved fractions, with the exception of urban catchments.

Regarding the varying grain size distribution depending on catchment type, Egemose et al. (2015) describes that very fine particles need longer residence time. As the inflow of stormwater from urban catchments in their study contained very fine particles, the majority of metals in the outflow from ponds were in particulate form since the fine particles did not have enough residence time to settle.

The catchment type clearly influences the metal concentration, particle sizes and metal species in the inflow to the ponds. Following is a description of how in-pond processes affect which phase the metals are in, dissolved versus particulate, in the concentrations in the outlet. Egemose et al. (2015) saw that there was a direct positive relation between metal concentration in the sediments and the inflow concentration of particulate metals. They also observed that while the metal concentration in the sediment increased with age, it was not always proportional and they explain that it can be due to dynamic loading of the ponds and due to varying grain size distribution of the particulate matter in the inflow to the stormwater ponds. They expected the metal content in sediments to increase with time, due to mineralization processes, but only the concentration of Pb increased significantly. They discovered less metal content in the sediment than expected based on retention rates, and explained that the most likely reason for that is mineralization processes and resuspension. The degradation of organic matter by microorganism can influence metal speciation and lead to an increase of dissolved metals, and that having a dry period before a rain event during a study might affect the results as there can been an increase of dissolved metals during that dry period (Egemose et al., 2015). Joshi and Balasubramanian (2010) explains that abrupt changes in environmental condition can increase the dissolved fraction of metals through the environmentally mobile fraction of metals sorbed to suspended solids becoming dissolved in the water after an abrupt change in for example pH. They explain that the environmentally mobile fraction of the total concentration (dissolved, environmentally mobile and stable) was a significantly large part in their study with the concentration of certain metals in the environmentally mobile fraction being equal or larger than the dissolved fraction concentration. If there are abrupt changes in environmental conditions then the concentration for the dissolved fraction could increase. They explain that the metal with highest environmentally mobile fraction in the runoff from the residential area in their study was Cr, followed by Ti, Fe, and Zn.

Apart from catchment type, and in-pond-processes there are also other variables that impact the removal efficiency of a pond, such as the ratio between pond volume and impervious part of catchment area (Egemose et al., 2015). Egemose et al. (2015) found that the larger the ratio the better the retention. Their study also revealed that pond age has a great impact on retention. New ponds, below 2 years of age, had a positive removal of all metals to some extent. The net removal for the first years is most likely caused by adsorption kinetics. They declare that older ponds only removed Pb, Ni and Zn, where the removal decreased a lot over the years, but stayed positive. Ponds older than 1–2 years showed negative retention of the metals Cu, Cr and Cd, most likely due to low particulate content. In their study they found that physical parameters such as size of pond had larger impacts than chemical ones such as pH or organic matter, but they also mention that it is hard to interpret precisely which parameters affect the retention in the ponds, as several parameters act at the same time, and many physical and chemical parameters are interconnected.

In the stormwater ponds studied by Egemose et al. (2015) metal concentration, at the

outlet for Cd, Pb, Ni and Zn were below toxic levels reported in other literature. The dissolved Cu and Cr concentrations were below the toxic level for many of the ponds, but at toxic level for some of the ponds. While most of the outlet metal concentrations were not exceeding toxic levels reported in other literature, several metals either exceeded the Danish quality standard or were close to the limits of the standard.

2.4 Method on stormwater sampling and analysis

To evaluate the efficiency of stormwater ponds in retaining pollutants and particles, various studies have employed different water sampling techniques. The following studies— Gillis (2017), Nayeb Yazdi et al. (2021), and Pettersson (1999) — provide insights into methodologies used for collecting and analyzing stormwater samples at pond inlets and outlets.

Nayeb Yazdi et al. (2021) conducted stormwater sampling over a one-year period, monitoring 30 storm events using automated sampling stations at three inlets and one outlet. Each inlet was equipped with an automatic sampler (Teledyne-ISCO 6712), a rain gauge (ISCO 674) and an area-velocity meter (ISCO 2150) to measure inflows. The outlet-station featured a Palmer-Bowlus flume, a bubbler flow meter (ISCO 730) and a water quality data sonde for continuous monitoring of parameters such as water level, pH, temperature, oxidation/reduction potential, conductivity, turbidity, and dissolved oxygen. Hydraulic retention time was estimated for each event. Water samples collected from these events underwent laboratory analysis for total P, ammonia, nitrite, TSS and particle size distribution.

Similarly, Gillis (2017) employed ISCO 6700 and 6712 automatic samplers to capture stormwater at pond inflow and outflow points during a variety of rainfall events. Three samplers were positioned at stormwater inlets carrying runoff into the pond and one at the outlet. Sampling intervals were adjusted to capture pollutant variations, with shorter intervals (10 minutes) at the beginning of rainfall events to capture the first flush—when contaminant concentrations are highest—before transitioning to longer intervals (30 minutes). The ISCO samplers were triggered to begin sampling when the water level exceeded a predefined threshold, detected using an ISCO 750 area-velocity module with acoustic Doppler technology. Additionally, meteorological data were collected using a rain gauge to correlate precipitation intensity with pollutant transport. Data from the samplers, including sample times, water levels, and velocities, were retrieved via a field computer running Flowlink software. Additionally, meteorological data was collected, such as the rain intensity via leveled tipping bucket rain gauge (TR-525USW), which counted the number of tips in 15 minute intervals. Collected water samples were analyzed in the laboratory for TSS and particle size distribution.

Pettersson (1999) also relied on ISCO automatic samplers to collect flow-weighted stormwater samples at the inlets and outlets of three stormwater ponds. The ISCO 3700 samplers were equipped with peristaltic pumps and programmed to take only flow-weighted samples during storm events. Water discharge rates were measured using pressure probes: one in the inlet pipe, where flow was calculated using Manning's formula, and another in the pond, where discharge was determined using a 90° V-notch weir formula. The system was further supported by a rain gauge (ISCO 674) and a multi-probe water quality monitor (YSI 600) installed at the outlet, which continuously recorded parameters such as dissolved oxygen, pH, specific conductivity, and temper-

ature. Field data were logged and transmitted either directly to a laptop on-site or remotely via modem. The laboratory analysis of the collected water samples included TSS, VSS, heavy metals, total N, and total P.

Overall, all three studies utilized ISCO automatic sampling for their reliability in collecting stormwater samples under variable hydrological conditions. Nayeb Yazdi et al. (2021) and Pettersson (1999) both employed flow-weighted sampling to ensure pollutant loads were accurately represented, but they differed in their discharge measurement techniques: Nayeb Yazdi et al. (2021) used a Palmer-Bowlus flume and bubbler flow meter, whereas Pettersson (1999) relied on pressure probes and hydraulic formulas. In contrast, Gillis (2017) combined both flow-weighted and time-weighted sampling to capture the first-flush effect, adjusting sampling intervals dynamically. Additionally, Gillis (2017) integrated Doppler-based flow detection, while the other two studies primarily depended on traditional flow measurement techniques. These methodological variations highlight different priorities in stormwater research—whether focusing on pollutant load representation, first-flush dynamics, or precise hydrological monitoring. In terms of laboratory analysis, all three studies measured TSS and particle distribution, but Pettersson (1999) uniquely examined VSS, heavy metals, and nutrient levels (total N and P), while Nayeb Yazdi et al. (2021) additionally analyzed ammonia and nitrite. These methodological variations are caused by different research priorities, whether focusing on pollutant load representation, first-flush dynamics, or precise hydrological and chemical monitoring. Other underlying cause can be differences in budget, time frame and availability of tools and know-how.

2.5 Stormwater modeling

There are several different kinds of tools available to model stormwater management systems and ponds, and in the following subchapter (2.5.1) a brief overview of a selection of them will be presented. Thereafter, MIKE modeling is the focus of subchapter 2.5.2.

2.5.1 Different modeling tools

Svensson and Andersson-Sköld (2021) reviewed dispersion and fate models for microplastics from tire and road wear. Hydrological models simulate water conditions and flows using meteorological and hydrological parameters such as precipitation, evaporation, and infiltration. These models often include soil moisture, snowmelt, and groundwater calculations and can incorporate pollutant transport. However, they generally use one-dimensional flow representation.

Water quality (fate) models focus on pollutant transport in watercourses but require inputs from hydrological models or measured flow data. Examples include STREAM-EU, which simulates organic compound transport, and WASP, which models pollutants like nitrogen, phosphorus, and metals (Svensson & Andersson-Sköld, 2021). Besseling et al. (2017) adapted the NanoDUFLOW model, which was originally designed for nanoparticles, to study microplastics transport in the Dommel River, Netherlands. This model accounted for advection, aggregation, sedimentation, and resuspension, showing that particle size was the main factor influencing dispersion.

Hydrodynamic models calculate water flow using physical principles, according to Svensson and Andersson-Sköld (2021). While one-dimensional models describe longi-

tudinal transport, three-dimensional models, such as MIKE 3 FM, MIKE 11, TELEMAC, and Delft3D, offer high-resolution flow simulations in water bodies. Eisakhani et al. (2012) used an approach involving the use of MIKE 11, a 1D model, which has been applied to simulate the transport of biochemical oxygen demand (BOD) and chemical oxygen demand (COD) in river and channel systems. It is a one-dimensional hydrodynamic and water quality model used to simulate river and channel transport processes. So, while primarily used for open-channel flow, MIKE 11 can provide insights into pollutant dynamics in stormwater management systems, including the fate of dissolved and particulate contaminants.

Computational Fluid Dynamics (CFD) modeling is a numerical approach that solves fluid flow equations to simulate how water and suspended materials move within a defined environment. It allows detailed analysis of flow behavior, sediment transport, and contaminant dispersion in water systems (Ansys, 2025). It can be used to simulate simulate a submerged jet in a rectangular pond and optimizing a pond with regard to length, width, tail water depth, bottom roughness, and the offset of the pipe for the jet from the bottom of pond based on energy dissipation (P. Li et al., 2019). It also has been utilized in combination with a Lagrangian multiphase approach, to simulate the transport of buoyant microplastics and observing what the dominant mechanism is for transport of microplastics from water phase to sediments and for spreading microplastics across the pond (Molazadeh et al., 2023). Furthermore, it can also be employed supplemented with Lagrangian particle tracking, to develop a new boundary condition to simulate realistic sedimentation in a full-scale detention basin (Yan et al., 2014).

Discrete Phase Models (DPM) are computational approaches used in CFD to simulate the behavior of individual particles, droplets, or bubbles within a continuous fluid phase (Zahari et al., 2018). This study, Zhu et al. (2020), used a Lagrangian DPM to simulate the sediment transport and distribution of metals in a stormwater retention basin during dry weather.

Stormwater models assess runoff and water quality environments. The Storm Water Management Model (SWMM), developed by the US EPA, is widely used to simulate hydrological and transport processes to support the design of drainage systems and evaluation of Best Management Practices (BMPs) (EPA, 2024; Rossman, 2010). While SWMM does not account for particle-specific processes, models such as StormTac, WinSLAMM, and SWNano provide additional capabilities for water quality assessment and nanoparticle transport (Svensson & Andersson-Sköld, 2021).

Similarly, the Environmental Fluid Dynamics Code (EFDC) supports 1D, 2D and 3D hydrodynamic and water quality modeling in contained water bodies. It integrates hydrodynamic, sediment-contaminant, and eutrophication processes, making it suitable for modeling enclosed and semi-enclosed water bodies such as lakes, reservoirs, and urban stormwater systems (EPA & Hayter, 2006). For instance, Shahidzadehasadi et al. (2024) utilized the EFDC+ with Lagrangian particle tracking to investigate particle transport dynamics. While their study involved marine applications, key insights—such as the influence of wind drag and the trade-offs between 2D and 3D modeling—remain relevant for modeling floating or suspended materials in confined systems. The study also emphasized the computational considerations associated with 3D simulations, highlighting the need for balance between model resolution and efficiency in long-term hydrodynamic analyses.

According to Gao and Li (2014), future model development trends include (1) combining multiple models to address complex scenarios, (2) integrating artificial intelligence with mechanistic and non-mechanistic models for improved accuracy, and (3) enhancing models with remote sensing, GIS, and GPS data for large-scale analysis.

2.5.2 Modeling of stormwater ponds using MIKE

MIKE 21 and MIKE 3 are presented by MIKE (2025a) as software tools for simulating water flow, currents and wave conditions in marine and coastal environments.

MIKE 21 focuses on 2D modeling, creating simulations of water levels, currents, temperature variations and floods in coastal and estuaries areas, and rivers. It also incorporates bathymetry and influence of external forces like wind. MIKE 3 expands this to hydrodynamic 3D modeling, increasing the in depth analysis of water flow dynamics. It's capturing wave-induced currents, storm surges, and weather-related influences, making it a useful tool for detailed environmental evaluations (MIKE, 2025a).

MIKE 3 Flow Model solves the three-dimensional Reynolds-averaged Navier-Stokes (RANS) equations (see equation 2.1 and 2.2) or the 3D shallow water equations to simulate water flow (MIKE, 2019). The focus of the present work will be on RANS. It incorporates a continuity equation to ensure conservation of mass:

$$\frac{\partial u}{\partial x} + \frac{\partial v}{\partial y} + \frac{\partial w}{\partial z} = 0 \tag{2.1}$$

where *u,v,w* are the velocities in the *x,y,z* directions. The momentum equation of RANS describes how the fluid moves in response to pressure gradients, body forces and viscosity. The conservative form of momentum equation for every direction can be expressed as:

$$\frac{\partial \bar{u}_i}{\partial t} + \bar{u}_j \frac{\partial \bar{u}_i}{\partial x_j} = -\frac{1}{\rho}\frac{\partial \bar{p}}{\partial x_i} + \nu \frac{\partial^2 \bar{u}_i}{\partial x_j^2} - \frac{\partial \overline{u_i' u_j'}}{\partial x_j} + F_i \tag{2.2}$$

Where the components are defined as shown in Table 2.4.

MIKE 3 modeling also entails a turbulence closure scheme to approximate how turbulent eddies affect the movement of the fluid. It uses a sigma coordinate system for the free surface, which stretches the vertical grid to follow the surface movement.

A finite volume method is used for spatial discretization in MIKE 3 (MIKE, 2019), where the equations are converted into a numerical form for computer simulations and solved in each computational cell. The model uses a semi-implicit scheme on time integration and implicit scheme on calculation vertical motion to prevent numerical instability. For solving the remaining terms in the numerical model that are not directly handled by the finite volume method, semi-implicit scheme, or implicit scheme for vertical motion, it is described that either first-order Euler method or a second-order Runge-Kutta scheme is used. For pressure computation in MIKE 3, a projection method is applied in the Navier-Stokes equation to handle pressure variations not related to water depth-related pressure. To handle shocks and discontinuities, an approximate Riemann solver is used, allowing robust simulations of phenomena where there are sudden changes in fluid properties such as sudden changes in water height or fast-moving waves or surges.

Symbol	Name	Description
$\bar{u}_i$	Mean velocity (i-th direction)	$i = 1$: x ($\bar{u}$), $i = 2$: y ($\bar{v}$), $i = 3$: z ($\bar{w}$)
$\bar{u}_j$	Mean velocity (j-th direction)	Used in convection term (summed over j)
x_j	Spatial coordinate (j-th direction)	$x_1 = x$, $x_2 = y$, $x_3 = z$
$\bar{p}$	Mean pressure	Time-averaged pressure field
ρ	Fluid density	Constant for incompressible flow
ν	Kinematic viscosity	$\nu = \mu/\rho$
$\frac{\partial \bar{u}_i}{\partial t}$	Local acceleration	Change of mean velocity over time
$\bar{u}_j \frac{\partial \bar{u}_i}{\partial x_j}$	Convective acceleration	Momentum transport by mean flow
$-\frac{1}{\rho}\frac{\partial \bar{p}}{\partial x_i}$	Pressure gradient force	Drives or resists flow
$\nu \frac{\partial^2 \bar{u}_i}{\partial x_j^2}$	Viscous diffusion	Diffusion of momentum due to viscosity
$-\frac{\partial \overline{u_i' u_j'}}{\partial x_j}$	Reynolds stress divergence	Turbulent momentum transport
$\overline{u_i' u_j'}$	Reynolds stress tensor	Averaged product of fluctuating velocities
F_i	Body force per unit mass	e.g. gravity, Coriolis, etc.
i, j	Tensor indices	i = direction of equation, j = summed direction

Table 2.4: Description of terms in the RANS momentum equation (tensor form)

MIKE 3 supports particle tracking through its Advection-Dispersion (AD) module and Lagrangian particle tracking (PT) module, which are coupled with the underlying hydrodynamic model to simulate the transport and fate of suspended substances or particles (MIKE, 2019) In the Lagrangian environment, the particles are represented as discrete units whose trajectories are calculated by solving Newton's second law using velocity fields derived from the hydrodynamic model. The particle position is updated based on advection from flow velocity and dispersion from turbulent diffusion, and the model can incorporate processes such as settling, resuspension, and buoyancy. The particle transport is influenced by 3D flow field, turbulence intensity and particle properties (size, density, settling velocity). Particle tracking in MIKE 3 is typically used for applications like sediment transport, microplastic dispersion, oil spill modeling, or tracer studies, where detailed insights into individual or grouped particle behavior over time are required (MIKE, 2017).

In MIKE 3, particle-like behavior such as the settling and resuspension of particulate matter can be simulated with the ECO Lab extension module (MIKE, 2019). Although ECO Lab does not track individual particles as in a Lagrangian model, it enables the representation of Eulerian particle tracking. The transport and fate of suspended particles (e.g. sediment, microplastics or particles bound to pollutants) is modeled as scalar concentrations within the 3D flow field. Settlement processes are usually implemented by defining a constant or dynamic settlement velocity and applying it as a vertical flow loss term scaled to the local water depth. In addition, ECO Lab allows the incorporation of physicochemical processes such as aggregation, sorption or resuspension by defining

user-defined differential equations and threshold conditions (e.g. based on the shear stress at the bed). This extension makes it possible to link hydrodynamic conditions from the MIKE 3 Flow Model FM with water quality or particle transport behavior, enabling the simulation of particulate fate in aquatic systems under complex flow scenarios (MIKE, 2025b).

Several studies have explored the application of MIKE models for hydrodynamic simulations in different contexts, providing insights relevant to stormwater treatment facilities. A study by German et al. (2005) utilized the MIKE 21 2D model to assess the impact of retrofitting measures on the hydraulic performance and removal efficiency of suspended solids in a stormwater pond. They assessed measures such as installing baffles, adding culverts under a causeway, and removing an existing island. By simulating the flow and sediment transport, the study demonstrated how structural modifications could enhance the pond's ability to retain pollutants and improve overall treatment efficiency.

Expanding the scope to a larger system, Bondelind et al. (2018) used the 3D hydrodynamic model MIKE 3 FM to simulate microplastics transport and deposition in a 16 km stretch of the Göta älv River. The model dynamically estimated flow based on river discharge and sea level measurements. While providing high spatial and temporal accuracy, it did not account for resuspension, biofouling, aggregation, or degradation. A key limitation, common to many models, is the reliance on assumptions about particle shape and density due to limited validation data.

Bentzen (2010) applied MIKE 3 specifically to wet detention ponds to simulate pollutant transport in wet detention ponds. Relevant physical processes such as wind, waves, deposition, erosion and sediment consolidation were taken into account. The model was calibrated using experiments in a controlled flume and validated against real data, showing good agreement with the measurements. The study underlines the usefulness of the model for evaluating the efficiency of pollutant removal in storm water treatment facilities, including the effects of wind on sedimentation. The model can be applied to both single discharge events and long-term assessments and is a valuable tool for optimizing the design and performance of wet detention ponds.

Building on this, Rama (2023) applied MIKE 3 FM to an actual Swedish stormwater pond, Järnbrott, to analyze flow patterns and assess the feasibility of implementing a forebay. This study narrows the scope further by linking hydrodynamic modeling directly to the design of forebays. It also demonstrates the challenges posed by spatial constraints, bathymetry accuracy and the lack of standardized criteria.

3 Methods

Below is the methodology for sampling, lab analysis, on-site measurements, retrieval of in-data for modeling from external sources, modeling and literature research. The pond chosen for analysis is based upon, partly accessibility to the site, and partly the willingness from the municipality to follow-up on the pond's performance.

3.1 Study area

The pond which is investigated is located at Kryddvägen, Angered in Sweden. The coordinates are 57°48'42.18"N 12°02'05.63"E. The pond is displayed in Figure 3.1 below.

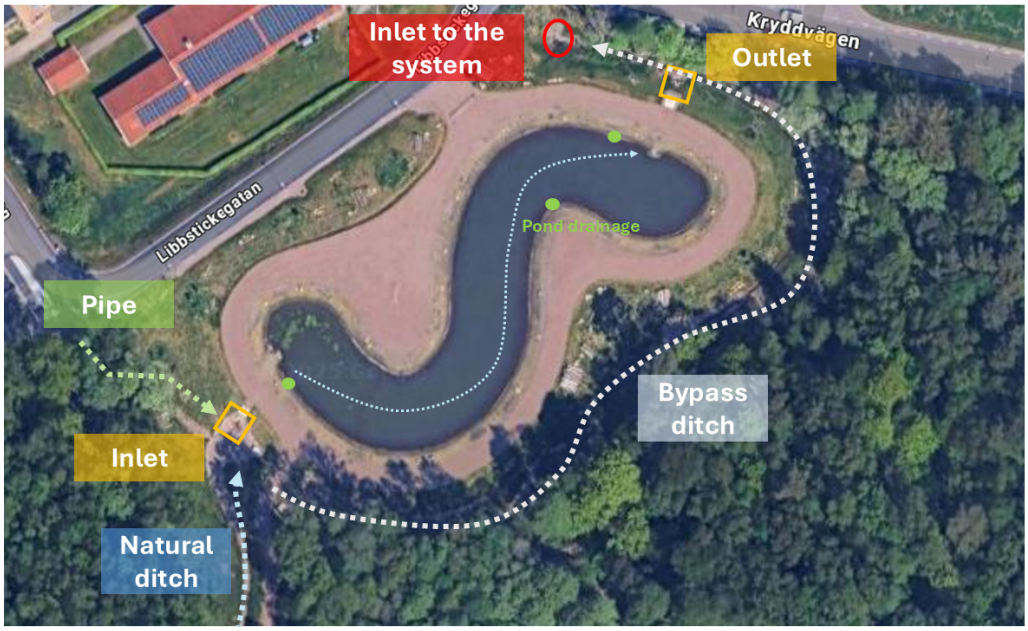

Figure 3.1: Overview of stormwater pond in Kryddvägen, Angered, Sweden with indicated flow path of approx. 102 meters in length (Image modified from Google Maps, accessed 20.03.2025, available at Google Maps).

The pond was built in 2021–2022, it has a water depth of 0.6 meters, and a surface area of around 2000 m^2, offering a pond volume of approx. 1200 m^3. The catchment area in Gårdsten, Göteborg for this pond is 26 ha and it is a mixed land use area consistent of residential areas, traffic area and forest area. Out of the 26 ha, only 6.5 ha is impervious surfaces such as buildings, roads and roofs. The pond volume-to-impervious-area ratio is around 0.018 m^3/m^2 The remaining catchment area is mainly forest area. The treated water from the pond then enters the Keillers damm through a conduit and then enters the final recipient from there, the river Göta älv. Below, in Figure 3.2, the catchment area for the pond can be observed.

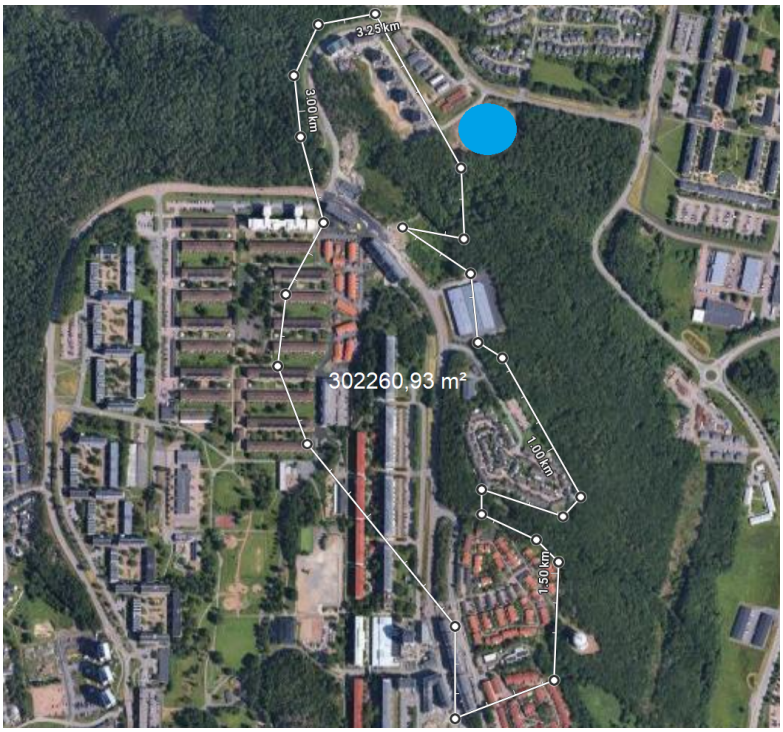

Figure 3.2: Overview of catchment area of the Kryddvägen pond (delimited by white contour). The pond's position is marked in blue (Image modified from Google Maps, accessed 20.03.2025, available at Google Maps).

In Figure 3.1 and 3.3, it is possible to see that stormwater from the catchment comes from two sources, one is from a pipe (catchment from residential area) and one is from a natural ditch. Before the inlet to the pond the two water streams are merged into one. The dimensioning flow used for the inlet pipe was 0.3 m^3/s. When the flow is greater, excess water goes through the by-pass ditch. The outlet is built as a weir and enables free overflow, when the water level reaches the tip of the weir (v-notch) at 63.75 m.a.s.l. The weir can be seen in Figure 3.3. Closure mechanisms are fitted to both the inlet and the outlet (Figure 3.3,top row to the left and to the right respectively), to allow the inflow and outflow of the pond to be blocked manually in the event of contamination in the catchment area (e.g. in the event of an oil spill). In the pond there are three drainage valves installed, which can be used to empty the pond to remove the sediment when needed.

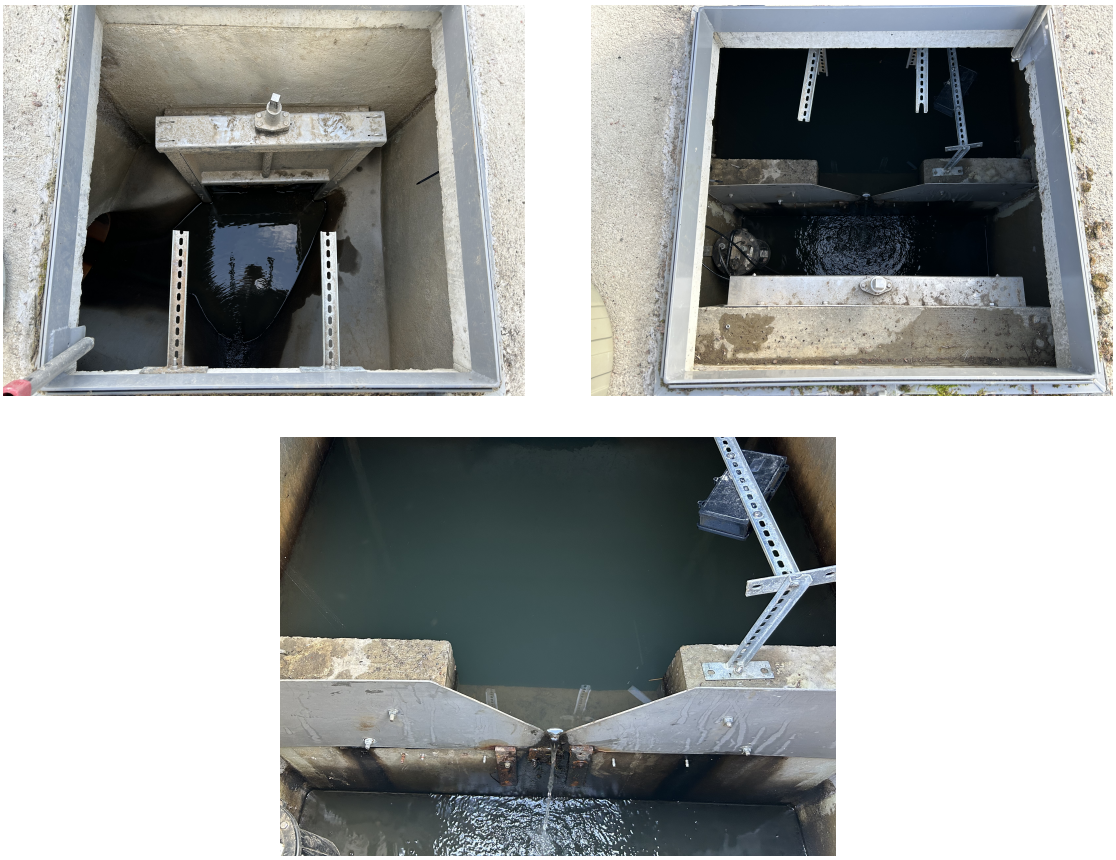

Figure 3.3: Inlet (left) and outlet (right) and a close up of the outlet-weir (bottom).

If a rain event occurs with a recurring interval of 20 years, excess water flows over a long overflow into a bypass ditch, where the rainwater is not treated by the rainwater pond. The runoff water from the pond and the excess water in the ditch are combined behind the pond outlet and fed into the municipality's pipe system.

Gothenburg has high precipitation levels with an average of 912 mm of rain/snow per year between 1991 and 2020 (SMHI, 2024). However, the amount of rain that falls each month varies, with the highest amount occurring in autumn with an average of 92.8 mm in August, 80 mm in September and 102.9 mm, in October. The lowest amount occurs in April with an average rainfall of 51.3 mm. The sampling period for the present work is in April/May. In April, the average rainfall is as mentioned 51.3 mm and the average temperature is 7.7°C, while the average rainfall is is 54.3 mm and the average temperature is 12.4°C, in May (SMHI, 2024).

3.2 Sampling

ISCO 6712 automated samplers from MJK Automation with the capacity to carry 24 one liter sampling bottles (Figure 3.4) were placed one each at the inlet and at the outlet of the pond. Each sampler was connected to a hose, which was placed at the bottom of the pipes at inlet and outlet. Through these, the ISCO samplers take in the rain water samples via a pump.

Figure 3.4: Opened ISCO-sampler, stacked with 24 bottles.

In addition, flow meters were installed and connected with the ISCO system to measure the flow and to set a trigger flow for the ISCO samplers to start taking samples. The installed flow meters are part of a ADS flow meter system consisting out of the Triton+^{TM} (signal conditioning, communications, data storage, and power functions) and a Peak Velocity Sensor^{TM} by ADS and were rented and maintained by DHI. The peak velocity sensors work based on the Doppler effect and were placed at the bottom of the pipes at inlet and outlet together next to the sampling hose.

The trigger flow at the inlet and outlet was set to different values, as the outlet requires a higher sensitivity in order to be able to take sufficient samples. This is the case because the pond has a low water level, especially after long dry periods, which has to fill up to 63.8 m.a.s.l. before the outlet can overflow and samples can be taken. Therefore, the trigger flow rate at the inlet for the first rain event was set to 5 L/s and at the outlet to 2 L/s. For the second and following rain events, the triggers were set to 8 and 5 L/s. The sampler was set to fill 2 bottles 10 minutes apart when triggered by the flow meter.

The weather conditions during sampling where documented using the weather forecast websites smhi.se and yr.no. Here, data on likability of rain event, rain intensity and wind force were collected. Additionally, a rain gauge was set up by DHI on a roof of a bicycle shelter close to Kryddvägen pond to monitor the rain amount and intensity. The gauge tipped over after filling up with 0.2 mm of rain. The sampling was carried out for six weeks from 17.04.–26.05.2025 with collected rains listed in Table 3.1.

Date	Duration	Antecedent Dry Days	Rain Depth [mm]
02.05.2025	06:20–07:50	11	4.4
22.05.2025	03:34–19:44	19	13.8
26.05.2025	13:48–15:57	1	6.2

Table 3.1: Summary of Rain Events from 17.04. to 17.06.2025. For the rain event on 22.05.2025: while the rain event lasted for approx. 13 h (incoming and outgoing flow measured by flow meter), samples were only captured over the first 8 h of the event, as the capacity of the samplers was reached.

3.3 Lab analysis

The sampling bottles taken on site from the ISCO samplers were transported to the laboratory. The filled bottles were stored in a fridge by 6°C when not processed the same day. To ensure sufficient sample volume for all laboratory analysis, consecutive pairs of 1 liter samples were mixed and aggregated into 2-liter samples. These samples were then analyzed for total and volatile suspended solids, nutrient content, organic carbon, nitrogen, turbidity, pH, and conductivity using standardized laboratory methods.

Total suspended solids and volatile suspended solids were determined using the ESS Method 340.2. The samples were filtrated through pre-weighted glass microfiber filters (diameter 55 mm) and dried at 105°C for TSS measurement. The filters were then ignited at 550°C to determine VSS by calculating the mass lost on ignition.

Total Phosphorus (TP) was measured using the HACH Test'n'Tubes PhosVer®3 reagent and acid persulfate digestion, following USEPA Method 8190. The device used gives orthophosphate (PO_4), phosphorus (P), and phosphate (P_2O_5), where P is the TP concentration and the others are different representation of the same phosphorous. The test range for the method is 0.02–1.10 mg/L P. For the first rain (2025-05-02) the inlet samples were diluted 2 times with deionized water prior to analysis due expectation of higher concentrations and the outlet samples were analyzed undiluted. For the second and third rain (2025-05-22 and 2025-05-26) neither inlet or outlet samples were diluted as the TP results from the first rain indicated that dilution wasn't needed.

Samples were also prepared for elemental analysis using Inductively Coupled Plasma Mass Spectrometry (ICP-MS). The samples were prepared by adding Nitric acid 69% and were then introduced to the ICP-MS model *iCAP Q* from Thermo scientific.

Total organic carbon TOC, dissolved organic carbon DOC, and Total Nitrogen (TN) were analyzed using a Shimadzu TOC-V CPH analyzer. For the first rain (2025-05-02) event the inlet samples were diluted 3× and outlet samples 2× prior to analysis to ensure values were within the instrument's calibration range. For the second rain (2025-05-22) and third rain (2025-05-26) neither inlet nor outlet samples were diluted due to the analysis of the first rain indicating that dilution wasn't needed. Samples were filtered for DOC and analyzed to the instrument's standard operating procedure.

pH was measured using a handheld VWR pH110 meter, calibrated with standard fluid beforehand. Electrical conductivity was determined using a VWR HCO 304 conductivity meter.

The event mean concentration EMC is commonly used to represent pollutant concentrations (Erickson et al., 2013). It is calculated as follows:

$$\text{EMC} = \frac{\sum_{i=1}^{n} C_i Q_i}{\sum_{i=1}^{n} Q_i} \tag{3.1}$$

where

- Q_i = flow during interval i
- C_i = concentration during interval i

Retention efficiency was calculated based on the EMC as pollutant load according to Erickson et al. (2013) as follows:

$$\text{Removal efficiency (summation of load)} = \left(\frac{EMC_I - EMC_E}{EMC_I}\right) \times 100\% \qquad (3.2)$$

where

- EMC_E = effluent event mean concentration as calculated by equation 3.1
- EMC_I = influent event mean concentration as calculated by equation 3.1

3.4 Modeling in MIKE

3.4.1 Geometry and computational mesh

The geometry of the pond was provided by the municipality as a DWG file. It was converted to a DXF format in AutoCAD, and then processed in JupyterLab to generate a .xyz file suitable for mesh generation (see Appendix A.1 for code).

A triangular computational mesh was created using the MIKE 3 Mesh Generator. The mesh consists of 1617 nodes and 2992 elements. The size of the triangular elements varies depending on geometric complexity, with areas ranging from 0.0204 m^2 to 1 m^2, and the smallest angle being 26°. Figure 3.5 shows the final mesh.

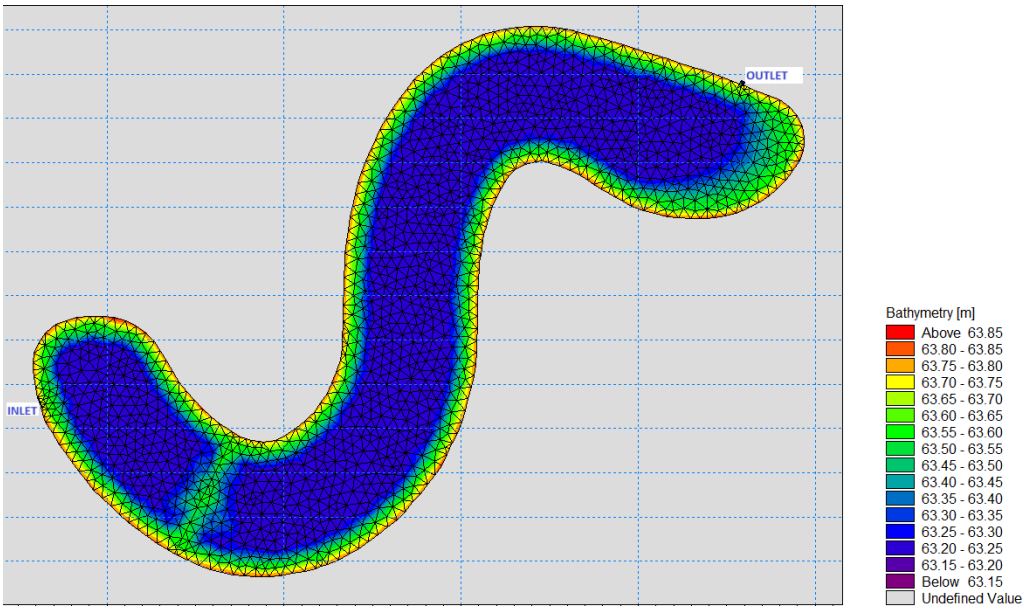

Figure 3.5: The final mesh file.

To set up boundary conditions, arcs were drawn and assigned properties: land boundaries (code 1), inlet (code 2), and outlet (code 3). These property codes enabled later differentiation and parameter assignment in the hydrodynamic model.

Mesh smoothing was applied (30 iterations) with constraints on mesh quality and fixed arc nodes. Following this, a compliance check was conducted to correct non-conforming elements. The final mesh met DHI's recommended Courant–Friedrichs–Lewy (CFL) number of 0.8. After interpolation, the mesh was exported in .mesh format for use in the hydrodynamic model.

3.4.2 Hydrodynamic modeling

The hydrodynamic simulation was conducted using the MIKE 3 Flow Model FM (DHI, 2019). A fully three-dimensional, time-dependent setup was implemented to simulate flow conditions in the pond during selected real rain events in April and May 2025. Five scenarios were modeled (see chapter 3.3.4, Table 3.6).

The vertical discretization was defined using the Sigma Equidistant method with 8 uniform layers each representing 12.5% of water depth. The initial water level was set to 63.8 m above sea level (m.a.s.l.). The model solves the three-dimensional incompressible Navier–Stokes equations. The hydraulic and physical properties of the model have been set as can be seen in Table 3.2.

Table 3.2: Hydraulic and physical model properties.

Parameter	**Value / Description**
Density	Water density formulation as function of temperature (reference: 10°C)
Horizontal eddy viscosity	Smagorinsky formulation, coefficient = 0.28
Vertical eddy viscosity	Two-equation turbulence model; min = 1.8×10^{-6} m^2/s, max = 0.4 m^2/s
Bed roughness	Constant roughness height: 0.035 m
Vegetation	not included
Coriolis force	spatially varying over the domain
Wind forcing	See reference scenario table
Ice coverage	Not included
Precipitation / evaporation	Not included
Infiltration	Not included
Wave radiation stress	Not included
Turbulence module	Default settings
Temperature / salinity module	Temp: -2.1 to 30°C; Salinity: 0–5 PSU; no heat exchange included

The model domain includes one inflow and one outflow, corresponding to the inlet and outlet of the pond (see Figures 3.1 and 3.5). The inflow was implemented as a source boundary, with flow rates derived from measured or scenario-based hydrograph (see Table 3.6). The inlet boundary was set to free outflow conditions. The outflow was implemented as a structure-type boundary using a weir with defined physical characteristics. The outflow boundary was also set to free outflow. The land boundary surrounding the pond was defined as a no-flow boundary with zero normal velocity. Parameters for the weir are summarized in Table 3.3.

Table 3.3: Implemented weir parameters.

Parameter	Value	Unit
Width	0.5	m
Height	0.25	m
Weir coefficient	1.38	$\frac{m^{\frac{1}{2}}}{s}$
Weir exponent	2.5	-
Invert level	63.75	m

3.4.3 Particle tracking

Particle tracking module was set up to provide insight on how TWP are transported within the pond and where TWP of different size classes would settle during a rain event. The properties of the particles relevant for the model have been chosen and sorted into three classes based on literature (Gaggini et al., 2024; Järlskog et al., 2022; Knight et al., 2020). As no laboratory analysis of TWP or size distribution measurement could be carried out, the TSS concentration is used as a surrogate parameter for potential TWP concentrations in the model. The basis for this assumption is the strong correlation in behavior between TWP and TSS established by Gaggini et al. (2024).

The classes implemented into the particle tracking module can be seen in Table 3.4. Although a wide range of different particle sizes is given in the literature, three particle sizes were chosen for the simulations to represent TWP, which cover the size range in the literature (according to Kovochich et al., 2021, TWP is usually <120 μm). In this way, the very fine size fraction is also avoided, as it cannot be easily sedimented.

Particle mass and settling velocity for each class were calculated as follows:

The particle mass m_p was calculated using

$$m_p = \frac{4}{3} \times \pi \times r^3 \times \rho_p \tag{3.3}$$

where *r* is the particle radius and ρ_p is the particle density.

The terminal settling velocity *v* of a spherical particle in water is determined by balancing gravitational, buoyant, and drag forces:

$$\frac{4}{3}\pi r^3(\rho_p - \rho_f)g = \frac{1}{2}C_d\rho_f\pi r^2 v^2 \tag{3.4}$$

where ρ_p is the particle density, ρ_f the fluid density, C_d drag coefficient and g gravitational acceleration The Reynolds number *Re* is defined as:

$$Re = \frac{2rv\rho_f}{\mu} \tag{3.5}$$

The drag coefficient C_d for spherical particles with *Re* < 1000 is approximated by:

$$C_d = \frac{24}{Re}\left(1 + 0.15Re^{0.687}\right) \tag{3.6}$$

This nonlinear system is solved iteratively by assuming an initial velocity (e.g., from Stokes' law), updating Re and C_d, and refining v until convergence. The results of these calculations are documented in Table 3.4 and were implemented as stated here in the particle tracking module.

Table 3.4: Particle properties used in the model.

Class	Particle size (μm)	Density (g/m³)	Mass (mg)	Settling velocity (m/s)
1	10	1900	9.94838E-07	4.90E-05
2	50	1900	0.000124355	1.20E-03
3	100	1900	0.000994838	4.51E-03

The settings for the particle tracking module were set up as presented in Table 3.5.

Table 3.5: Particle tracking model properties.

Parameter	Value / Description
Classes	See Table 3.4
Sources	Point source, positioned on top inlet boundary
Decay	Not included
Settling	Constant, class dependent
Dispersion	Dispersion coefficient formulation
- Horizontal Dispersion	Constant, 0.001 m^2/s
- Vertical Dispersion	Constant, 1.1E-05 m^2/s
Erosion	Not included
Drift Profile	Use raw data from hydrodynamics
Density	Water density formulation from hydrodynamic model

3.4.4 Simulated scenarios

To investigate hydrodynamic behavior and particle transport under various conditions, four modeling scenarios were developed. Each scenario represents a specific set of boundary conditions, ranging from idealized to more realistic setups. The scenario conditions are presented in detail in Table 3.6.

Table 3.6: Definition of simulated hydrodynamic and particle tracking scenarios. The time series for Scenario 4–6 are based on measured data (see Figures 4.29, 4.33 & 4.37 for inflow and duration; Figures 4.1, 4.2 & 4.3 for flux input and A2.1, A2.2 & A2.3 for the wind time series).

	Scenario 1	**Scenario 2**	**Scenario 3**	**Scenario 4**	**Scenario 5**	**Scenario 6**
Title	Basecase	Basecase with wind	20-year rain event	Rain 2025-05-02	Rain 2025-05-22	Rain 2025-05-26
Inflow	10 L/s	10 L/s	300 L/s	Fig. 4.29	Fig. 4.33	Fig. 4.37
Duration	12 h	4 h	4 h	12 h, 07:00–19:00	12 h, 03:00–15:00	12 h, 13:30–01:30
Wind -Velocity -Direction	 - -	 7 m/s 270°	 - -	 Tab. A2.1 Tab. A2.1	 Tab. A2.2 Tab. A2.2	 Tab. A2.3 Tab. A2.3
Particle flux input	5 constant inputs	-	-	Time series	Time series	-
Particle number	999,995 per class	-	-	1,000,000 per class	1,000,000 per class	-
Particle per pulse	199,999 per class	-	-	Follows TSS curve	Follows TSS curve	-

Scenario 1 represents the base case and models the pond under constant conditions. A steady inflow of 10 L/s, representing an average flow rate into the pond, was used. No wind forcing was applied. This setup was selected to observe undisturbed flow patterns and establish a reference condition for comparison with more complex scenarios.

Scenario 2 builds on the base case by introducing wind forcing to examine the effect of surface wind on flow conditions and particle dynamics. A constant wind with a direction of 270° (westerly) and a velocity of 7 m/s, which reflects the prevailing wind direction and average wind speed in Gothenburg (SMHI, 2024). This scenario allows for the assessment of wind-induced surface mixing.

Scenario 3 represents an extreme weather event, precipitation with a return period of 20 years. The precipitation intensity was set to 30 mm/h, in accordance with national climate projections and technical design values (SMHI, 2025; Sörensen & Rana, 2013). The duration of the storm event was set to 4 hours, to ensure that the simulation reached steady state. Inflow corresponding to 30 mm/h over the 26 ha catchment area results in approximately 1029 L/s, though in practice and in the simulation only 300 L/s are routed into the pond due to bypass activation during high flows. This scenario is designed to test the pond's capacity and behavior under design storm conditions.

Scenario 4–6 are based on actual meteorological and hydrological data, including rain gauge and flow meter recordings. These simulations intended to reflect realistic and temporally resolved events. Wind was based on measured conditions from smhi.se, enabling a close-to-life model calibration and validation. In Scenario 4, the flow was set to zero starting from time step 62 (12:10) due to lack of further data over the remaining time of the simulation (12 h). Wind forcing held on for the complete run of the simulation.

For comparability, the particle load of a total of 1,000,000 particles was set up for all simulated scenarios with implemented particle tracking (Scenario 1, 4, and 5). In the

Scenario 1, the release was configured as five pulses of equal particle amounts during the first five time steps of the simulation.

To avoid triggering a warning related to MIKE 3's internal particle mass checks — specifically, "Source value smaller than minimum, source value clipped" — the number of particles per pulse was adjusted slightly. This warning occurs when the emitted flux or total mass per time step is smaller than the minimum particle mass defined for a class in the setup. To resolve this while maintaining total mass and flux accuracy, the particle number was reduced marginally from 200,000 to 199,999 per time step, ensuring that each particle's mass remained above the specified minimum threshold.

In the rain event scenarios (Scenario 4 and 5), particle inputs were dynamically defined using the time-varying TSS concentration profile measured at the inlet during experiments. This approach reflects more realistic inflow conditions by directly incorporating experimentally observed variations in particle concentrations over time.

The total particle mass entering the pond during simulation can be seen in Table 3.7.

Table 3.7: Total mass (mg) entering the Kryddvägen pond during simulation across different scenarios.

	Total mass [mg]	
Class	**Scenario 1**	**Scenario 4, 5**
Class 1	0.995	0.995
Class 2	124.354	124.355
Class 3	994.833	994.838

4 Results

4.1 Water quality analysis

The first rain event of the sample-period that yielded in samples being taken at both inlet and outlet by the auto-samplers occurred on 2025-05-02. The second rain event which yielded samples being taken at both inlet and outlet occurred on 2025-05-22. A third rain event occurred 2025-05-26.

As mentioned in section 3.3, the analyzed water quality parameters were total suspended solids (TSS) and volatile suspended solids (VSS), turbidity, pH, conductivity, total organic carbon and dissolved organic carbon (TOC/DOC), total nitrogen and dissolved nitrogen (TN/DN), total phosphorous (TP) and dissolved metal concentration.

4.1.1 TSS and VSS

In Figure 4.1, it can be seen that TSS and VSS are much higher at the inlet compared to the outlet for rain event 2025-05-02, which indicates that the majority of particles entering the pond are not discharged into the connected stormwater network. It is also clear that TSS is significantly higher than VSS, which indicates that most particles are inorganic in the pond. TSS in the inlet ranges from 99.47 to 497 mg/L, and the VSS at the inlet is around 11-15% of the TSS. The TSS at the outlet ranges from 10.68 to 15.24 mg/L, and the VSS at the outlet is around 30 to 40% of the TSS, depending on sample.

The results from TSS/VSS analysis for rain event 2 show that TSS is higher at the inlet compared to the outlet, especially when comparing the first flush inlet samples to outlet samples (see Figure 4.2). The TSS concentrations at the inflow ranges from 28.2 mg/L to 209 mg/L, and the TSS concentrations at the outflow ranges from 3.5 mg/L to 37.7 mg/L.

It should be noted that VSS is given as error bars due to an error in filter preparation where the filters were dried at 105 degrees instead of burned at 550 degrees. The VSS results were corrected using the average weight loss of five blank filters from the same batch (rinsed with milliQ and burned at 550 degreed), and by the minimum and maximum measured weight loss as indicated by the error bars.

While there is a significant portion of organic particles in the inflow, the vast majority is inorganic for all samples except for one, I8 at 07:25. That sample seems to deviate from pattern and may be an anomaly caused by the filter losing more weight than the blank filters tested. If disregarding I8, the VSS is around 8 to 22% of TSS at the inlet. At the outlet, the combined uncertainty from low VSS concentrations relative to filter weight loss hinders clear determination of organic versus inorganic content. Based on VSS values corrected by the average weight loss in blanks, organic particles represent 17.5 to 49% of TSS at the outlet, except in O2 and O8 were they represent 58 to 68%. When comparing TSS to the minimum VSS, the results show that the organic fraction is reduced to around 50 to 52% for O2 and O8, while the other samples organic fraction is reduced to around 12 to 41% of the TSS concentration. Comparing TSS with the maximum VSS after correcting for weight loss, the results show organic particles dominate at the outlet (56 to 84% of TSS), except for the last four samples which had 24 to 36% of organic particles. Sample O7 was an outlier with higher VSS than TSS, likely caused by the filter losing significantly more weight, than the blank filters tested.

In Figure 4.3 it can be seen that the TSS at the inlet is reduced with time and that the TSS at the outlet is much lower than at the inlet, with inlet TSS concentrations ranging from 115.3 mg/L to 932 mg/L and outlet concentrations ranging from 12.3 mg/L to 16 mg/L. About 8 to 13% of particles in the inflow are organic and about 15-31% of particles in the outflow are organic.

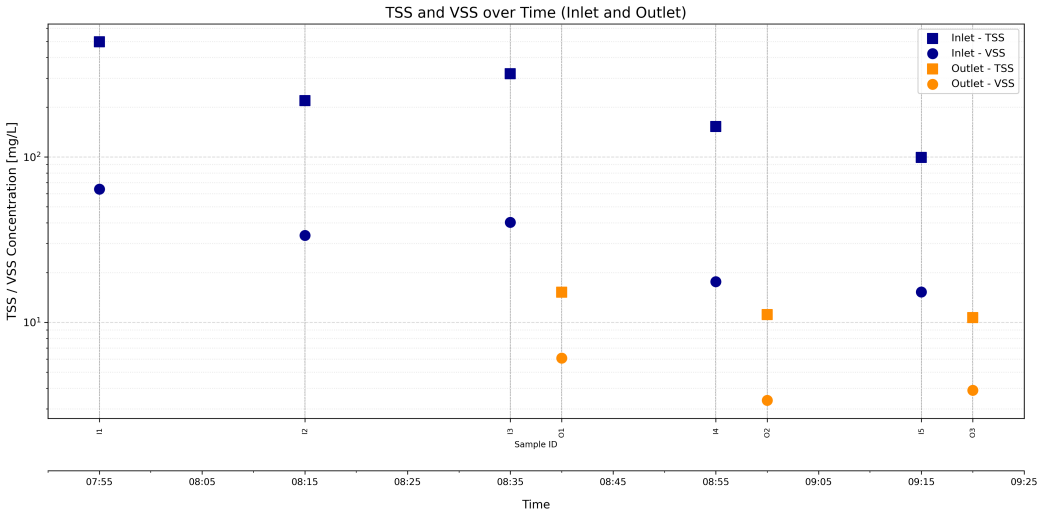

Figure 4.1: TSS and VSS in each sample from inlet (I1–I5) and outlet (O1–O3) over time. Rain event 2025-05-02.

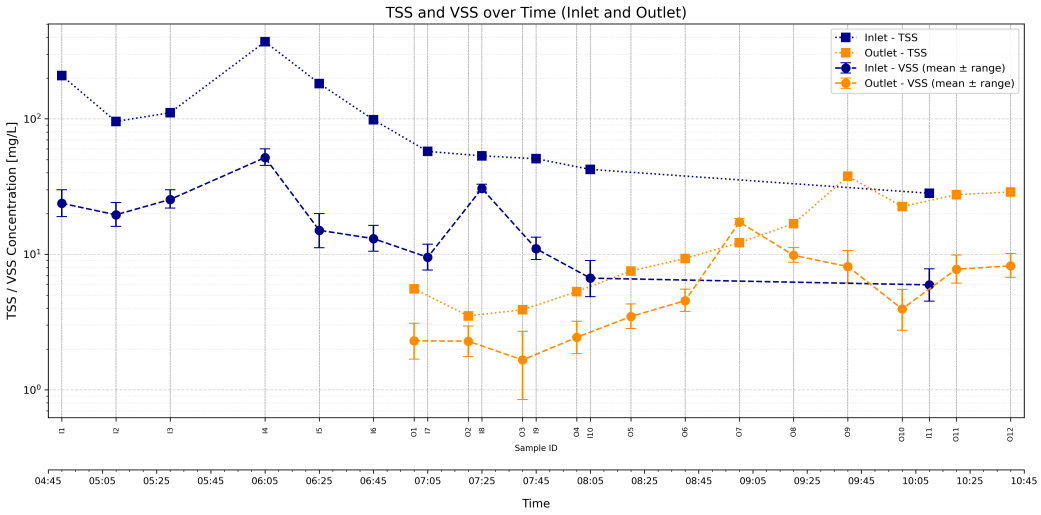

Figure 4.2: TSS and VSS in each sample from inlet (I1–I11) and outlet (O1–O12) over time. Rain event 2025-05-22. Note that caution should be taken when analyzing the VSS due to error in filter preparation where the filters where dried instead of burnt causing unintended additional weight loss. For VSS results, the values are corrected by the average filter weight loss from blank filters. The error bars indicate VSS values corrected by the minimum and maximum filter weight loss observed from the blank test.

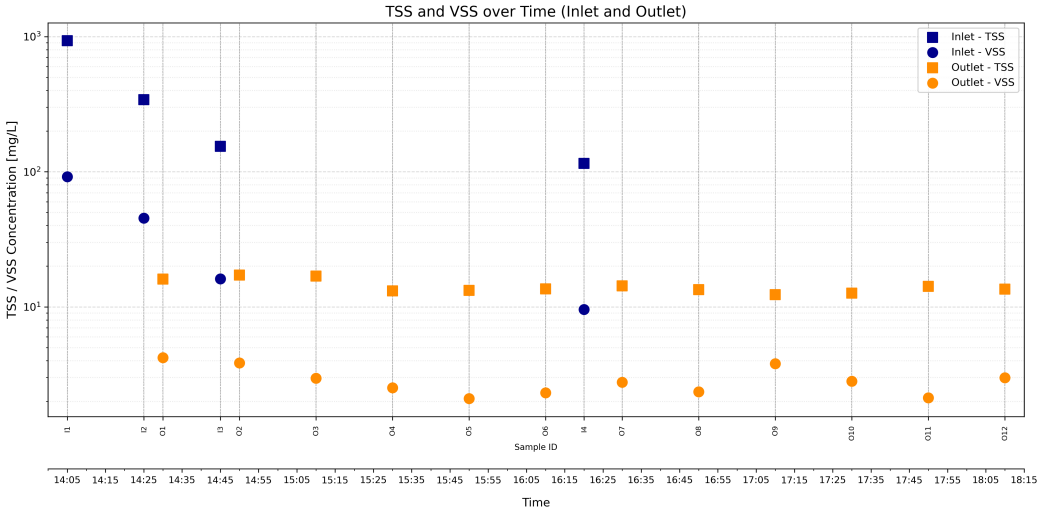

Figure 4.3: TSS and VSS in each sample from inlet (I1–I4) and outlet (O1–O12) over time. Rain event 2025-05-26.

The event mean concentration was calculated for the three rain events with regards to TSS and VSS, and can be seen in Table 4.1. The third rain event displayed the highest mean concentration for TSS and VSS in the inflow, followed by the first rain event and lastly the second rain event. In the outlet, the event mean concentration for TSS was the highest for the second rain event, followed by the third and lastly the first rain event. The mean concentration for VSS in the outlet was the highest for the second rain event followed by the first and lastly the third rain event.

The retention efficiency of the pond regarding VSS and TSS was calculated using EMC, and can be seen in Table 4.1. For both, TSS and VSS, a high retention efficiency during rain events could be reached (up to 97.41%). Overall TSS was reduced better than VSS.

Table 4.1: Event mean concentrations and retention efficiencies for rain events.

Rain	**Event mean concentration (EMC) [mg/L]**				**Retention efficiency (%)**	
event	**TSS**$_{in}$	**TSS**$_{out}$	**VSS**$_{in}$	**VSS**$_{out}$	**TSS**	**VSS**
1	311.98	11.95	40.99	4.21	96.17	89.74
2	180.52	15.34	23.39	6.22	91.50	73.39
3	545.01	14.14	57.32	2.87	97.41	94.99

4.1.2 Turbidity

As can be seen in Figure 4.4, the pattern of turbidity aligns well with the pattern of TSS in Figure 4.1. The turbidity in the samples from rain event 2025-05-02 declines with time at the inlet from 261 to 92 FAU, with sample I2 being an exception. Turbidity remains roughly the same at the outlet over time (20 and 17 FAU). The turbidity in the samples from rain event 2025-05-22 (see Figure 4.5) has a somewhat similar pattern for inlet to that of rain event 2025-05-02 (see Figure 4.4), where the turbidity decreases from the first sample to the second and then an increase occurs for 1-2 samples and then decrease. The time horizon for when in time the increase and decrease occurs, are however different, where the second peak of turbidity occurs after 40 minutes for the first rain event (2025-05-02) and after 1 hour and 20 minutes for the second rain event

(2025-05-22). The highest turbidity in the inlet for the second rain was 244 FAU, and the lowest turbidity was 49 FAU. The turbidity at the outlet increases with time for the second rain. The highest turbidity at the outlet for the second rain event was 50 FAU and the lowest was 4 FAU. As can be seen in Figure 4.6, the turbidity for rain event 2025-05-26 aligns well with TSS curve seen in Figure 4.3. The turbidity decreases with time at the inlet, from 662 FAU to 83 FAU, but remains roughly the same at the outlet, between 19-23 FAU over time, with the exception of O9 which had 1 FAU.

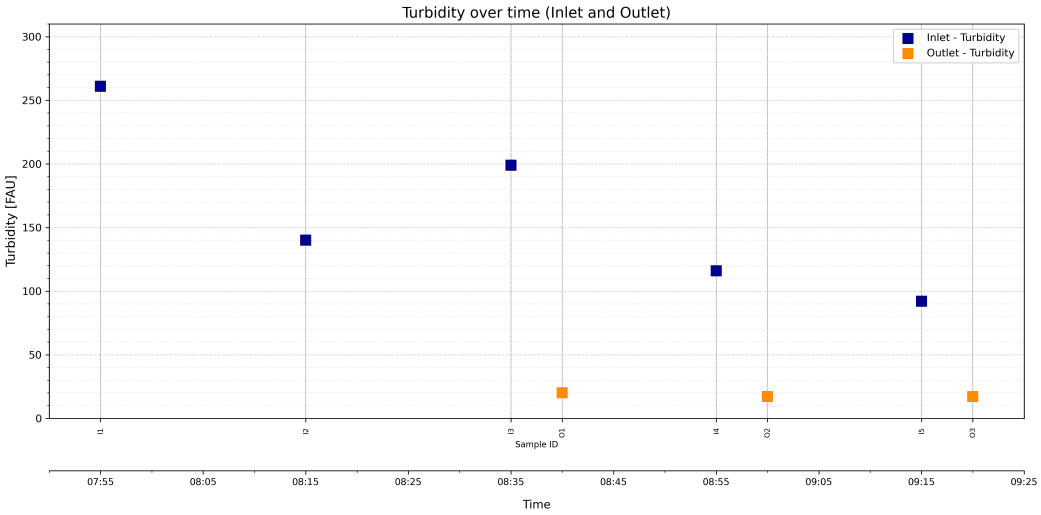

Figure 4.4: Turbidity in each sample from inlet (I1–I5) and outlet (O1–O3) over time. Rain event 2025-05-02.

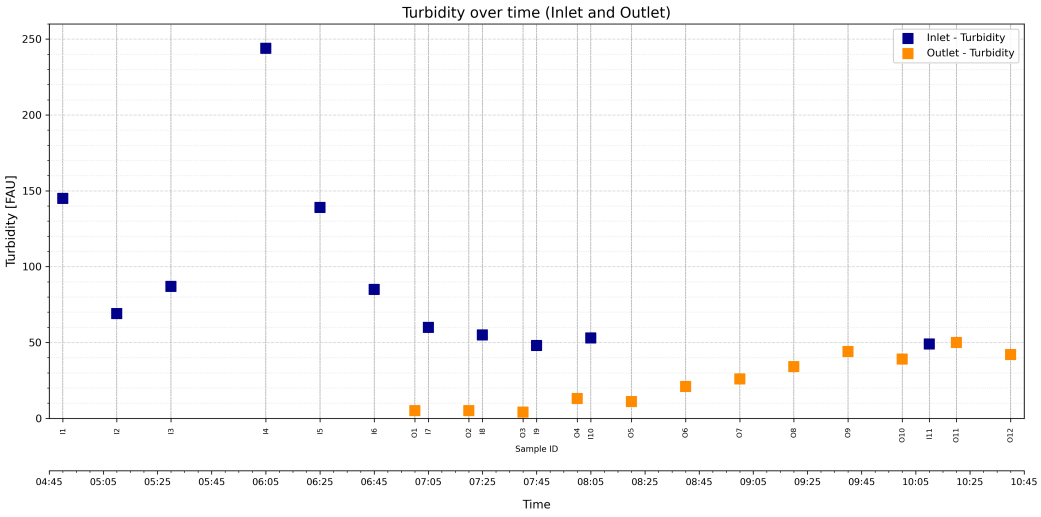

Figure 4.5: Turbidity in each sample from inlet (I1–I11) and outlet (O1–O12) over time. Rain event 2025-05-22

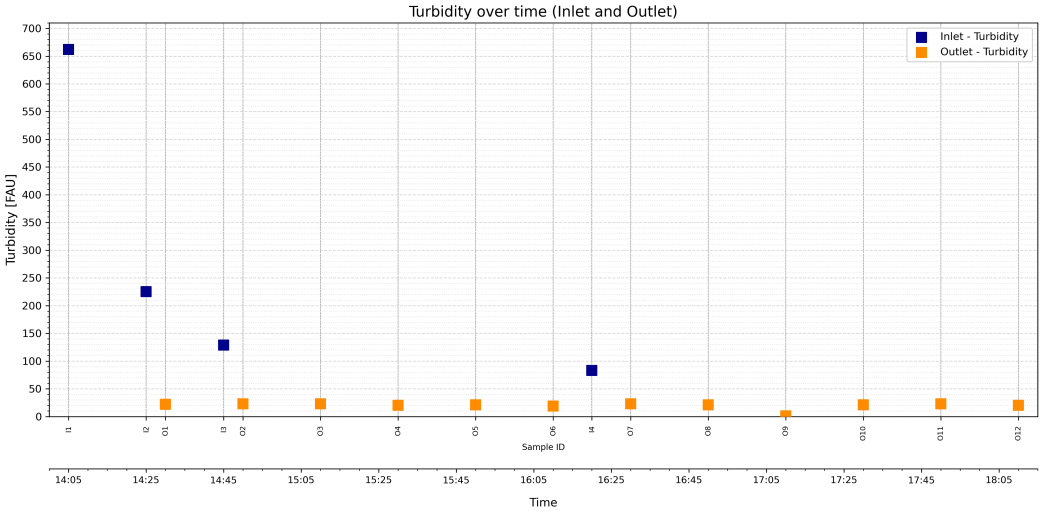

Figure 4.6: Turbidity in each sample from inlet (I1–I4) and outlet (O1–O12) over time. Rain event 2025-05-26.

4.1.3 pH

Figure 4.7, Figure 4.8 and Figure 4.9 shows that the pH in the inlet is lower than in the outlet, but that both inlet and outlet has pH near 7. The water that enters the pond is slightly acidic. Starting from 6.24 the pH at the inlet increases up to 6.5 for the first rain event (2025-05-02). Starting from 6.49 the pH in the inflow increases to 6.82 for the second rain event rain (2025-05-22), and starting from 6.31 the pH in the inflow increases to 6.48 for the third rain event (2025-05-26). The pH at the outlet is around 7.2 for all samples from the outlet for the first rain event but varies between 6.96 to 7.15 for the outlet samples yielded by the second rain event. The pH at the outlet for the third rain event has slightly lower pH than both the first and second rain event, with pH that ranges from 6.79 to 6.93.

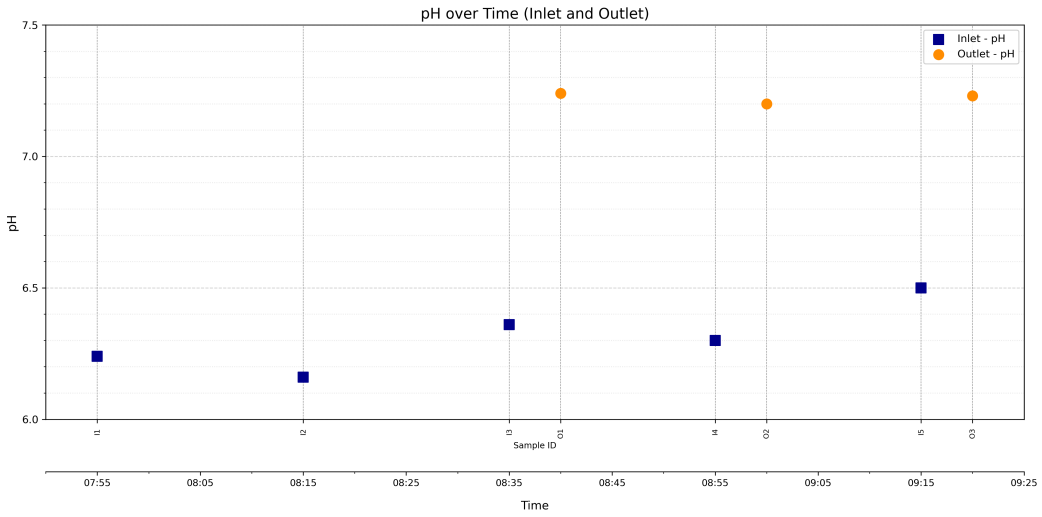

Figure 4.7: pH in each sample from inlet (I1–I5) and outlet (O1–O3) over time. Rain event 2025-05-02.

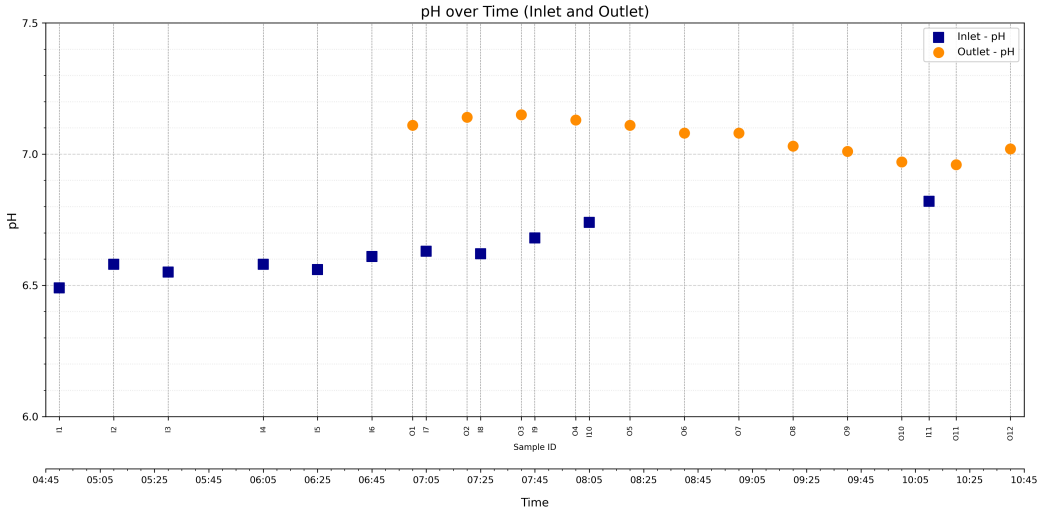

Figure 4.8: pH in each sample from inlet (I1–I11) and outlet (O1–O12) over time. Rain event 2025-05-22.

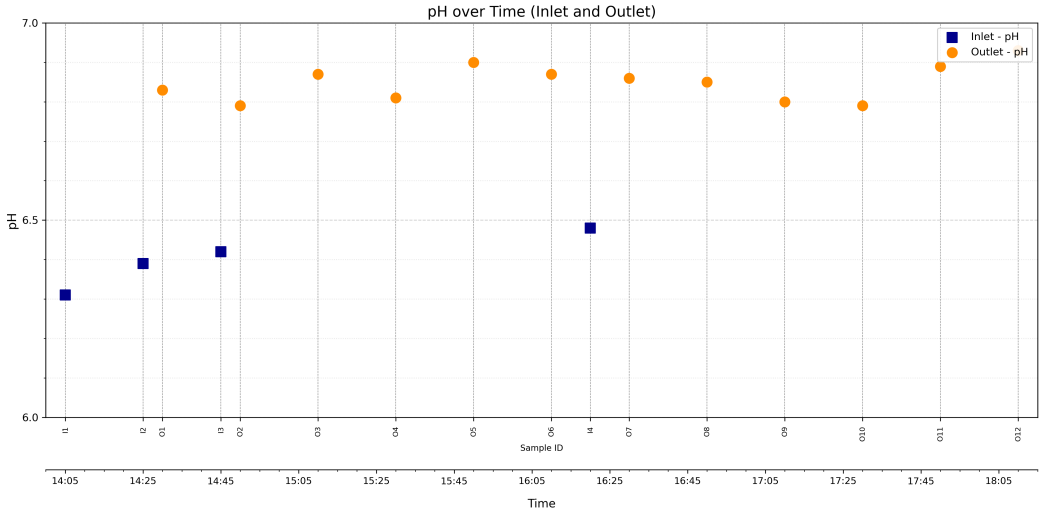

Figure 4.9: pH in each sample from inlet (I1–I4) and outlet (O1–O12) over time. Rain event 2025-05-26.

4.1.4 Conductivity

As can be seen in Figure 4.10, 4.11 and 4.12, the conductivity is much higher at outlet (approximatly 410 µS/cm for rain event 2025-05-02, between around 290–410 µS/cm for rain event 2025-05-22, and between 132–138 µS/cm), compared to conductivity at the inlet. The inlet conductivity varies between around 50–150 µS/cm for rain event 2025-05-02, between around 40–210 µS/cm for rain event 2025-05-22 and between 46–98 µS/cm for rain event 2025-05-26. Overall, the conductivity in the pond is relatively low.

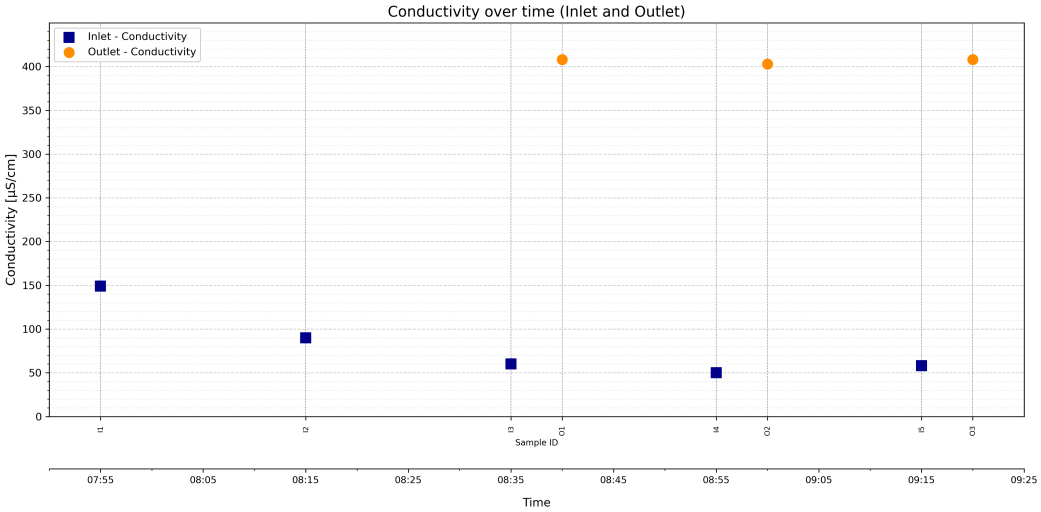

Figure 4.10: Conductivity (µS/cm) in each sample from inlet (I1–I5) and outlet (O1–O3) over time. Rain event 2025-05-02.

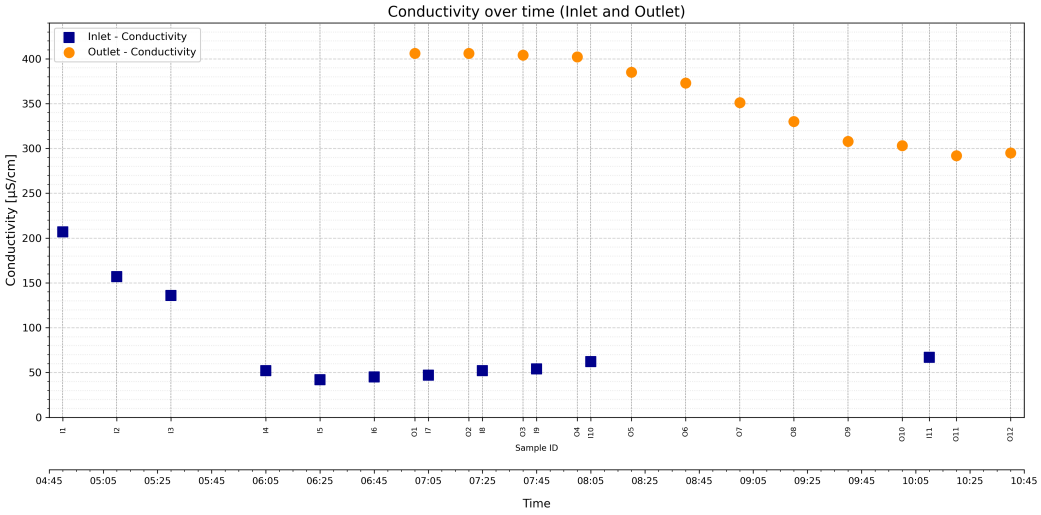

Figure 4.11: Conductivity (µS/cm) in each sample from inlet (I1–I11) and outlet (O1–O12) over time. Rain event 2025-05-22.

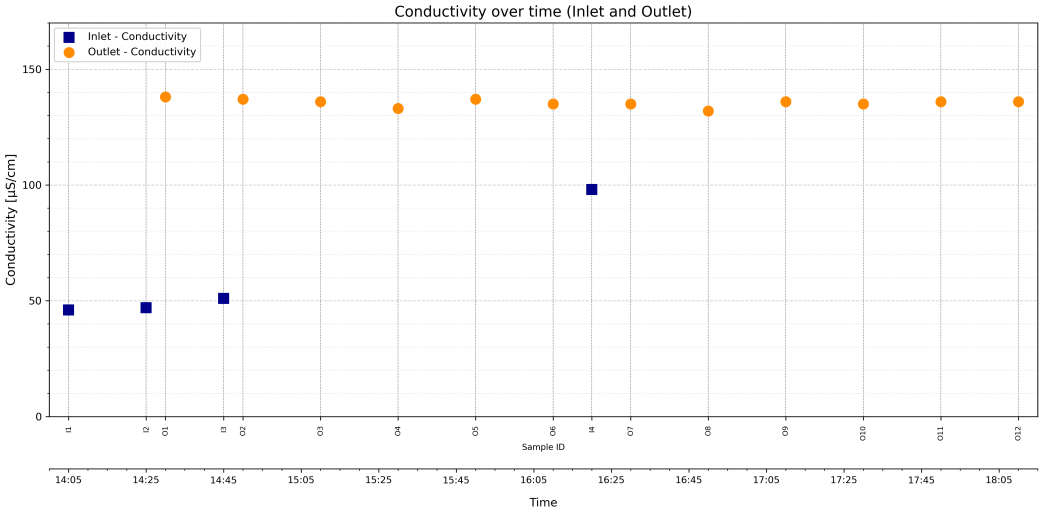

Figure 4.12: Conductivity (µS/cm) in each sample from inlet (I1–I4) and outlet (O1–O12) over time. Rain event 2025-05-26.

4.1.5 TOC and DOC

Figure 4.13 and Figure 4.14 shows that TOC and DOC are higher in the first inlet samples than in the outlet samples and that there is trend in the inlet where the TOC/DOC is reduced as time passes. Additionally, it can be seen in that the later inlet samples has around the same TOC/DOC values as outlet samples.

TOC at the inlet for rain event 2025-05-02 decreases from 30.30 to 8.29 mg/L, while DOC decreases from 27.40 to 11.48 mg/L. The TOC (using average value of replicates) at the inlet for rain event 2025-05-22 decreases from 51.69 mg/L to 12.58 mg/L, while DOC (using average value of replicates) decreases from 52.97 mg/L to 12.82 mg/L.

At the outlet, for rain event 2025-05-02, the TOC concentration remains between 9.45 and 8.20 mg/L and DOC lays between 8.06 and 8.34 mg/L. At the outlet, for rain event 2025-05-22 it can be seen in Figure 4.14 that the TOC and DOC at first decreases for the first couple of samples but then increases for several samples to then decrease slightly for the later samples. TOC at the outlet for rain event 2025-05-22 ranges from 10.75 mg/L to 22.02 mg/L and DOC at the outlet ranges from 10.2 mg/L to 22.16 mg/L.

While the TOC and DOC have a decreasing trend in the inflow for the first and second rain, they have an increasing trend for rain event 2025-05-26 as seen in Figure 4.15. The outlet TOC and DOC concentrations for the third rain event (2025-05-26) are similar to those from the first rain event (2025-05-02), while the inlet TOC and DOC concentrations are significantly lower for the third rain event.

The higher DOC concentrations compared to TOC concentrations found in several samples from the different rain events is discussed further in chapter 5, section 5.1.4.

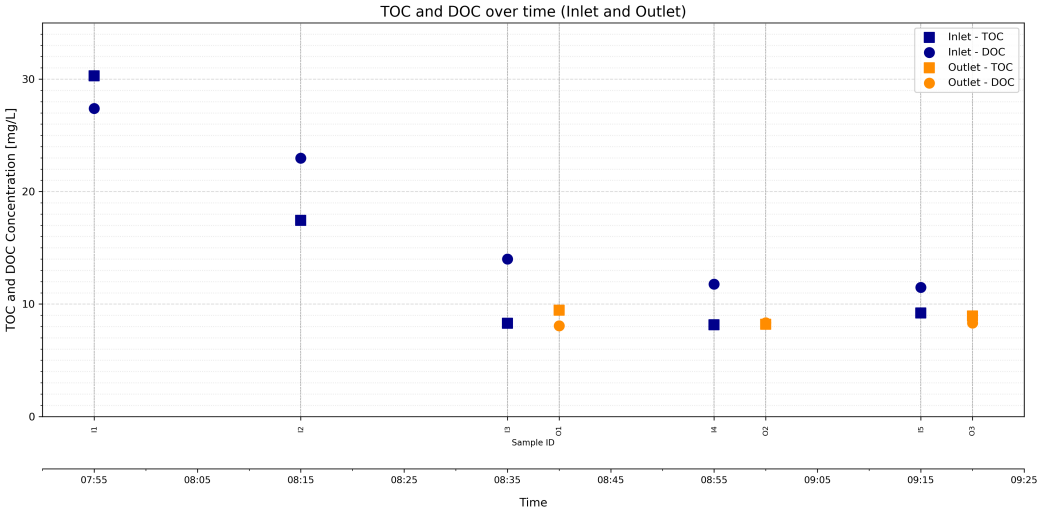

Figure 4.13: TOC and DOC in each sample from inlet (I1–I5) and outlet (O1–O3) over time. Rain event 2025-05-02

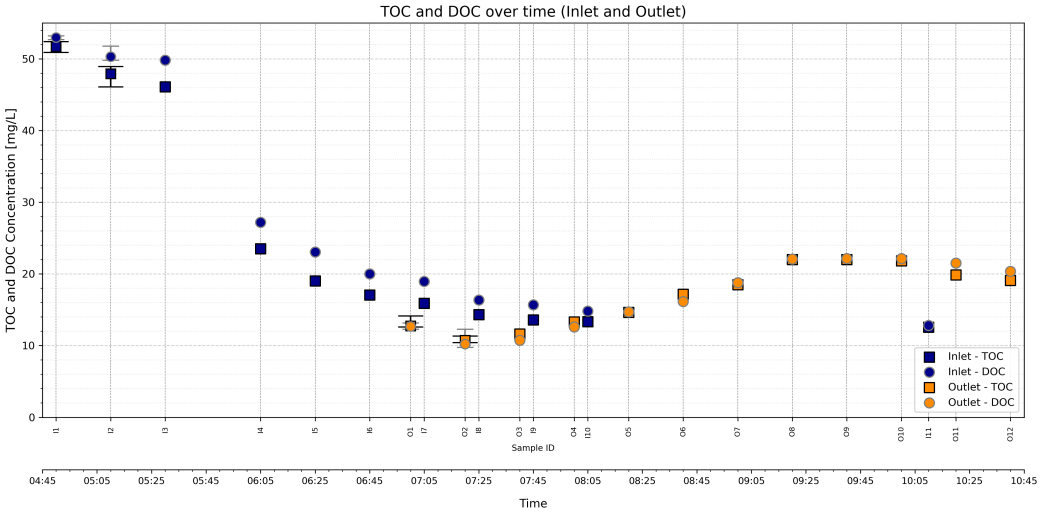

Figure 4.14: TOC and DOC in each sample from inlet (I1–I11) and outlet (O1–O12) over time. Triplicates of TOC and DOC were made for I1, I2, O1, O2, and mean value and error bars showing minimum and maximum values are shown for those samples. Rain event 2025-05-22.

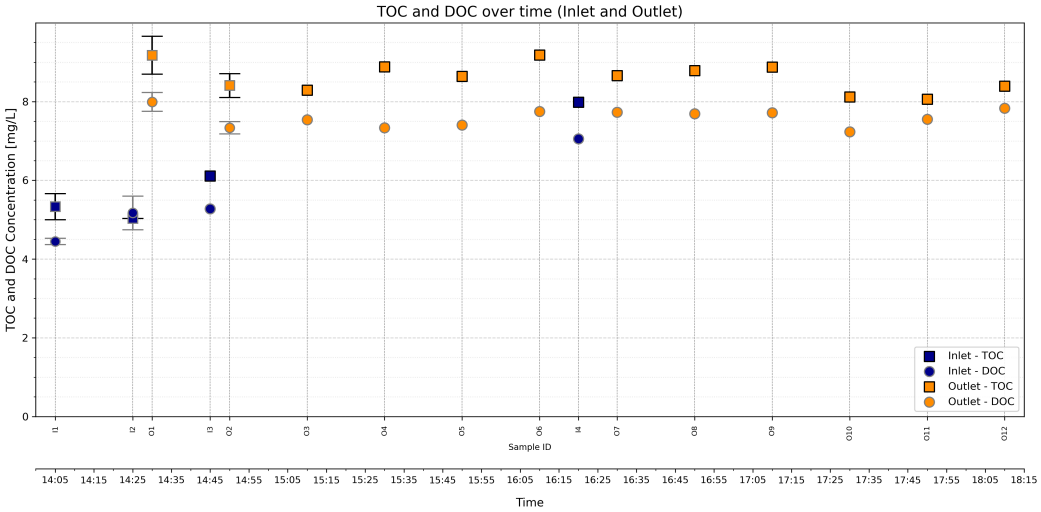

Figure 4.15: TOC and DOC in each sample from inlet (I1–I4) and outlet (O1–O12) over time. Duplicates of TOC and DOC were made for I1, I2, O1, O2, and a mean value and error bars showing minimum and maximum values are shown for those samples. Rain event 2025-05-26.

The EMC was calculated for the three rain events with regards to TOC and DOC, and can be seen in Table 4.2. The highest TOC and DOC concentrations are found for the second rain event followed by the first and lastly the third rain event.

The retention efficiency of the pond regarding DOC and TOC was calculated using EMC. The retention efficiency for the three rain events can be seen in Table 4.2. The retention efficiency varies drastically between the rain events. The highest retention efficiency is found for the first rain event, which had 46% retention efficiency for TOC and 57% for DOC. Retention of TOC and DOC also occurs for the second rain event but with around 50% less efficiency. The third rain event shows an increase in TOC and DOC from inlet to outlet, leading to negative retention values. The TOC increases with around 51% and the DOC with 47%.

Table 4.2: Event mean concentrations and retention efficiencies for rain events.

Rain event	**Event mean concentration (EMC) [mg/L]**				**Retention efficiency (%)**	
	TOC$_{in}$	**TOC**$_{out}$	**DOC**$_{in}$	**DOC**$_{out}$	**TOC**	**DOC**
1	16.26	8.77	19.17	8.26	46.10	56.90
2	22.32	17.18	24.07	17.24	23.04	28.35
3	5.71	8.62	5.15	7.58	-50.02	-47.22

4.1.6 TN and DN

As seen for TOC/DOC, also the TN/DN results (Figure 4.16, Figure 4.17 and Figure 4.18) showed higher dissolved concentrations than total for some samples. This was unexpected and is further discussed in section 5.1.4.

The pattern of TN and DN at the inlet is similar to that of TOC and DOC with a decreasing TN and DN with time for the first two rains and an increasing trend for the third rain event. The TN stops decreasing after some time, for rain 2025-05-02 it stops

decreasing after about 1 hour and for rain 2025-05-22 it stops decreasing after around 1 hour and 30 minutes. After the decrease in TN and DN, the values are rather stable for the remaining time of each rain event, with values around 0.9-1.2 [mg/L] for TN and 1.0-1.6 [mg/L] for DN.

At the inlet, TN and DN has a decreasing trend for both rain event 2025-05-02 and rain event 2025-05-22. For rain 2025-05-02, TN and DN concentrations decreased over time from 3.54 to 0.88 mg/L and 3.32 to 1.28, respectively. For rain 2025-05-22, the TN and DN levels decreased from 4.12 to 0.93 mg/L and 4.09 to 1.04 mg/L, respectively. Unlike the first two rain events, rain 2025-05-26 had an increasing trend of TN and DN concentrations over time, with TN increasing from 0.66 to 0.89 mg/L and DN increasing from 0.65 to 0.85 mg/L. The TN and DN levels at the inlet was lower for the third rain event (2025-05-26) than for the first two.

At the outlet, TN and DN concentrations were relativity constant, ranging from 0.35 to 0.33 mg/L and 0.29 to 0.32 mg/L, respectively, for rain 2025-05-02. On 2025-05-22, both TN and DN outlet levels were higher, ranging from 0.58 to 1.39 mg/L and 0.47 to 1.35 mg/L, respectively. On the 2025-05-26, TN and DN outlet values were similar to those from 2025-05-02, with TN ranging from 0.35 to 0.42 mg/L and DN from 0.44 to 0.50 mg/L, showing slight variation.

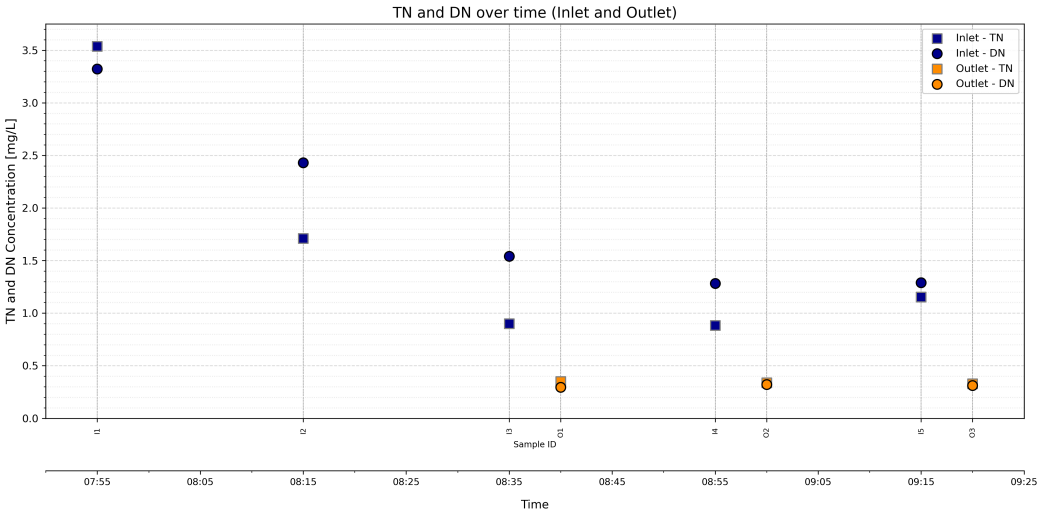

Figure 4.16: Total nitrogen (TN) and dissolved nitrogen (DN) in each sample from inlet (I1–I5) and outlet (O1–O3) over time. Rain event 2025-05-02.

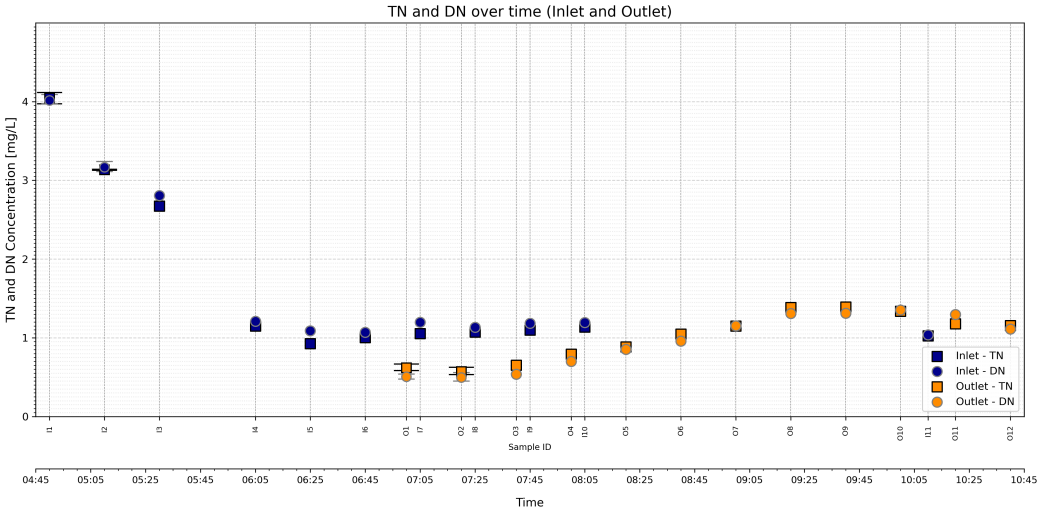

Figure 4.17: Total nitrogen (TN) and dissolved nitrogen (DN) in each sample from inlet (I1–I11) and outlet (O1–O12) over time. Triplicates of TN and DN were made for I1, I2, O1, O2, and mean value and error bars showing minimum and maximum values are shown for those samples. Rain event 2025-05-22.

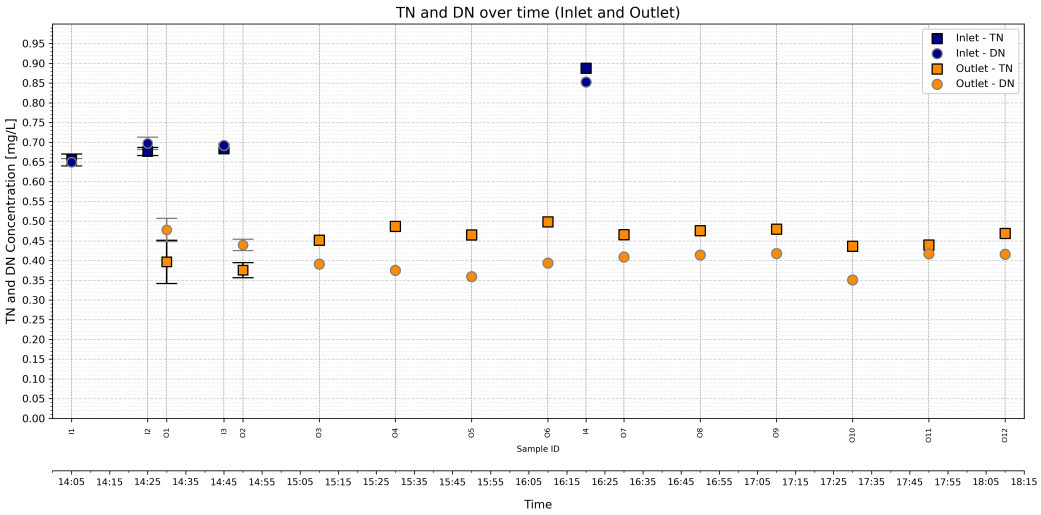

Figure 4.18: Total nitrogen (TN) and dissolved nitrogen (DN) in each sample from inlet (I1–I4) and outlet (O1–O12) over time. Duplicates of TN and DN were made for I1, I2, O1, O2, and a mean value and error bars showing minimum and maximum values are shown for those samples. Rain event 2025-05-26.

The EMC was calculated for the three rain events with regards to TN and DN, and can be seen in Table 4.3. The highest TN and DN concentrations in the inflow are found for the first rain event followed by the second and lastly the third rain event, while the highest TN and DN concentration in the outflow are found for the second rain even, followed by the third and lastly the first rain event.

The retention efficiency of the pond regarding DN and TN was calculated using EMC (see Table 4.3). The retention efficiency varies significantly between the rains. The highest retention of TN and DN is found for the first rain event. Rain event three had

higher retention efficiency than rain event two, but much lower retention efficiency than the first rain event.

Table 4.3: Event mean concentrations and retention efficiencies for rain events.

Rain event	Event mean concentration (EMC) [mg/L]				Retention efficiency (%)	
	TN_{in}	TN_{out}	DN_{in}	DN_{out}	TN	DN
1	1.80	0.34	2.17	0.31	81.19	85.65
2	1.33	1.03	1.33	0.99	22.55	25.83
3	0.70	0.47	0.70	0.39	33.47	43.84

4.1.7 TP

As can be seen by comparing Figure 4.19 to Figure 4.20 and 4.21, the pattern of TP is not the same for the rain event on 2025-05-02 and the rain events on 2025-05-22 and 2025-05-26. The first rain, 2025-05-02, has an increasing trend for the inlet, where the phosphorus is 0 at first and increases and reaches a maximum value of 0.6 mg/L. The inlet values for TP for rain 2025-05-22 decrease with time, although not steadily. The first sample's (I1) TP value (0.13 mg/L) is significantly higher than the last sample's (I11) TP value (0.01 mg/L), and the TP values from rain event 2025-05-26 have a similar trend although with lower TP values.

The outlet samples do not show any trends or patterns for the first rain, which can be expected since there are only three outlet samples for that rain event, see Figure 4.19, and the values at the outlet range from 0.03 to 0.07 mg/L. The concentration of phosphorus at the outlet is roughly in the same size-range as for the last three inlet samples, I3, I4 and I5. The outlet samples from the second rain (2025-05-22) indicates a slightly increasing trend, although not steadily, see Figure 4.20. The outlet TP values for the second rain ranges from 0-0.06 mg/L, and are rather similar to the inlet concentrations with the exception of I1. The outlet TP concentrations from the samples yielded by rain event 2025-05-26 show no trend and are in the same size range as the TP in the inflow, see Figure 4.21, ranging from 0 to 0.05 mg/L.

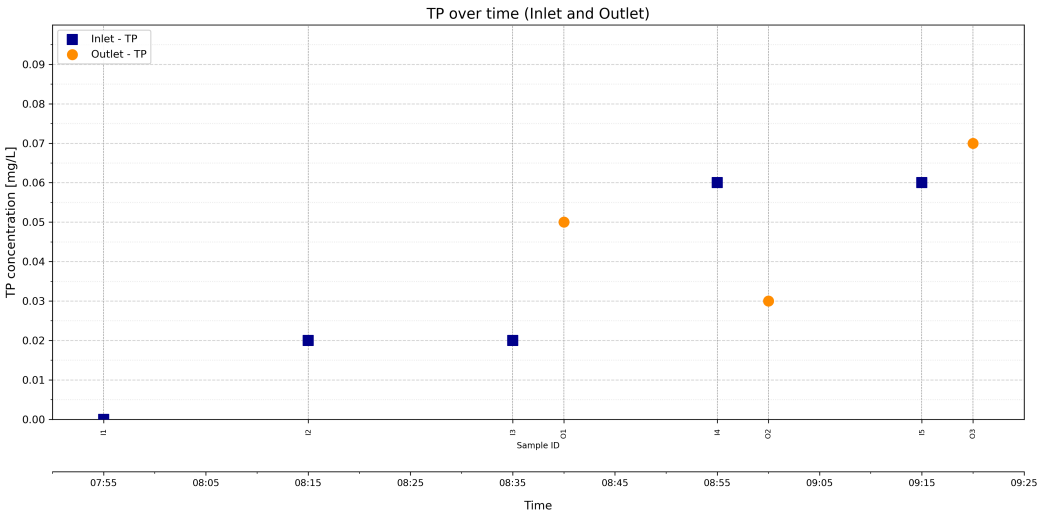

Figure 4.19: Total phosphorous in each sample from inlet (I1–I5) and outlet (O1–O3) over time. Rain event 2025-05-02.

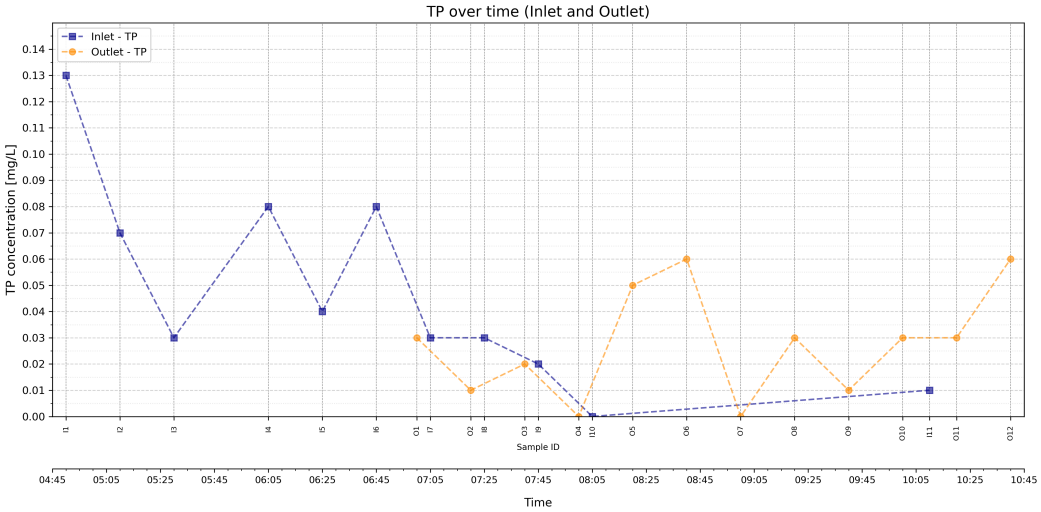

Figure 4.20: Total phosphorous in each sample from inlet (I1–I11) and outlet (O1–O12) over time. Rain event 2025-05-22.

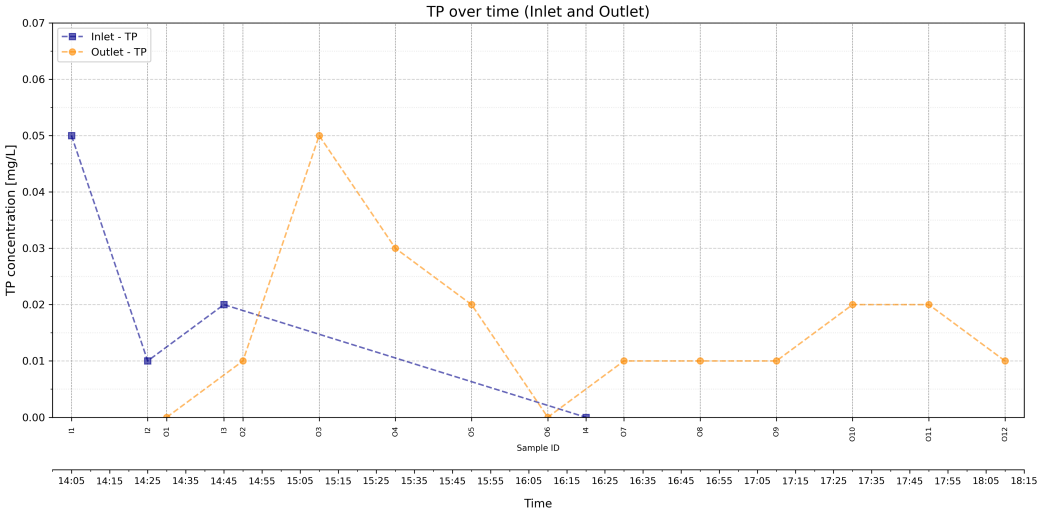

Figure 4.21: Total phosphorous in each sample from inlet (I1–I4) and outlet (O1–O12) over time. Rain event 2025-05-26

The EMC was calculated for the three rain events with regards to TP, and can be seen in Table 4.4. The highest EMC in the outlet was for rain event 1, while the highest EMC in the inlet was for rain event 2.

The retention efficiency of the pond regarding TP was calculated using EMC and can be seen in Table 4.4. The largest retention efficiency of TP is found for rain event two, followed by rain event three. The first rain event has an increase of TP from inlet to outlet meaning that there is a release of 150% more TP in the outlet compared the inlet.

Table 4.4: Event mean concentrations and retention efficiencies for rain events.

Rain event	Event mean concentration (EMC) [mg/L]		Retention efficiency (%)
	$\mathbf{TP}_{in}$	$\mathbf{TP}_{out}$	
1	0.02	0.050	-150
2	0.055	0.028	49.29
3	0.027	0.016	39.31

4.1.8 Metals

Dissolved metal concentration were only analyzed for rain event 2025-05-02 due to time constraints. As can be seen in Table 4.5, the dissolved metals Al, Cr, Mn, and Co clearly decrease in the pond, from inlet to outlet, whereas Ti, Mo, and Ba increase from inlet to outlet. The other metals have more similar dissolved metal concentrations between inlet and outlet. Some dissolved metals like Fe, Ni, Cu, Sb and Pb, while mostly having similar values between inlet and outlet, have a significant higher inlet value for the first one or two samples. Results for Na, K and Ca are excluded from Table 4.5 due to values far outside the reliable calibration range of the ICP-MS.

Table 4.5: Dissolved metal concentration in [μg/L] for the five inlet samples (I1-I5) and three outlet samples (O1-03) from rain event 2025-05-02

Metals	I1	I2	I3	I4	I5	O1	O2	O3
Mg	2104.06	1196.97	883.63	786.72	971.63	Outside reliable range	Outside reliable range	Outside reliable range
Al	103.87	115.84	301.53	90.91	111.6	78.75	81.95	88.98
Ti	34.61	25.15	17.16	15.22	18.84	51.76	97.03	95.47
V	2.7	2.79	2.46	2.15	2.1	2.56	3.12	3.13
Cr	1.24	1.12	0.91	0.89	0.9	0.18	0.22	0.24
Mn	84.88	58.07	46.95	48	45.64	22.53	25.42	26.48
Fe	214.73	234.96	163.34	126.05	170.21	144.72	156.92	143.01
Co	0.73	0.65	0.5	0.71	0.5	0.11	0.1	0.11
Ni	3.14	2.42	1.8	1.49	1.54	1.65	1.75	1.72
Cu	14.52	11.78	7.5	6.57	7.56	7.98	5.82	5.43
Zn	185.46	159.72	97.59	99.6	95.47	12.09	11.79	12.67
Mo	0.94	0.62	0.47	0.41	0.43	1.35	1.67	1.52
Cd	0.04	0.02	0.01	0.02	0.02	0.02	0.03	0.02
Sb	1.51	0.91	0.77	0.6	0.7	0.72	0.88	0.84
Ba	10.19	7.7	4.3	3.93	5.05	35.64	41.52	40.18
Pb	0.23	0.22	0.15	0.13	0.18	0.14	0.15	0.15

The event mean concentration was calculated for all metals (see Table 4.6) except Mg since there were no outlet values for Mg within the calibration range.

The retention efficiencies for the dissolved metals (Table 4.6) show high retention efficiency for Co, Cr and Zn, whereas Cd, Sb, Pb, Fe, Ni, Cu, Al, and Mn have low to moderate retentions efficiency. The other metals, Ti, V, Mo and Ba have negative retention, i.e. there is no retention and the concentration at outlet is larger than at inlet. Ba, Ti and Mo increased the most from inlet to outlet.

Table 4.6: Event mean concentrations and retention efficiencies for rain events.

Dissolved metals	**Event mean concentration (EMC) [mg/L]**		**Retention efficiency (%)**
	In	**Out**	
Al	169.69	83.77	50.63
Ti	23.43	85.75	-265.98
V	2.54	2.99	-17.80
Cr	1.042	0.22	79.09
Mn	59.71	25.12	57.92
Fe	188.17	148.94	20.85
Co	0.62	0.11	83.02
Ni	2.24	1.72	23.55
Cu	10.21	6.19	39.40
Zn	135.20	12.18	90.99
Mo	0.62	1.54	-148.42
Cd	0.022	0.02	9.55
Sb	0.97	0.83	15.00
Ba	6.61	39.64	-498.78
Pb	0.19	0.15	20.44

4.2 Hydrodynamic Modeling

Hydrodynamic modeling was done for 6 scenarios, 3 with constant inflow and 3 based on real recorded rain events. The details of the various scenarios can be found in Table 3.6.

4.2.1 Scenario 1 - Basecase

The water level in Kryddvägen pond is represented by the simulation output "surface elevation". The mean surface elevation (see Figure 4.22) increases up to 63.84 m.a.s.l. After almost 2 hours of simulation time the water level starts to flatten out, and reaches steady state conditions after about 4 hours simulation time. Therefore, the results presented below are for the last timestep.

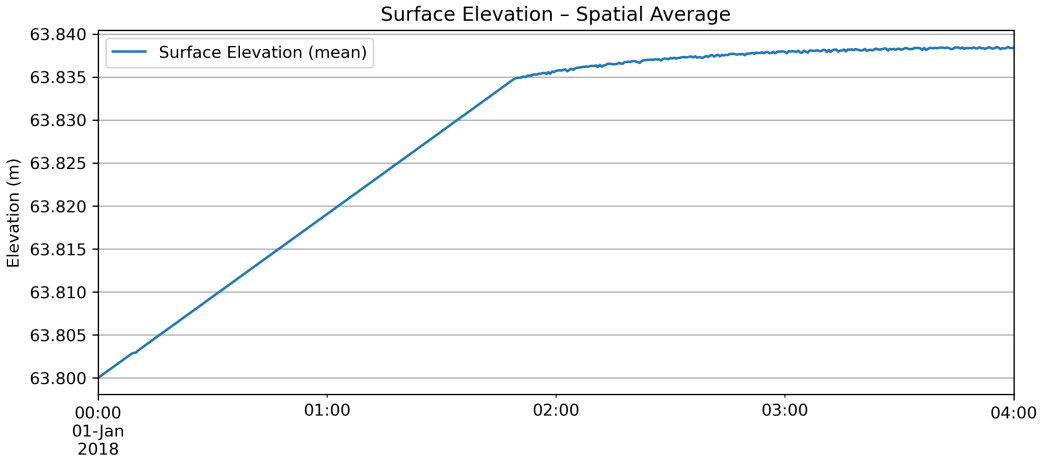

Figure 4.22: Average surface elevation in the pond.

To assess the velocities close to the outlet, three points with same x and y location (see Figure 4.23) were monitored at different depths: one point at the top of the pond (63.8 m.a.s.l), one at mid depth (63.5 m.a.s.l) and one at the bottom (63.2 m.a.s.l).

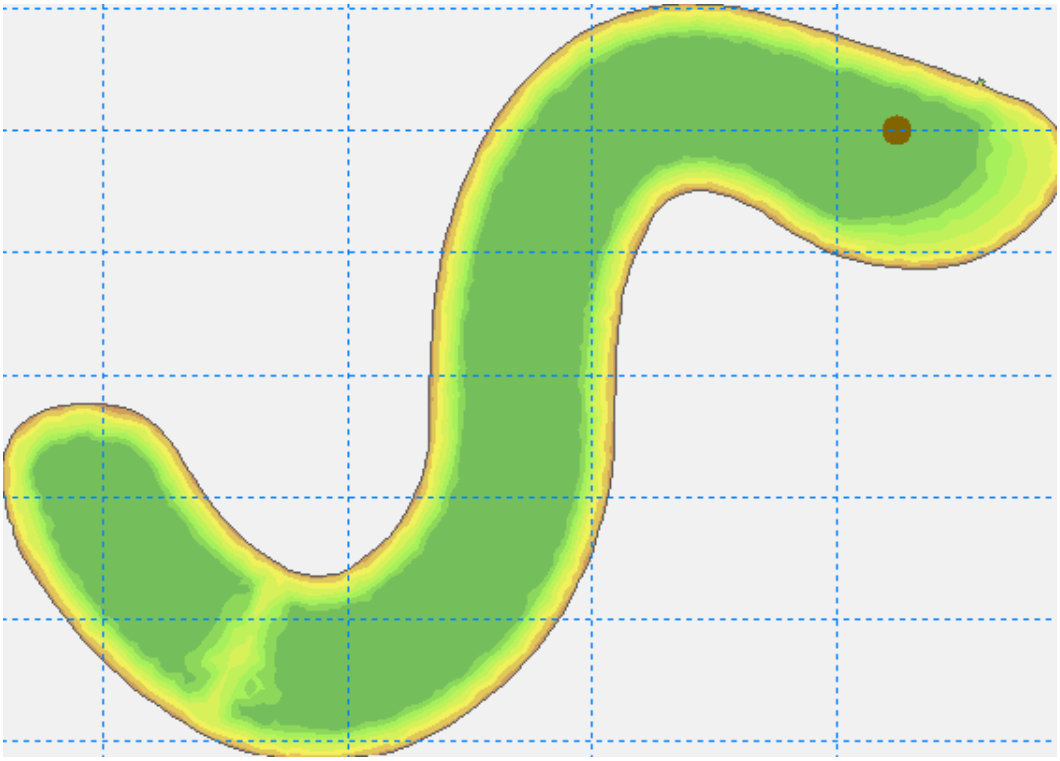

Figure 4.23: Location of three points for analysis. All the points have same x and y position but exist at different depths.

As can be seen in Table 4.7 the velocities in the pond, near the outlet, at the last timestep when the simulation has reached steady state, are very low. Table 4.7 shows that the speed is largest in the top point followed closely by the middle point. The lowest speed is found in the bottom point.

Table 4.7: Velocity values at the last time step in different point depths (see Figure 4.23) for Scenario 1 in m/s.

Point	Speed
Top	0.002
Middle	0.002
Bottom	0.001

A volume series output was also produced from which velocities and velocity patterns throughout the entire pond were analyzed. At the final time step of the simulation — when steady state is reached — the velocity distribution across the mesh's sigma layers 1, 3, 6 and 8 is shown in Figure 4.24. The flow path is clearly visible, with dominant velocities in the range of 0.004–0.005 m/s. Areas with near-zero velocity are observed along the pond bed and near most shorelines, indicating zones of minimal mixing or stagnation. A notable circulation zone is present directly in front of the inlet, with its extent limited by the 40 cm internal barrier.

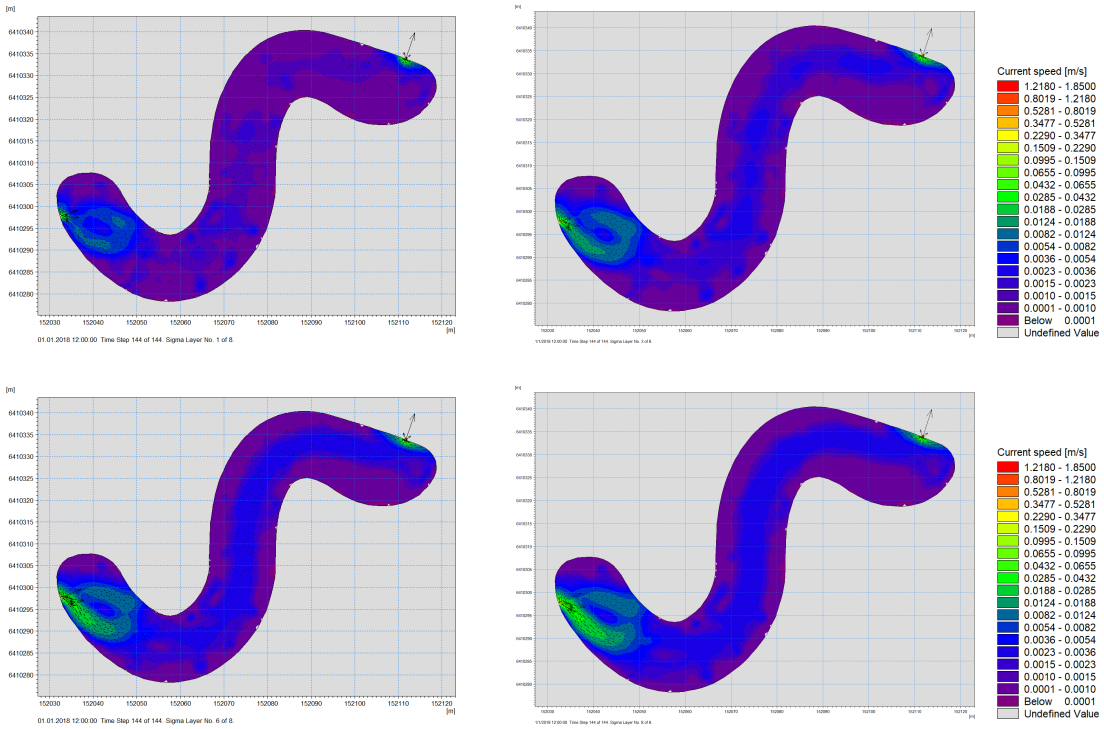

Figure 4.24: Velocity distribution in Scenario 1 across layers 1 (top left image), 3 (top right image), 6 (bottom left image) and 8 (bottom right image), representing surfaces from near-bed (layer 1) to near-surface (layer 8).

In Scenario 1 with 10 L/s there is generally low mean velocity in the pond across all layers (0.002 – 0.005 m/s). As can be seen in Table 4.8, the maximum speed reached in the named layers during the simulation is 0.446 m/s in layer 1 and can likely be localized near the inlet or outlet but do not dominate overall behavior (see Figure 4.24).

Table 4.8: Velocity values for Scenario 1 at at the last time step in m/s.

Layer	Min Speed	Max Speed	Mean Speed
1	2e-06	0.447	0.005
3	3e-06	0.041	0.002
6	2e-06	0.019	0.002
8	0	0.242	0.004

4.2.2 Scenario 2 - Basecase with windforcing

As shown in Figure 4.25, the mean surface elevation rises to approximately 63.84 m.a.s.l. The increase slows significantly after 2 hours and reaches steady state after about 4 hours. The results below are based on the final timestep.

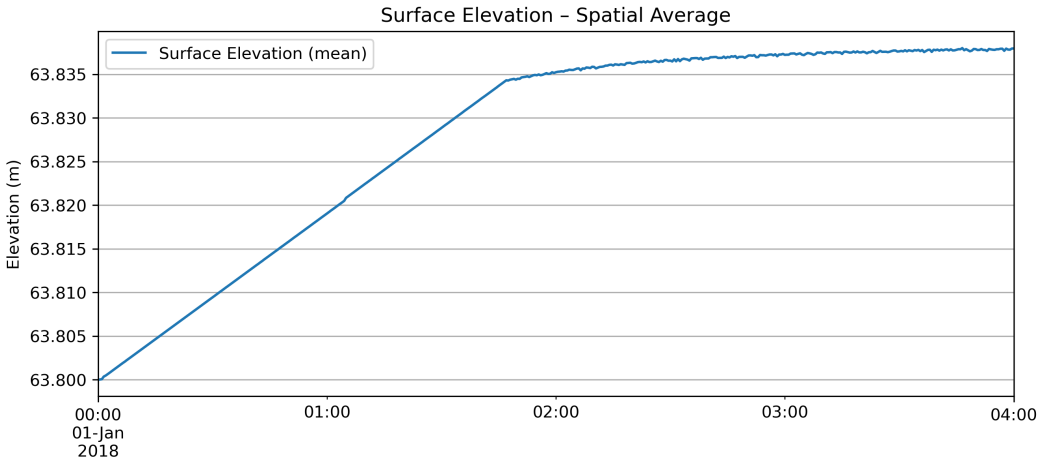

Figure 4.25: Average surface elevation in the pond, Scenario 2

As for Scenario 1, the velocities in three points near the outlet (see Figure 4.23), the Table 4.9 shows that the highest speed can be found in the top point, followed by the bottom point and lastly the middle point. Compared to Scenario 1, the speed in the top point increased with a factor of about 26, while the speed in the middle point increased with a factor of around 7 and the bottom point with a factor of around 24.

Table 4.9: Velocity values at the last time step in different point depths (see Figure 4.23) for Scenario 2 in m/s.

Point	Speed
Top	0.036
Middle	0.011
Bottom	0.023

A volume series was analyzed with regard to velocities and velocity patterns in the pond and these were compared to the velocities and velocity patterns of Scenario 1. The ve-

locity pattern under wind influence is shown in Figure 4.26. In layer 8, the surface layer, wind-driven flow is dominant, with vectors indicating a strong west-to-east direction. Compared to Scenario 1, overall flow velocities are slightly higher, with values predominantly in the range of 0.043–0.066 m/s. A circulation area is also observed in front of the outlet, most pronounced in layer 6. While near-zero velocities are still evident in the pond center and along the shores, these stagnation zones are less extensive than in the windless case. Interestingly, in layer 1, there is a visible reverse flow from the outlet back toward the inlet, likely induced by wind-driven recirculation dynamics.

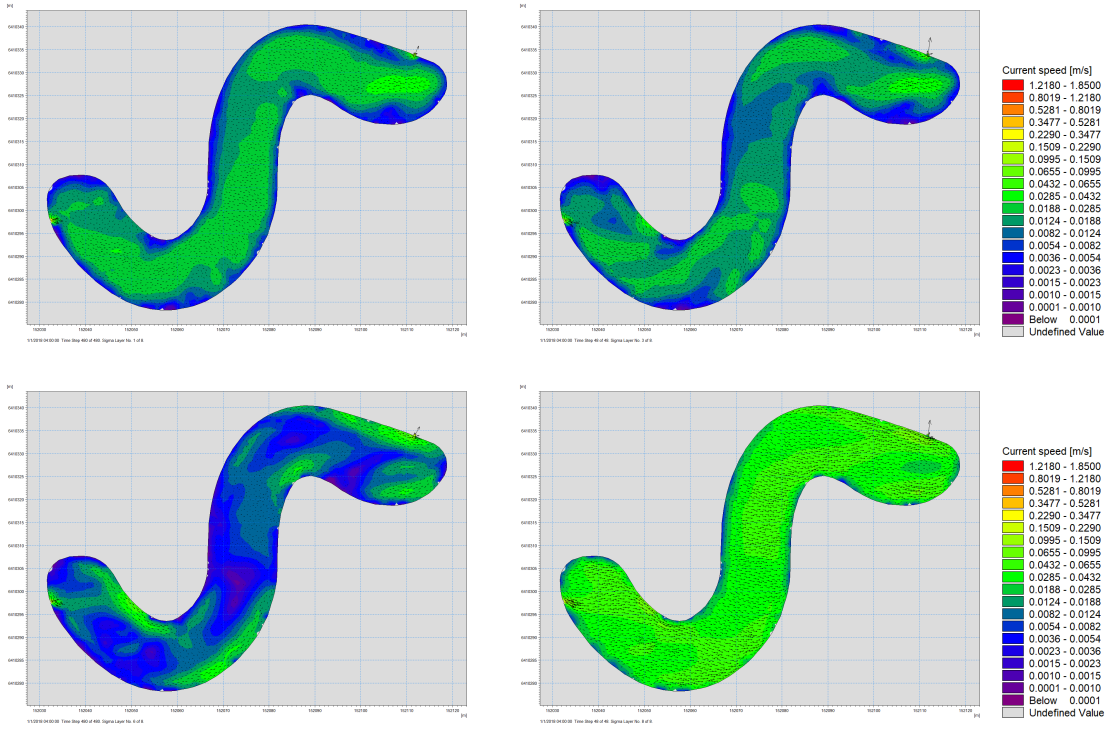

Figure 4.26: Velocity distribution in Scenario 2 across layers 1 (top left image), 3 (top right image), 6 (bottom left image) and 8 (bottom right image), representing surfaces from near-bed (layer 1) to near-surface (layer 8).

The mean velocities displayed in Table 4.10 increase significantly in all layers (0.018–0.019 m/s). This indicates that compared to Scenario 1 wind enhances mixing, especially at the surface (layer 8) and upper-middle layers. Minimum speeds remain low, indicating persistent quiescent zones.

Table 4.10: Velocity values for Scenario 2 at at the last time step in m/s.

Layer	Min Speed	Max Speed	Mean Speed
1	1.97e-04	0.438	0.019
3	2.09e-04	0.069	0.018
6	5.3e-05	0.076	0.018
8	1.81e-04	0.236	0.018

4.2.3 Scenario 3 - 20 year rain event

Similarly to Scenarios 1 and 2, an area series, a series of points near the outlet (see Figure 4.23) and a volume series were analyzed. From the area series the mean surface elevation was extracted at the last time step and in Figure 4.27 it is observable that the mean surface elevation stabilizes and reaches steady state at around 64.17 m.a.s.l. after 4 hours.

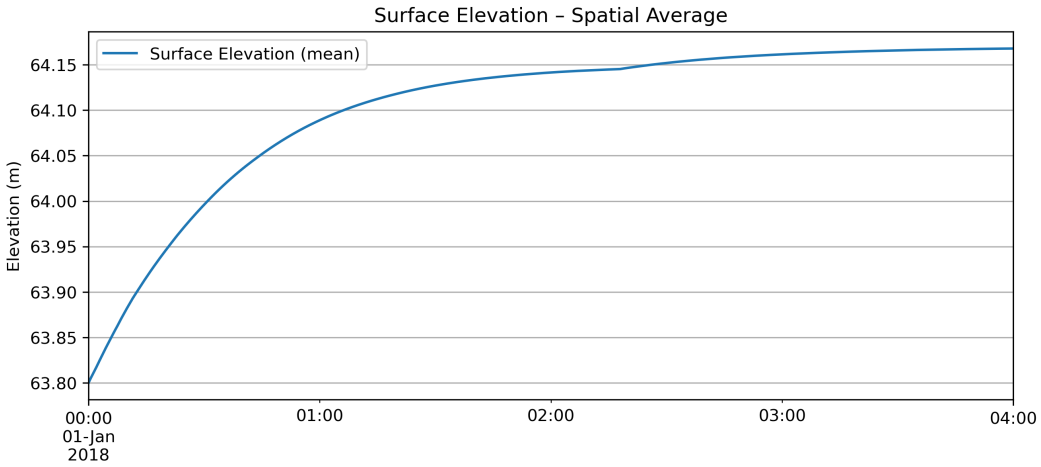

Figure 4.27: Average surface elevation in the pond, Scenario 3

When comparing Table 4.11 to Table 4.7, it is clear the speed at the last time step at the chosen points (see Figure 4.23) are significantly higher in Scenario 3 which has much larger inflow, than Scenario 1. The speed in the top and middle point increased by a factor of around 20 and the speed in the bottom point increased by a factor of around 25. Comparing Scenario 2 and 3, it is found that the speed in the top point and in the bottom point are very similar and that the middle point speed is a factor of almost 3 higher.

Table 4.11: Velocity values at the last time step in different point depths (see Figure 4.23) for Scenario 3 in m/s.

Point	Speed
Top	0.035
Middle	0.034
Bottom	0.024

For Scenario 3, just as for the previous scenarios, a volume series output file was analyzed with regard to velocities and velocity patterns. Figure 4.28 shows the final velocity pattern for high inflow conditions. The increased discharge significantly alters the hydrodynamics compared to the lower inflow scenarios.

The primary flow path is clearly delineated by elevated velocities (0.043–0.066 m/s) in the main channel. Peak velocities reach 1.12–1.85 m/s and occur directly at the inlet and outlet, shown in red. A well-defined circulation zone develops in front of the inlet, extending from shore to shore and bounded by the submerged barrier. Outside the main flow path, areas with low velocity persist, especially near the outlet and along the left

pond perimeter.

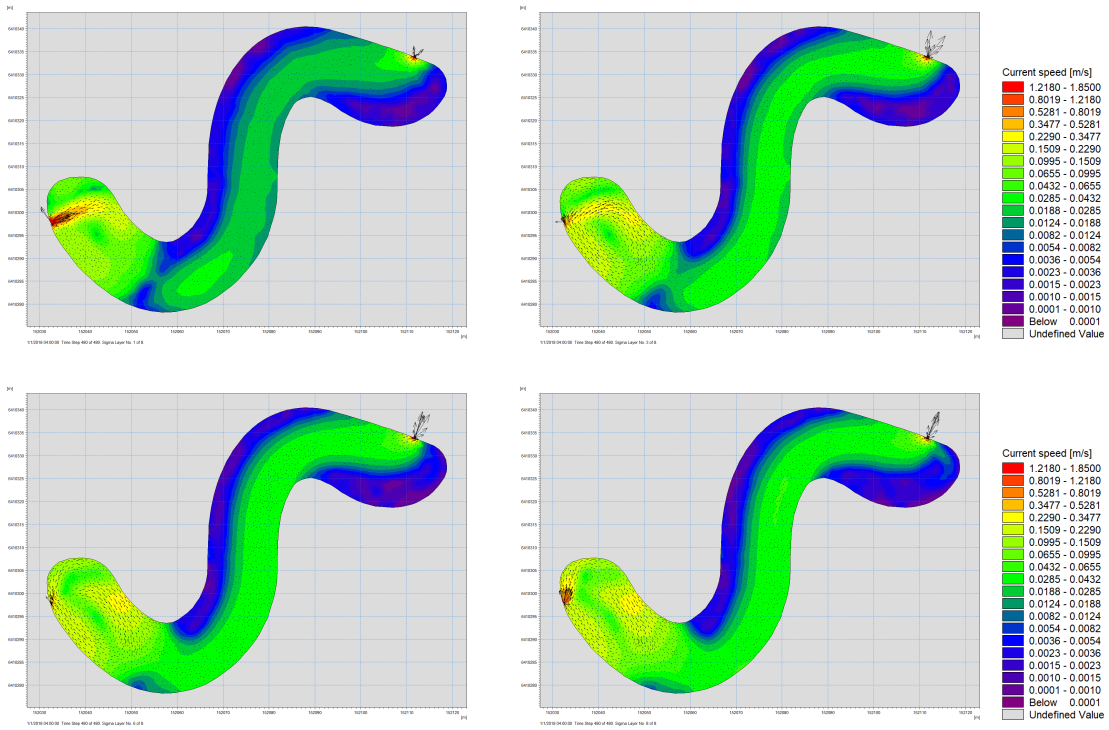

Figure 4.28: Velocity distribution in Scenario 3 across layers 1 (top left image), 3 (top right image), 6 (bottom left image) and 8 (bottom right image), representing surfaces from near-bed (layer 1) to near-surface (layer 8).

In Table 4.12 the displayed mean velocities are much higher (up to 0.080 m/s in layer 1), with max speeds reaching 5.7 m/s (likely at inlet and outlet). There is significant velocity across all layers due to high inflow rates, except for in the low flow zones with min velocities between 6.9e-05 and 5.4e-04 m/s.

Table 4.12: Velocity values for Scenario 3 at at the last time step in m/s.

Layer	Min Speed	Max Speed	Mean Speed
1	6.9e-05	5.714	0.079
3	1.02e-04	0.254	0.029
6	5.4e-04	0.853	0.035
8	1.6e-04	2.439	0.067

4.2.4 Scenario 4 - Rain of the 2025-05-02

In Figure 4.29 the rain intensity of the rain event is illustrated alongside the corresponding inflow into Kryddvägen pond. It can be seen that the flow data follow the trend of the rain intensity with two peaks, up to 50 L/s and 63.8 L/s at 08:00 and 08:40 at the inlet. At the outlet the outflow sets in with 2 L/s at 08:45 and peaks with 14.7 L/s at 10:35.

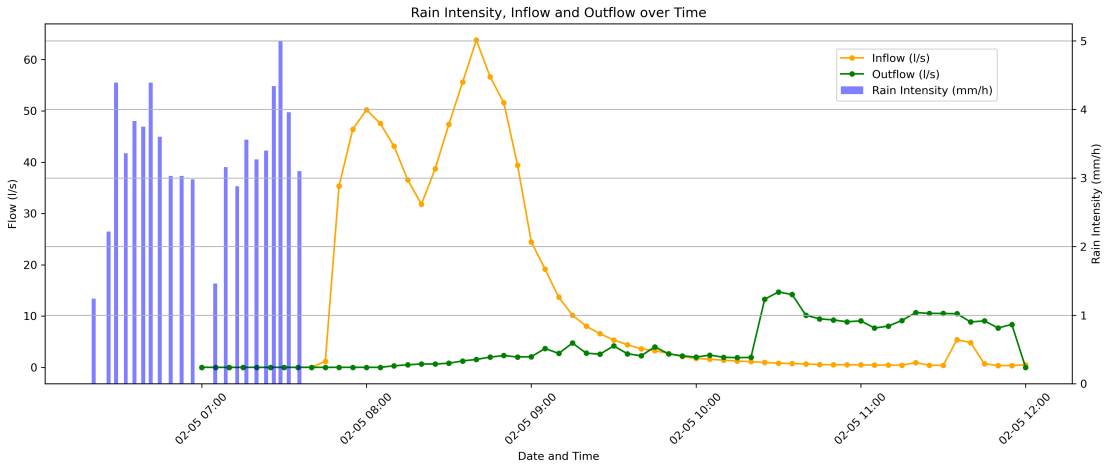

Figure 4.29: Measured in- and outflow to the pond over time (left-hand side y-axis) and measured rain intensity (right-hand side y-axis) for rain event on 2025-05-02.

The mean simulated surface elevation showed only slight variance in elevation and remains approximately at 63.799 m.a.s.l. (Figure 4.30).

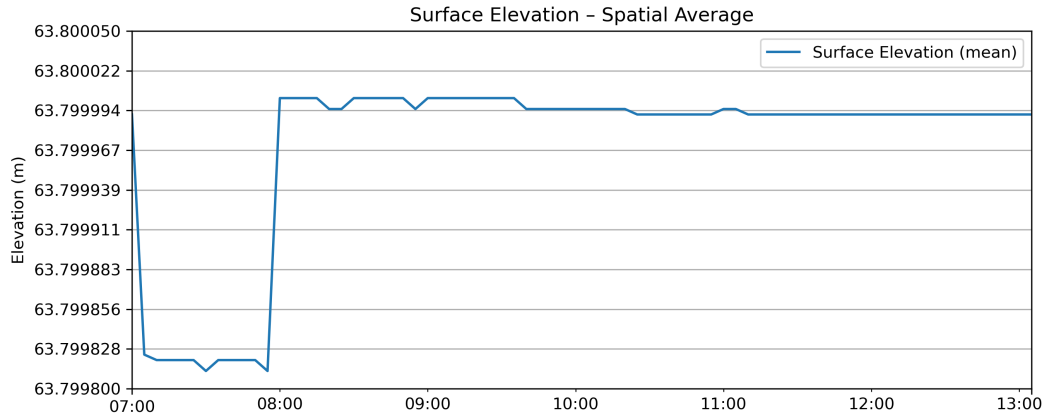

Figure 4.30: Average surface elevation in the pond, Scenario 4.

Similarly to the other scenarios, a series of points were analyzed near the outlet (see Figure 4.23). When comparing Table 4.13 to the corresponding tables in Scenario 1-3, it is evident that the mean and maximum speeds in the chosen points (see Figure 4.23) for Scenario 4 are very similar to the speeds found for the last timestep for Scenario 2 which was the base-case of constant inflow of 10 L/s with the addition of a west wind of 7 m/s.

Table 4.13: Velocity values throughout the whole simulation in different point depths (see Figure 4.23) for Scenario 4 in [m/s].

Point	Min	Mean	Max
Top	0	0.040	0.060
Middle	0	0.008	0.014
Bottom	0	0.019	0.030

The Figure 4.31 presents the velocity distribution in layer 1 and 6 (based on volume series output file) during the peak inflow of the rain event, where inflow rates reached up to 63.81 L/s. Despite elevated inflow, velocities in both the inlet and outlet remained low (0.001–0.004 m/s). A dry cell is present directly at the outlet, which may suggest that discharge had not commenced in the simulation—contrary to the measurements——pointing to discrepancies between the simulated and actual initial pond volume.

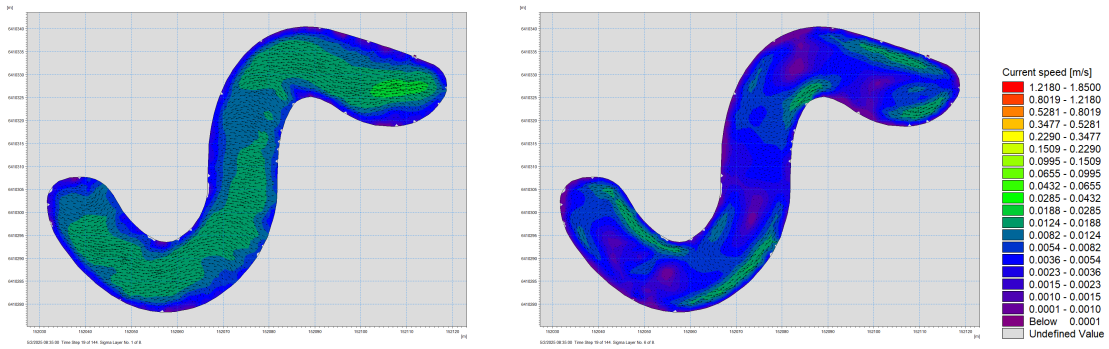

Figure 4.31: Velocity distribution in Scenario 4 at 08:35 (time step 19) across layer 1 (left) and 6 (right).

Later in the event and during low flow conditions (3-5 L/s), at time step 54 (11:30) the wind's influence became dominant (up to 9.7 m/s from west) and caused velocity values up to 0.067 m/s at higher layers (7 and 8), significantly shaping the surface hydrodynamics. Figure 4.32 illustrates the hydrodynamic conditions in layer 6, where a well-defined circulation pattern is highlighted, less disturbed by surface wind and more representative of the pond's geometry-driven flow. Layer 1 shows a change in flow direction, indicative of internal recirculation.

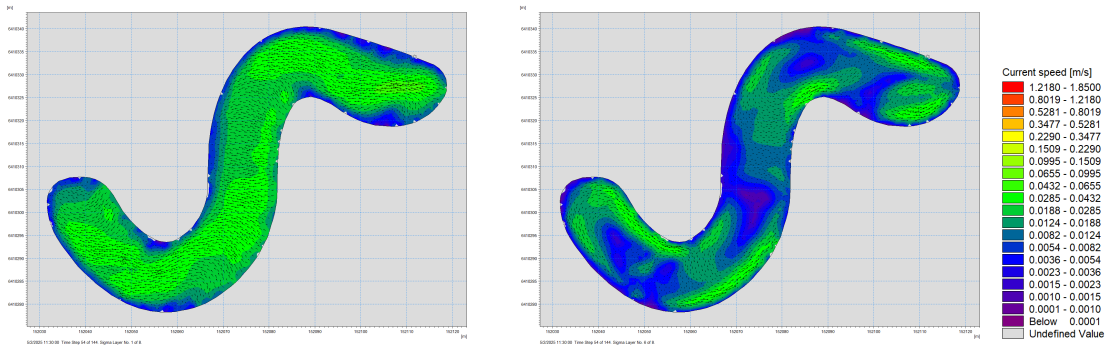

Figure 4.32: Velocity distribution in Scenario 4 at 11:30 (time step 54) across layer 1 and 6

In Table 4.14 the mean velocities remain moderate (0.011 m/s), even under max inflow (63 L/s). Outlet was inactive. Between time step 19 and 54 the max and mean speed almost double, likely corresponding to increased wind force.

Table 4.14: Velocity values for Scenario 4 at the time steps 19 and 54 in m/s.

Time Step / Time	Layer	Min Speed	Max Speed	Mean Speed
19 / 08:35	1	7.025e-05	0.044	0.010
19 / 08:35	3	1.613e-04	0.044	0.011
19 / 08:35	6	5.152e-05	0.049	0.011
19 / 08:35	8	5.207e-12	0.043	0.011
54 / 11:30	1	8.744e-05	0.010	0.023
54 / 11:30	3	2.672e-04	0.098	0.025
54 / 11:30	6	1.197e-04	0.103	0.025
54 / 11:30	8	3.711e-04	0.095	0.024

4.2.5 Scenario 5 - Rain of the 2025-05-22

In Figure 4.33 the rain intensity of the rain event is illustrated alongside the corresponding inflow into Kryddvägen pond. It can be seen that the flow data follow the trend of the rain intensity. The highest intensity peaks in 68 mm/h, followed by an inflow of 67.60 L/s into the pond.

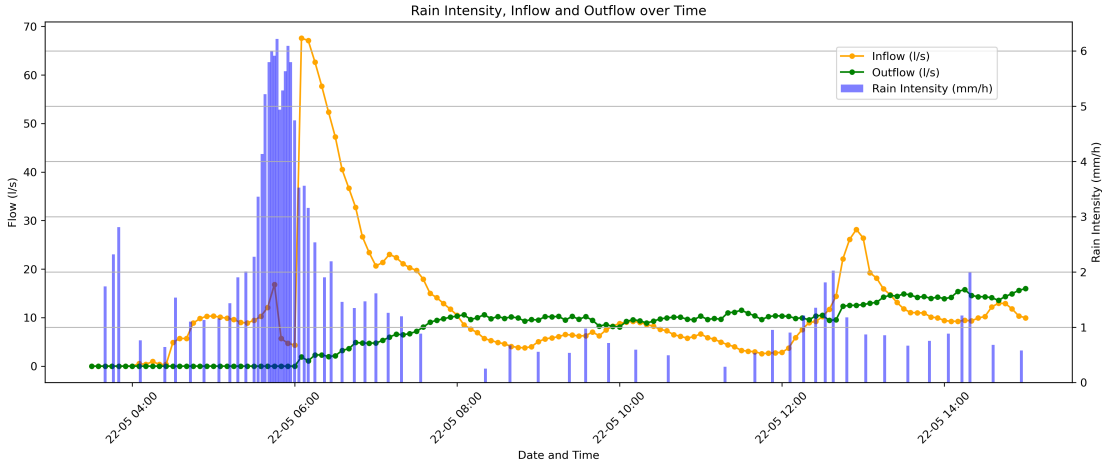

Figure 4.33: Measured in- and outflow to the pond over time (left-hand side y-axis) and measured rain intensity (right-hand side y-axis) for rain event on 2025-05-22.

The mean surface elevation for Scenario 5 (Figure 4.34) seems to follow the inflow curve seen in Figure 4.33 to some extent and with some delay. The maximum mean surface elevation is 63.8 m.a.s.l..

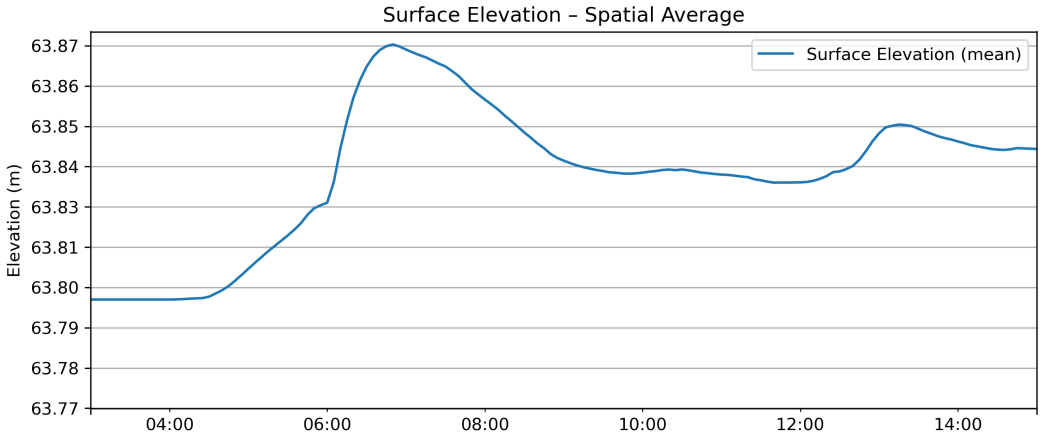

Figure 4.34: Average surface elevation in the pond, Scenario 5

The point series for Scenario 5 (see Table 4.15) reveals that the speed in specific points close to the outlet (see Figure 4.23) are rather similar to the speeds found in Scenario 4 (Table 4.13) and Scenario 2 (Table 4.9).

Table 4.15: Velocity values throughout the whole simulation in different point depths (see Figure 4.23) for Scenario 5 in [m/s].

Point	Min	Mean	Max
Top	0	0.025	0.034
Middle	0	0.015	0.022
Bottom	0	0.020	0.025

Volume series (4.35) at different layers show that at time step 38 (06:10) of the simulation, the system experienced peak inflows between 67.60 and 62.64 L/s. Velocities at the inlet in layers 6 to 8 ranged from 0.64 to 0.84 m/s, with even higher values (up to 1.32 m/s) recorded in intermediate layers (2 and 3). The vertical section through the inlet, on the other hand, only shows the maximum velocities in the upper layers higher up the inlet. These discrepancies could be attributed to the scaling of the visualization or the numerical dispersion in the layer-by-layer velocities.

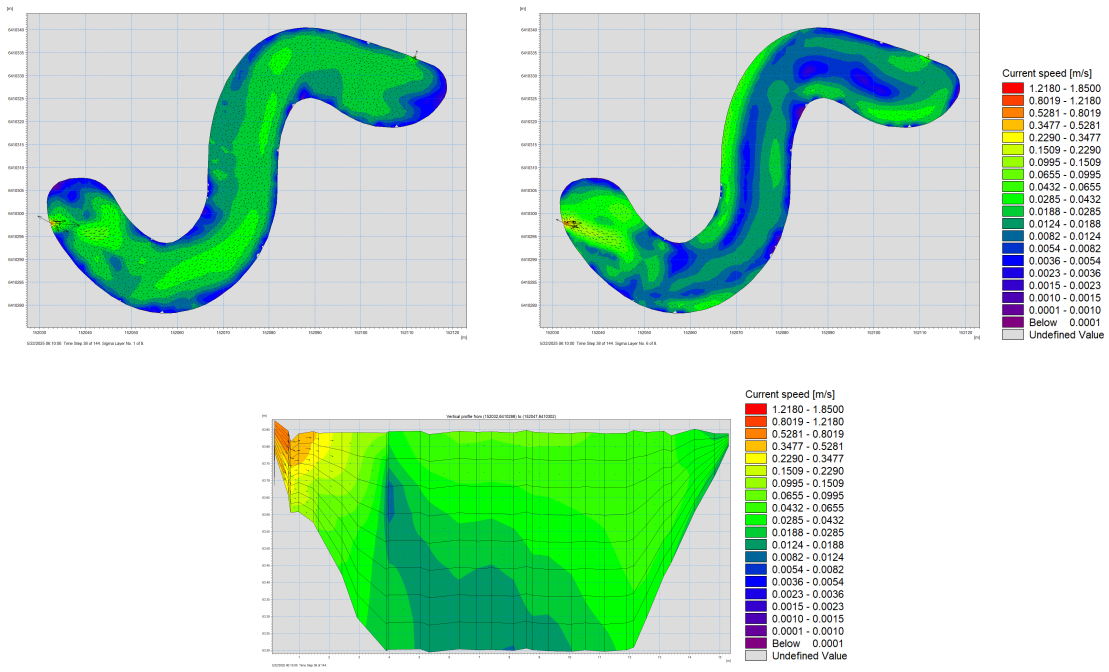

Figure 4.35: Velocity pattern in Scenario 5 at 06:10 (time step 38) across layer 1 and 6 and vertical cut through inlet.

Later in the event, at time step 103 (11:35), the system had stabilized to low flow conditions with inflow between 2.58 and 3.24 L/s. The corresponding Figure 4.36 shows very low velocities throughout the pond: 0.03–0.01 m/s at the inlet, and 0.022–0.018 m/s at the outlet. Circulation zones persist in front of both the inlet and outlet, while near-zero velocities occur along the shores.

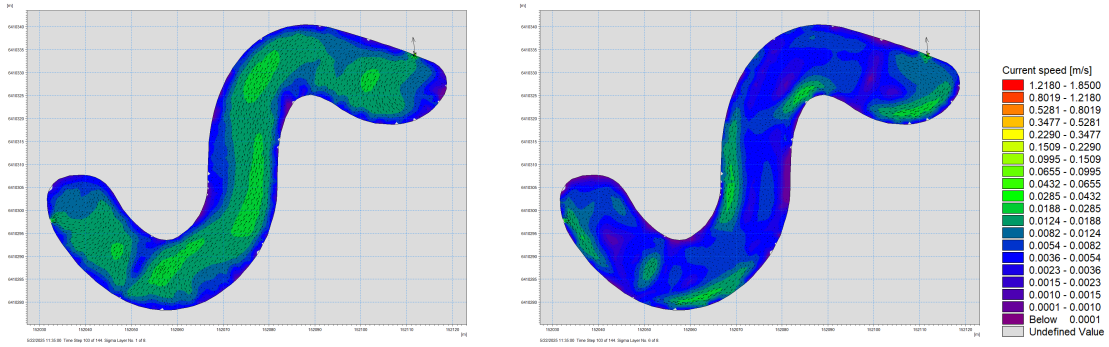

Figure 4.36: Velocity distribution in Scenario 5 at 11:35 (time step 103) across layer 1 and 6.

Table 4.16 lists the velocity statistics at two time steps. During time step 38 there are higher mean velocities in all layers (0.021–0.033 m/s), with local spikes above 2 m/s, compared to time step 103. There, the system returns to very low mean speeds (0.011–0.013 m/s).

Table 4.16: Velocity values for Scenario 5 at the time steps 38 and 103 in m/s.

Time Step / Time	Layer	Min Speed	Max Speed	Mean Speed
38 / 06:10	1	0	2.133	0.033
38 / 06:10	3	1.29e-04	0.095	0.021
38 / 06:10	6	2.9e-05	0.103	0.021
38 / 06:10	8	7.0e-05	0.246	0.023
103 / 11:35	1	0	0.050	0.011
103 / 11:35	3	4.4e-05	0.050	0.013
103 / 11:35	6	3.3e-05	0.052	0.013
103 / 11:35	8	1.08e-4	0.190	0.013

4.2.6 Scenario 6 - Rain of the 2025-05-26

The mean surface elevation for Scenario 6 (seen in Figure 4.38) seem to follow the inflow curve seen in Figure 4.37 to some extent and with some delay. As can be seen, there is high rain intensity in the beginning which corresponds to the fast increase of surface elevation in the beginning.

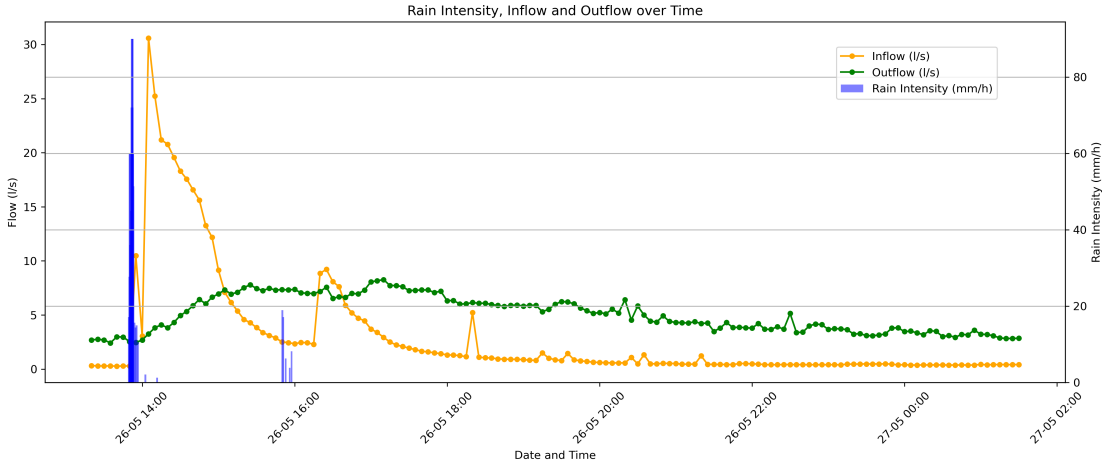

Figure 4.37: Measured in- and outflow to the pond over time (left-hand side y-axis) and measured rain intensity (right-hand side y-axis) for rain event on 2025-05-26.

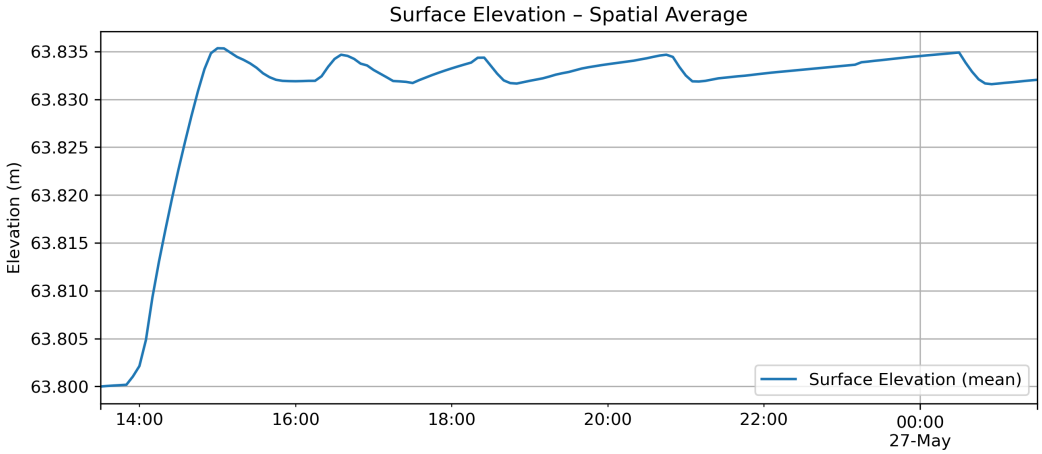

Figure 4.38: Average surface elevation in the pond, Scenario 6

The point series for Scenario 6 (see Table 4.17) reveals that the speed for the points close to the outlet (see Figure 4.23) is slightly lower, around a factor of 1.5–2.5 lower, for Scenario 6 compared to Scenario 4 and 5, depending on depth of point. It is also visible that the top point has the highest speed followed by the bottom point and lastly the middle point, which also was observed for Scenario 2, 4 and 5.

Table 4.17: Velocity values throughout the whole simulation in different point depths (see Figure 4.23) for Scenario 6 in [m/s].

Point	Min	Mean	Max
Top	0	0.016	0.023
Middle	0	0.004	0.008
Bottom	0	0.009	0.013

Scenario 6 was analyzed using volume output data at two representative time steps: shortly after peak inflow (time step 10) and near the end of the simulation (time step 142). At time step 10 (14:20) just after peak inflow of 30.59 L/s, there formed a circulation zone between inlet and barrier, as seen in the scenarios before. The flow velocities at the banks and upstream of the outlet are low, as indicated by the blue and purple flow velocity range (0.0001–0.004 m/s), possibly indicating areas of stagnant water and thus no flow exchange zones for untreated water.

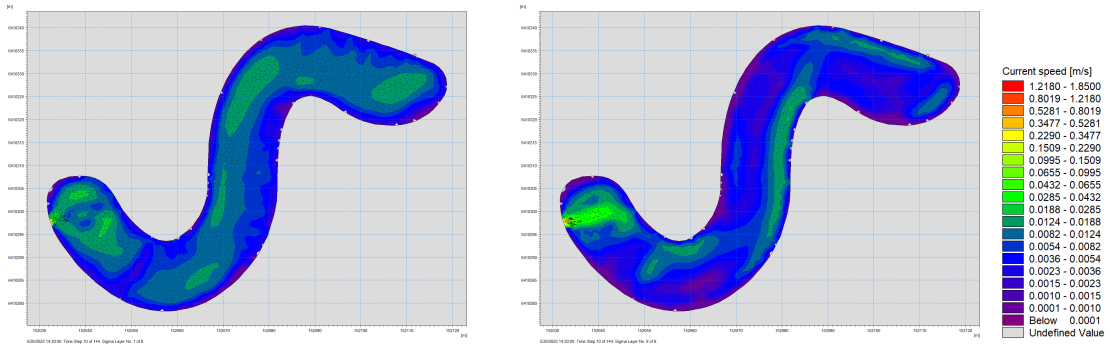

Figure 4.39: Velocity distribution in Scenario 6 at 14:20 (time step 10) across layer 1 and 6.

The velocity distribution at the end of the simulation time step 142 (01:20, 2025-05-27) is shown in Figure 4.40. The low inflow and outflow (0.14 L/s and 2.83 L/s, respectively) lead to several circulation and close-to-zero velocity throughout the pond. Across layer 1 there is also a distinct backflow visible, indicating water circulation pattern spanning the pond's full length. Such circulation, if too strong, may resuspend settled sediments, especially fine particles. On the other hand, enhanced mixing can improve oxygen distribution, reducing the risk of anoxic zones near the bottom.

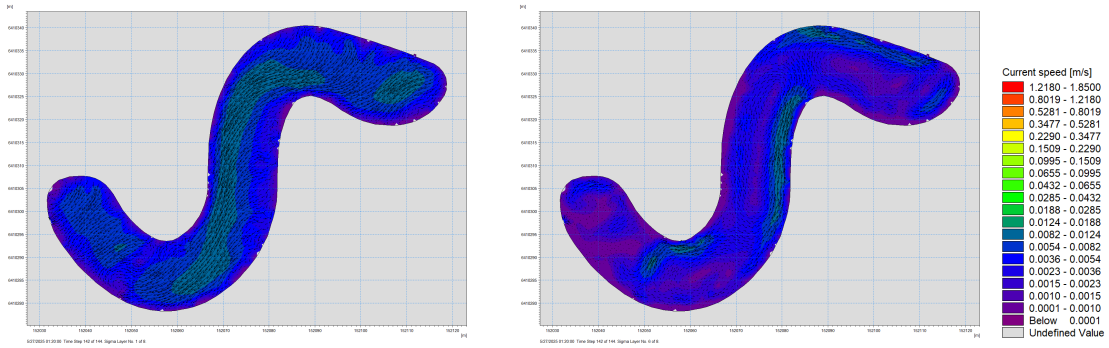

Figure 4.40: Velocity distribution in Scenario 6 at 01:20, 2025-05-27 (time step 142) across layer 1 and 6.

As can be seen in Table 4.18, velocity values of time step 10 and 142 show that the upper layer (layer 1) experienced the highest local velocities (up to 0.77 m/s), likely near the inlet. However, mean velocities remained low across all layers (approximately 0.009–0.014 m/s), with calmer conditions (0.0001–0.004 m/s) observed along the pond edges and before the outlet. By time step 142 the flow is reduced and near-stagnant conditions set in across the water body (min speed 8.834e-12 m/s). Mean velocities decreased across all layers to values between 0.005 and 0.006 m/s.

Table 4.18: Velocity values for Scenario 4 at the time steps 10 and 142 in m/s.

Time Step / Period	Layer	Min Speed	Max Speed	Mean Speed
10 / 14:20	1	2.388e-05	0.766	0.014
10 / 14:20	3	6.089e-05	0.038	0.009
10 / 14:20	6	4.285e-05	0.124	0.010
10 / 14:20	8	2.916e-06	0.079	0.010
142 / 01:20	1	1.297e-06	0.025	0.005
142 / 01:20	3	2.499e-05	0.025	0.006
142 / 01:20	6	2.962e-05	0.027	0.006
142 / 01:20	8	8.834e-12	0.025	0.006

4.3 Particle tracking

Particle tracking was conducted for simulations of Scenario 1, 4 and 5. The results from the particle tracking can be found in Appendix B. However, the particle tracking results were not deemed reliable and remain preliminary due to time constraints that prevented further refinement. In the simulation results a great loss in total particle mass was observed over the course of the simulations (see Figure B1.1, B2.2, and B3.3), which could not be accounted for. In order to resolve the issue with the mass loss, modifications would have had to be made either with the particle tracking module and/or the bathymetry and model mesh, with a subsequent re-running of all scenarios. Despite the mass loss issue, the results are still discussed to some extent but the conclusion drawn and the indications the particle tracking provides should be viewed with caution.

5 Discussion

5.1 Function of pond based on water quality analysis

Several water quality parameters have been analyzed, and overall it has been found that for all parameters except phosphorous, there is a clear distinction between the values at inlet and outlet.

5.1.1 TSS, VSS and Turbidity

Results for turbidity and TSS/VSS show the temporal profile of turbidity during the rain events correlates well with the pattern of TSS and turbidity and TSS/VSS are significantly lower at outlet compared to inlet. The pond also showed high retention efficiencies regarding the elevated TSS (91.50–97.41%) and VSS (73.39–94.99%) which is a strong indicator for the pond functioning as it should based upon its main purpose, which is to sediment particles.

These findings support the validity of using TSS concentrations as a reference for particle inputs in the MIKE 3 particle tracking model. Importantly, literature indicates that TWP concentrations in stormwater are closely linked to TSS and VSS levels (Gaggini et al., 2024; Rødland et al., 2022). For example, Gaggini et al. (2024) reported strong correlations between TWP and TSS (r = 0.87) and organic content (r = 0.72). This suggests that the sedimentation behavior observed in the pond, especially the high removal of TSS and VSS, may also apply to TWP, reinforcing the pond's potential to mitigate such persistent pollutants. However, direct measurement of TWP would be needed to confirm this.

The TSS/VSS analysis from the rain event 2025-05-02 showed that a large portion of the particles are inorganic, both at inlet and at outlet. For rain event 2025-05-22, the filter preparation error leads to uncertainty especially for outlet with regards to if there is more organic or inorganic particles. The inflow however, has more inorganic than organic particles regardless of where in the margin the true VSS lies, with the exception of I8, which likely is an anomaly caused by significantly greater filter loss for the specific filter used than what was observed for the blank tests. The TSS/VSS analysis for rain event 2025-05-26 shows that for both inlet and outlet, the inorganic particles dominate.

Despite rain event 2025-05-22 featuring a longer duration, higher peak rain intensity (up to 68 mm/h), and more antecedent dry days, all conditions typically associated with elevated pollutant buildup, the event yielded surprisingly low EMC values for both TSS and VSS at the inlet. Several factors may explain this discrepancy. First, the initial peak intensity (28 mm/h) occurred before sampling began, suggesting that a substantial portion of the first-flush pollutant load, especially coarser or loosely attached sediments, may have been washed off and missed by the ISCO samplers (Maniquiz-Redillas et al., 2022). Second, light and buoyant particles such as pollen, which were expected in greater abundance during spring, tend to float on the surface and may not have been adequately captured by sampling hoses positioned at the pipe bottom. Additionally, hydrophobic conditions on paved surfaces after prolonged dryness can delay runoff formation and limit early particle mobilization. This can inhibit the detachment and transport of particulate matter during early runoff. In such cases, rainfall may initially run off

without mobilizing significant solids, particularly coarser or more strongly bound particles (EPA, 2025). However, dissolved and fine organic compounds such as leachate from decaying vegetation, oils, or atmospheric deposition can still be mobilized without requiring particle detachment. Soil affected by a long dry period and then hit by intense rain could have lead to soil erosion and an increase in dissolved or colloidal organics in the runoff, as well (Rugendo et al., 2023; Sønderup et al., 2016). This is supported by the comparatively high concentrations of TOC, DOC, TN, and DN observed during this event, indicating substantial organic loading in dissolved or colloidal form. These findings imply that while solids may remain in place under certain surface conditions, pollutants in dissolved phases can still be transported early and effectively, underscoring the need to consider both particulate and dissolved fractions when assessing stormwater quality. The incomplete capture of the event's later hours (only the first 8 of 12 hours were sampled) may have further limited representation of slowly mobilized fine particles or delayed drainage from less responsive surfaces. Interestingly, the subsequent rain event 2025-05-26, although shorter and less intense, showed higher TSS and VSS—possibly reflecting cumulative mobilization effects, re-wetting of pollutant-laden surfaces, and more effective particle wash-off.

Göteborgs stad (2020) has set guideline values for discharges of polluted water into stormwater networks and recipients in Gothenburg which can be seen in Table 2.1. The guideline value for suspended particles is 25 mg/L and the highest TSS value at the outlet for rain event 2025-05-02 was 15.2 mg/L which is well beneath the limit. For rain event 2025-05-22, three out of twelve outlet samples had higher concentration than the guideline value and the highest TSS concentration was 37.7 mg/L. For rain event 2025-05-26, the TSS concentration was well beneath the guideline value for all outlet samples and the highest TSS concentration observed was 17.2 mg/L.

5.1.2 pH and conductivity

The municipal guideline for pH, seen in Table 2.1, is that pH should be within 6.5 and 9. The pH at the inlet for the three rain events is below pH 7 for all samples. The pH in the first four inlet samples from rain event 2025-05-02 as well as the pH in the first inlet sample from rain event 2025-05-22, and the pH in all inlet samples from rain event 2025-05-26, is below the guideline values, meaning that some of the stormwater coming in is slightly too acidic to be released into recipient. Treatment in the pond is enough to level the pH though, as the measurements in the outlet show a neutral pH of around 7.2 for rain event 2025-05-02, 6.96–7.15 for rain event 2025-05-22, and 6.79–6.93 for rain event 2025-05-26, which is inside the guideline range.

The conductivity in the pond is generally low and indicates low concentration of dissolved ions and is not critical for water quality. The low conductivity is expected since the sampling campaign was carried out in late spring. To be noted is that winter road maintenance is carried out in the city, both for main roads, and for minor roads, with the spreading of de-icing salt, among other practices (Göteborgs Stad, n.d.). This means that a sampling campaign carried out during winter/early spring could yield very different results due to the increased seasonal load of ions.

5.1.3 TOC/DOC and TN/DN

The TOC guideline, seen in Table 2.1, is 12 mg/L and the TOC in the outlet samples for rain event 2025-05-02 were all below 10 mg/L, and reached a retention efficiency of

46.10%. However, most of the outlet samples from rain event 2025-05-22 were above 12 mg/L, with a retention efficiency halfed compared to the former rain event. The samples above the guideline value were O1, O4–O12 and the highest measured TOC value in the outlet for that rain was 22.16 mg/L, which is about 10 mg/L too high. A reason as to why TOC was well within the limit for the first rain, but not for the second rain could be that there was a lot of pollen during rain event 2025-05-22, which could be seen floating in the pond in low velocity zones. Pollen was not seen during the previous rain event. Another reason for the significantly higher TOC values for the second rain compared to the first rain could be found in the antecedent dry days of the rain events, with several more dry days before rain event 2025-05-22 (19 days) compared to 2025-05-02 (11 days). Furthermore, a reason for higher TOC values in the second rain compared to the first rain can be that the second rain was longer than the first, leading to pollutants being collected for longer time. Lastly, higher peak rain intensity may also have contributed to the higher TOC values in the second rain event. The third rain event, 2025-05-26 had a maximum TOC concentration of 9.18 mg/L in the outlet which is beneath the guideline value, even though the retention efficiency was negative (-51.02%) and more organics were released from the pond than were present in the incoming stormwater. There were only a few days between the 2025-05-22 and 2025-05-26 rain events and only one dry day prior to the 2025-06-26 rain event. This, and that the sampling was stretched out over a longer period of time (6 hours more) for rain event 2025-05-22 compared to the the third rain event, could explain why the TOC and DOC concentration are so much lower for the third rain event compared to the second.

The guideline for nitrogen, seen in Table 2.1, is 1.25 mg/L. The values for TN in the samples from the rain on 2025-05-02 are equal or smaller than 0.35 mg/L, the values for TN in the samples from rain 2025-05-22 are equal or lower than 1.391 mg/L and the values for TN in the samples from rain event 2025-05-26 are equal of lower than 0.5 mg/L. For rain event 2025-05-02 and rain event 2025-05-26 the guideline value is met, with great margin, throughout all samples. However, three out of 12 outlet samples that exceed the guideline value for rain 2025-05-22, with about 0.086–0.141 mg/L, probably due to more antecedent dry days before rain event 2025-05-22 and the rain on 2025-05-22 going on for a longer period of time.

As could be viewed in Figure 4.13 and Figure 4.16, there were samples for which the TOC or TN had a lower value than the dissolved value although by definition the dissolved value should be a subgroup to the total value. Initially, it was hypothesized that the discrepancy in TOC, DOC, TN, and DN results was caused by the freezing of samples prior to analysis for preservation. However, upon reviewing a set of grab sample analyses—conducted before the installation of the automatic samplers and not included in this report—a similar discrepancy was observed even though the samples had not been subjected to freezing. The exact cause for the dissolved values occasionally being higher than the total values remains uncertain. Some possible explanations are sample heterogeneity between vials, the instrument mechanics, and the high content of inorganic suspended solids indicated by TSS/VSS analysis.

Replicate analysis of TOC, DOC, TN and DN performed on selected samples from the rain events 2025-05-22 and 2025-05-26, showed some variability comparable to the differences between total and dissolved concentrations, suggesting heterogeneity in the sub-samples.

The unfiltered samples for TOC and TN analysis contain a significant amount of inorganic particles based on TSS/VSS results. The instrument withdraws the same sample volume from each vial but the amount of measurable parameters within the water withdrawn, used to calculate TOC, TN, DOC and DN, could differ between filtered and unfiltered samples due to the existence of a lot of inorganic particles in unfiltered sample water. The needle taking the sample withdraws sample water with measurable parameters (TOC and TN) that also contains a lot of inorganic particles which are not measurable by the instrument and thus is not measured but also are not water, affecting the calculations of the TOC, DOC, TN and DN values as the volume of inorganic particles are not a part of the calculation of the parameter values. Ultimately this could cause the dissolved values to be higher than the total values, especially when the dissolved fraction represents a large portion of the TOC and TN content. As the dissolved values are only slightly above the total values, this indicates that a lot of the organic carbon and nitrogen is in dissolved form and that the existence of a significant amount of inorganic particles in the unfiltered water is the reason for the discrepancy. Another possible reason could be that the unfiltered samples are very heterogeneous and that a significant portion of particles settle before analysis has been completed leading to the instrument only withdrawing sample volume from a part of the vial with cleaner sample water, leading to particles that may have been deposited at the bottom of the vial to not be registered.

5.1.4 TP

While TSS, TOC, pH, and TN have been within/below the guideline values at the outlet, total phosphorous in the outlet samples exceed the guideline value of 0.050 mg/L slightly. The sample O2 from rain event 2025-05-02 is below 0.050 mg/L but O3 is slightly above (see TP in Figure 4.19), with TP being and 0.07 mg/L in O3. TP concentration also was increased at the outlet, resulting in a retention efficiency of -150%. No trend could be seen for the outlet with regards to TP for the rain events 2025-05-02 and 2025-05-26, and only a weak increasing trend for rain 2025-05-22. The samples from rain event 2025-05-22 exceeded the TP guideline for sample O6 and O12 slightly (by 0.01 mg/L), but the rest of the samples showed TP values lower or equal to the guideline, as well as a retention of 49.29%. For the third rain event, 2025-05-26, TP guideline value was met for all outlet samples and 39.31% could be retained during the rain event. Generally, the inlet and outlet TP concentrations are within the same range for the various rain events.

When measuring TP, there are three values possible to read, P (which is TP), PO_4, and P_2O_5 which are other expressions of the same phosphorus. The test range for the method is 0.02–1.10 mg/L P. For rain 2025-05-02 I1 was below that range and I10, I11, O2, O4, O7, O9 were below the range for rain 2025-05-22. For rain event 2025-05-26, the TP was below that range for samples I2, I4, O1, O2, O6–O9, and O12. Therefore, those results should be viewed with caution.

5.1.5 Metals

Municipal guideline values were available for the metals Cd, Cr, Cu, Ni, Pb and Zn that were analyzed for the rain event 2025-05-02 (Table 2.1). The guideline values are for total metal concentration, while dissolved metals were measured in this work. For metals Cd, Ni, and Pb, assuming that the dissolved form represents 50% of the

total concentration (Vorne & Waara, 2021), the guideline value are met, as maximum measured dissolved concentrations at the outlet were 0.03 μg/L, 1.75μg/L and was 0.15 μg/L, respectively, which is much lower compared to the guideline values for total concentration of 0.9 μg/L, 68 μg/L and 28 μg/L, respectively. Similarly, the maximum dissolved Cr concentration at the outlet was 0.24 μg/L and given that the guideline value for total concentration is much higher at 7 μg/L it is likely that the guideline is met also for Cr. For Cu and Zn, the maximum concentrations over all samples were relatively high compared to the guideline values: 7.58 μg/L and 12.67 μg/L, which represent 80% and 42.3% of the guideline value, respectively. Therefore there could be a risk of the total concentrations of these metals exceed guidelines.

It is notable that the Kryddvägen pond showed the highest retention efficiency regarding the metals Zn (79.09%) followed by Co (83.02%) indicating effective removal of these metals. Ba and Ti concentrations at the outlet on the other hand were enriched compared to inlet concentrations (retention efficiency of -498.78 and -265.98%), hinting on antecedent concentrations or remobilization from sediments. However, these are not part of the municipal guidelines and are not categorized in terms of aquatic threshold.

5.2 Differences in hydrodynamics affect the water level, velocities and particle movement in the pond

5.2.1 Water level

In Scenarios 1 and 2, the surface water level increased from the initial elevation of 63.8 m.a.s.l. to an average of 63.84 m.a.s.l.. The water level reaches stabilises reaching stead-state after about 4 hours of simulation time. In Scenario 3, which represents an extreme inflow event, the water level rises to a steady state at around 64.17 m.a.s.l., which poses an level rise of nearly 0.37 meters.

It is important to note that actual water level rises would be slightly lower than the simulated values, ranging from less than 1 mm to approximately 3 cm, depending on the scenario. This discrepancy results from model simplifications. Figure 5.1 illustrates the difference: while the model assumes vertical water rise along a fixed boundary, real-world topography includes sloped terrain outside the mesh, which would absorb some of the volume and result in a lower surface elevation.

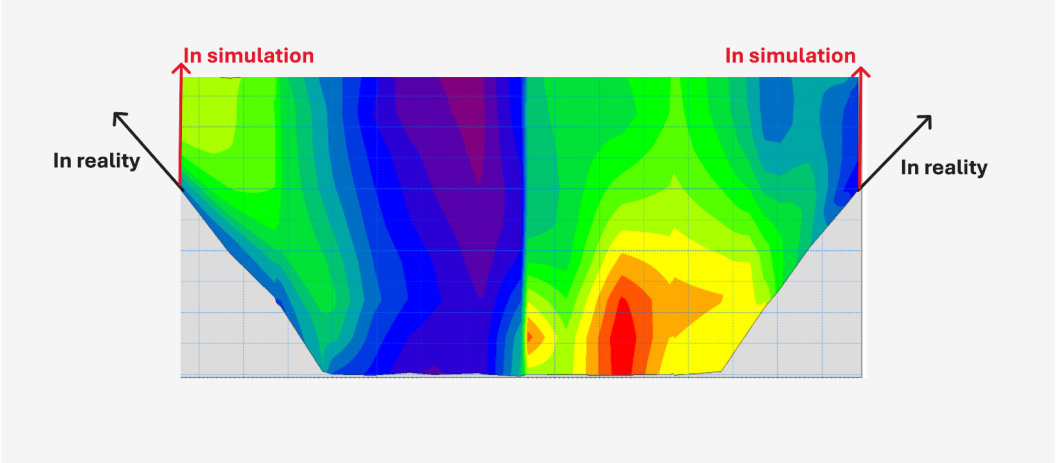

Figure 5.1: Explanatory figure showing the differences between simulated and actual water rise.

Scenario 4 showed minimal surface level change, remaining around 63.8 m.a.s.l. In Scenario 5, the surface elevation fluctuated, correlating with inflow peaks with some time lag. The maximum mean simulated elevation was 63.87 m.a.s.l., and at the final timestep, it had stabilized at 63.84 m.a.s.l.

5.2.2 Velocity in pond

In the low-flow Scenarios 1 and 2, a defined main flow path and a circulation zone near the outlet were observed. Wind in Scenario 2 enhanced circulation compared to Scenario 1, potentially resuspending fine particles or delaying their settling, especially in the upper water layers. Surface flow was predominantly wind-driven from west to east, while near-bed velocities remained low, promoting sedimentation. Localized reverse flow near the bed and enhanced circulation near the outlet further suggest that wind-induced shear was the dominant mixing mechanism under low inflow. The stagnation zones on the banks of the pond observed in Scenario 1 were also mitigated by the mixing due to wind action, possibly restoring the usable volume of the pond.

In Scenario 3, high inflow rates led to strong, directional flows with peak velocities at the inlet and outlet, likely hindering sedimentation of finer particles. Only heavy sediments may settle in protected or low-flow zones (e.g. between inlet and barrier). Circulation is most prominent near the inlet, constrained by the submerged barrier. Purple areas along the shore can be found here as well, which indicate stagnation and loss of usable sedimentation capacity during high flow events.

During the rain events (Scenario 4, 5 and 6), even during the inflow peak, the pond maintained low average velocities throughout the water column. This indicates that the pond's design, particularly the internal barrier and elongated S-shape, effectively dampens incoming flow energy. Circulation zones developed near both the inlet and outlet, while most of the pond exhibited minimal flow. There is also circulation over the entire length of the pond, visible by the backflow just above the pond bed. This suggests enhanced internal mixing without necessarily increasing turbulence in upper layers. Such circulation improves retention efficiency by reducing dead zones and distributing sedimentation potential more evenly across the pond volume. Although wind temporarily redistributed surface flows, it did not significantly disturb the lower layers, allowing favorable conditions for sedimentation to persist for most of the event.

The observed velocity patterns under different runoff conditions are consistent with standard stormwater pond design principles. For example, the effectiveness of the internal barrier and elongated S-shape supports literature recommendations that emphasize long flow paths and a high length to width ratio to promote plug flow and sedimentation (Davis, 2020). The persistent low velocities across the pond during rain events reflect successful implementation of flow-directing features, such as the barrier and irregular pond shape with high length-to-width ratio, that reduce turbulence and enhance treatment efficiency. (Davis, 2020; Kadlec & Wallace, 2009).

Moreover, the localized sedimentation dynamics in Scenarios 1–3 demonstrate how design elements like submerged barriers and forebays can help stratify flow regimes, targeting both coarse and fine particle removal (Scholz, 2023; USEPA, 2004). On the

other hand, there is potential for stagnant water along the shores and the middle of the pond, especially during low wind velocities. Inflowing water might bypass these zones, hindering sediments from resuspending, but also restricting sediment transport and oxygen exchange. As per Kadlec and Wallace (2009) and Ferguson (1998) this might lead to a decrease of the effective pond volume and introduce inefficient water treatment.

When examining the Kryddvägen pond, it could be seen that vegetation establishes itself in areas where circulation occurred in the simulations: Figure 5.2 shows a dense vegetation zone growing in front of the inlet and overlapping with the position of the circulation zone in several simulations. The effect of the vegetation was not included in the simulations but is likely to have a large effect on both the flow field and the retention efficiencies for certain pollutants, as it has been found to promote sedimentation by distributing incoming water more evenly and reduce sediment erosion, contributing to pollutant filtering and flow attenuation (USEPA, 2004). While the vegetation likely has a large effect on retention and flow field it should be carefully maintained. Otherwise, the vegetation may cause blockage of the inlet and overgrow the barrier.

Figure 5.2: Vegetation in front of the inlet in Kryddvägen pond

Overall, these results highlight the pond's dual behavior: brief periods of high-energy inflow can disrupt sedimentation, potentially resuspending settled particles. However, once the inflow subsides, the system returns to a low-velocity regime that supports effective particle settling. Thus, sedimentation efficiency varies dynamically, with the pond alternating between phases of transport and deposition depending on rainfall intensity and duration.

5.2.3 Particle tracking

For scenario 1, 4 and 5 particle tracking of TWP was simulated, however, due to great (unaccounted for) mass loss identified by performing mass balance equations, the results are unreliable and can at best give an indication of how particles are transported and sedimented in the pond. The mass loss was probably caused by the existence of

dry cells at inlet where intermittent wetting and drying likely led to particle deletion or exclusion from the active transport domain. To resolve it would likely require changes in bathymetry and model mesh and re-running all scenarios, and this could not be done within the time-frame for this thesis. The results from the simulations and analyses of mass balance does emphasize the importance of careful boundary configuration and highlight the sensitivity of Lagrangian particle tracking models to small-scale hydrodynamic and topographic features. The results underscore the value of performing mass balance checks to uncover potential inconsistencies that might go unnoticed if only the final spatial distributions are analyzed.

The results from the particle tracking are as mention unreliable, but observing the results does give indications regarding sedimentation and transport patterns. Indications from the three scenarios simulated include that the finest TWP fraction simulated (10 μm) may reach the outlet under low but constant flow conditions (Scenario 1), but may settle under conditions where inflow declines to the end of a rain event (seen in Scenario 4 and 5). The coarser particle fractions (50 μm and 100 μm) seem to sediment early in the pond geometry, before the barrier which aligns with sedimentation behavior under calm conditions, which was also discussed in chapter 5.2.2.

As expected by sedimentation physics, the coarser the particle, the greater the total and settled mass. Coarser particles are heavier and settle more rapidly, especially under calm or low-flow conditions. The results, though not fully reliable, could indicate that only a very small fraction or none of particles simulated reach the outlet, depending on scenario. The TSS concentrations found in laboratory analysis indicate that either finer particles (<10 μm) were captured at the outlet as those can be transported further, or resuspension occurs or there are particles suspended in the pond before the rain event recorded started. It is possible that a combination of these possibilities are true.

5.2.4 Overall retention efficiency as per modeling

The combined analysis of hydrodynamic conditions and particle tracking across scenarios indicates that the Kryddvägen pond performs effectively as a sedimentation system under typical and moderate flow events. The pond's internal design, particularly its elongated shape, submerged barrier, and resulting low velocities, supports extensive sedimentation across most of its area, especially for medium and coarse TWP. Retention efficiency is highest during low-flow conditions, with over 95% of coarser TWP settling near the inlet and before the barrier. During high inflow events, particle transport of TWP increases and retention drops, especially for fine particles, but the system rapidly returns to a low-velocity regime favorable for sedimentation. However, very low velocities may also introduce inefficiencies, as seen in certain simulations where flow stagnation along pond margins and in interior corners could reduce oxygen exchange and limit sediment transport. These zones can contribute to long-term accumulation without effective pollutant removal and biological treatment, or limiting the capacity for sedimentation.

The pond's performance is further influenced by wind, boundary configurations, and antecedent conditions, which may enhance or hinder short-term retention. While some mass balance inconsistencies highlight model limitations, the observed trends confirm that the pond generally supports high retention efficiency, particularly when inflow rates allow for extended residence time and minimal resuspension. When modeling various scenarios to investigate the influence of currents and wind, no sensitivity analyses were

carried out on how the density of the TWP and erosion, for example, affect sedimentation. Several studies state that a large portion of all TWP (by number) is in the ultrafine particle range, approx. 0.5–12 μm according to Sommer et al. (2018) and 1.6–20 μm (by mass) according to Gaggini et al. (2024). Several assumptions regarding the simulated TWP classes, shape and density were made in the project, which should be further assessed through sensitivity analyses for better interpretation of the results.

5.3 Integration of water quality analysis and modeling results

5.3.1 Combined assessment of retention efficiency

The retention efficiency of the pond was assessed by comparing inlet and outlet concentrations of key water quality parameters across three rain events, referencing both local guidelines and modeling outcomes.

The pond showed consistently high removal rates of suspended solids, with TSS reduction efficiencies between 91.50 and 97.41% and VSS reductions between 73.39 and 94.99%, aligning with its primary sedimentation function as stated in Ferguson (1998). These values are supported by turbidity trends and comply with the Gothenburg guideline of 25 mg/L for TSS in most samples, though a few exceeded this during the 2025-05-22 event. Modeling data (Section 5.2) also indicated lower velocities and effective sedimentation zones that likely contributed to the strong retention observed. Given strong correlation between TSS and TWP reported by Gaggini et al. (2024) and Rødland et al. (2022), it is likely that similarly high retention efficiency would apply to TWP if analyzed. This is further supported by Rasmussen et al. (2024) findings in a Danish stormwater pond, and aligns with preliminary—though unreliable—particle tracking results from this study.

pH values at the inlet were occasionally outside the acceptable range (6.5–9), but were consistently neutralized in the outlet, indicating effective buffering by the pond. Conductivity levels were low and not of concern, suggesting limited ionic pollution.

For organic carbon and nitrogen, removal performance varied with event characteristics. TOC and DOC exceeded the 12 mg/L guideline in several outlet samples during 2025-05-22, likely due to pollen accumulation, long dry periods, and higher runoff mobilization. These results show that dissolved forms of pollutants cannot be efficiently removed by the pond, especially during spring events with high availability of organic substances (low or negative retention efficiency, see Table 4.2).

While TN values were mostly below the 1.25 mg/L guideline, minor exceedances occurred during the same event. Overall, nitrogen removal was inconsistent, likely due to its predominantly dissolved form and the pond's limited ability to facilitate permanent removal via assimilation or denitrification, as also highlighted by Lusk et al. (2025). In several cases, dissolved nitrogen fractions were reported higher than total nitrogen, likely due to analytical inconsistencies or predominance of dissolved species—a pattern consistent with the low TSS conditions.

In contrast, phosphorous (TP) showed little change between inlet and outlet, with occasional slight exceedances of the 0.05 mg/L limit. A maximum retention of 49.29% and a negative retention of 150% suggests that phosphorous may remain largely in dissolved form or be influenced by measurement limitations, as some values fell outside reliable

detection ranges. This supports the findings by Lusk et al. (2025) that phosphorus and nitrogen are not permanently retained in ponds dominated by sedimentation, especially when available in dissolved forms.

Compared to the design benchmarks outlined by Sønderup et al. (2016)——which suggest optimal nutrient retention of 40–80% for ponds with features such as a vegetated sand filter, a minimum inlet–outlet distance of 50 m, a volume-to-impervious-area ratio of 0.025 m^3/m^2, and system age under 5 years——the Kryddvägen pond partially meets the criteria. With a flow path of about 102 m and a volume-to-impervious-area ratio of 0.0185 m^3/m^2 it approaches but does not fully reach the volumetric threshold. While it lacks a designed sand filter, a naturally formed vegetation zone has developed in front of the inlet. This may offer some limited nutrient uptake or flow attenuation, though its effect was not quantified in the current study.

Metal concentration were generally well below guideline values at the outlet, even when comparing dissolved forms to total concentration thresholds. Notably, Cd, Ni, Pb, and Cr levels were far below limits, while Cu and Zn were closer to guideline thresholds but still likely within acceptable margins, assuming a typical dissolved-to-total fraction.

As metals are often particulate-bound, especially in the case of Pb and Cr (Egemose et al., 2015), the removal efficiency of those are probably greater when measuring total concentration than it is when measuring dissolved concentration. However, according to literature retention is likely lower for Cu, which often has a higher dissolved faction and is more mobile under changing environmental conditions (Egemose et al., 2015). This aligns with literature stating that metal retention efficiency depends strongly on whether the metals are in dissolved or particulate form.

In summary, lab data indicate that the pond is effective at retaining particulate pollutants (e.g. TSS, VSS) and adjusting pH, consistent with the dominance of sedimentation-driven processes in pollutant removal. This aligns with model predictions and with established understanding that many pollutants, including heavy metals and nutrients, are bound to particles that settle in the pond (Ferguson, 1998). However, the more variable retention of dissolved substances (e.g. TOC, TN, TP) suggests that sedimentation alone is insufficient. Enhancing biological and chemical processes, such as microbial uptake, adsorption, and precipitation, may be necessary to improve the removal of dissolved pollutants (Kooi et al., 2017).

5.3.2 Model validation with water quality parameters

An objective for this thesis was to validate the model. However, this could not be done due to several factors. The particle tracking results show great mass loss which was unaccounted for which means that the results in Appendix for particle tracking shows only work in progress, and not reliable results. The great particle mass loss in the simulations prevented meaningful comparison of particle tracking results to the experimentally determined outlet concentrations. For full model validation, the unresolved problems creating unaccounted mass loss would need to be corrected. Furthermore, the simulated particle tracking of TWP is not directly comparable to the measured water quality parameters, as TWP concentrations were not measured.

6 Conclusion

The pond functions well with regards to its main purpose which is to sediment particles, as can be seen by the large differences between TSS at inlet versus TSS at outlet for the rain events 2025-05-02, 2025-05-22 and 2025-05-26. This is also visible in the resulting high retention efficiency values. The pond meets the guideline value for TSS at the outlet for rain event 2025-05-02 and rain event 2025-05-26, but three out of twelve outlet samples exceed the TSS guideline value for rain event 2025-05-22 which was a longer rain event with higher peak rain intensity compared to the other two rain events. The pond also meets the guideline values for other analyzed parameters rather well.

The phosphorous guideline value is not always met even for shorter rains like the one on 2025-05-02. Although the TP occasionally exceeds the guideline value, even during short events like 2025-05-02, the exceedance is minor. TOC more frequently exceeds guideline values during extended rainfall following long dry periods, likely due to a combination of pollen buildup in late spring and soil erosion from the forest area which is the largest part of the catchment area.

Regarding dissolved metal concentrations, for the 2025-05-02 rain event, all outlet samples were below the total concentration guideline thresholds. However, because only dissolved metals were measured (not total concentrations), and because no metal data was collected during the second rain (2025-05-22) which had higher pollution levels in the outlet in general, there is some built-in uncertainty in the results. This is particularly relevant for Cu, Zn, and Cd, which showed higher variability or were closer to guideline thresholds. Thus, caution is advised when interpreting the metal data.

The hydrodynamic simulations provide important insights into the performance of the pond under different flow and forcing scenarios. The internal barrier and pond geometry play a key role in creating low-velocity zones that promote effective sedimentation of coarse, traffic-related particles. Scenarios 1, 4, 5 and 6 clearly demonstrate this effect, with low velocities and circulation zones concentrated between the inlet and the barrier and along the opposing shore. The barrier's function as a flow-break and energy dissipator is particularly evident in scenarios with dynamic inflow conditions (e.g. Scenario 3).

Wind forcing, as can be seen especially when comparing Scenario 1 and 2, increases velocity and mixing in the surface layer but has limited influence on the lower water column. This stratification could ensure that heavier, sediment-bound particles still have the opportunity to settle. In contrast, calm conditions favor sedimentation but may risk localized stagnation, affecting water quality.

The hydrodynamic simulations confirm that while peak inflow events momentarily increase turbulence and could disturb already settled material, the pond's overall volume and geometry act as a buffer, allowing settling to resume once flows decrease. The pronounced backflow in the near-bottom layers (layer 1), observed across the entire pond, indicates a broad circulation pattern. While this may help alleviate stagnation, the associated very low velocities could reduce efficiency by resuspending fine particles. Nonetheless, intense rain events (as in Scenario 5) generate higher flow velocities and energy that may hinder sedimentation of finer particles or introduce resuspension. In addition, low wind velocities can lead to stagnation, particularly along the shoreline,

which could reduce the retention efficiency of the stormwater pond.

A critical finding during particle tracking from the mass balance analysis was the discrepancy between initial and final total particle mass, particularly in Scenario 1. Despite visualizations indicating that particles, especially coarse ones, remained near the inlet and sedimented, over 85% of particle mass appeared lost during the simulation. The issue could not be resolved within the time frame of the project, and while the results of particle tracking can give an indication of of potential transport and sedimentation patterns in the pond, they have to be viewed with caution. Lastly, discrepancy between the particle tracking results and the detection of suspended solids at the outlet in the experimental measurements, suggest that antecedent conditions, continuous low-flow transport, or resuspension were not fully captured in the simulations. Including these factors in future modeling efforts would help align simulated results with observed concentrations and improve predictions of fine particle behavior under varying hydrological regimes.

In summary, the pond shows strong performance in retaining sediment-bound pollutants, while the retention of dissolved substances remains more variable. The combination of laboratory observations and hydrodynamic simulation results provides valuable insights into the retention mechanisms and the hydraulic behavior of the system. The validation of the model and the detailed tracking of TWP transport could only be partially achieved. Nevertheless, the results make a useful contribution to understanding particle dynamics and highlight key areas for future model refinement and monitoring.

With regard to the objectives of the study, the hydrodynamic model of the stormwater retention basin was successfully developed and applied to several inflow scenarios. A targeted sampling campaign was also conducted in which traffic-related pollutants such as TWP, metals and suspended solids were successfully collected during three rain events. The goal of model validation was partially achieved: while the flow and precipitation measurements agreed quite well with the model results, the validation using water quality parameters was limited by not performing TWP analysis and the unresolved particle mass balance issues. Despite these limitations, the study provides a solid methodological basis for future assessments of pollutant transport and stormwater treatment performance.

To improve the ponds' long-term performance, several design and maintenance considerations can be recommended. Vegetation near the inlet should be carefully managed to prevent overgrowth, which could alter flow paths and reduce sedimentation efficiency. Additionally, structural design optimizations, such as the addition of baffles or modified inlet/outlet zones, could be explored to enhance retention of finer particles and improve flow control under dynamic inflow events. This would ensure hydraulic resilience during more extreme rainfall events expected in future climate scenarios. From a modeling perspective, several areas require further exploration. Incorporating antecedent conditions, such as background particle loads or ongoing low-flow transport, would help simulate more realistic scenarios. Including vegetation effects on flow and turbulence, as well as erosion and resuspension dynamics, would enhance the model's predictive capability. A sensitivity analysis on particle properties such as density, shape and size distribution, would help quantify uncertainty in settling behavior of particles and TWP. Future models should consider these finer fractions and explore their fate under varying hydraulic conditions.

References

Ansys. (2025). What is Computational Fluid Dynamics (CFD)? https://www.ansys.com/simulation-topics/what-is-computational-fluid-dynamics

Arthur Courtney, Baker Joel, & Bamford Holly. (2009). *Proceedings of the International Research Workshop on the Occurrence, Effects, and Fate of Microplastic Marine Debris* (tech. rep.). NOAA Technical Memorandum NOS-OR&R-30. www.MarineDebris.noaa.gov

Baensch-Baltruschat, B., Kocher, B., Stock, F., & Reifferscheid, G. (2020, September). Tyre and road wear particles (TRWP) - A review of generation, properties, emissions, human health risk, ecotoxicity, and fate in the environment. https://doi.org/10.1016/j.scitotenv.2020.137823

Barałkiewicz, D., Chudzińska, M., Szpakowska, B., Świerk, D., Gołdyn, R., & Dondajewska, R. (2014). Storm water contamination and its effect on the quality of urban surface waters. *Environmental Monitoring and Assessment*, *186*(10). https://doi.org/10.1007/s10661-014-3889-0

Barboza, L. G. A., Lopes, C., Oliveira, P., Bessa, F., Otero, V., Henriques, B., Raimundo, J., Caetano, M., Vale, C., & Guilhermino, L. (2020). Microplastics in wild fish from North East Atlantic Ocean and its potential for causing neurotoxic effects, lipid oxidative damage, and human health risks associated with ingestion exposure. *Science of the Total Environment*, *717*. https://doi.org/10.1016/j.scitotenv.2019.134625

Bentzen, T. R. (2010). 3D modelling of transport, deposition and resuspension of highway deposited sediments in wet detention ponds. *Water Science and Technology*, *62*(3), 736–742. https://doi.org/10.2166/wst.2010.363

Besseling, E., Quik, J. T., Sun, M., & Koelmans, A. A. (2017). Fate of nano- and microplastic in freshwater systems: A modeling study. *Environmental Pollution*, *220*, 540–548. https://doi.org/10.1016/j.envpol.2016.10.001

Betson, R. P. (1964). What is watershed runoff? *Journal of Geophysical Research*, *69*(8), 1541–1552. https://doi.org/10.1029/JZ069i008p01541

Bondelind, M., Nguyen, A., Sokolova, E., & Björklund, K. (2018). Transport of traffic-related microplastic particles in receiving water. *New Trends in Urban Drainage Modelling*, 317–321. https://doi.org/https://doi.org/10.1007/s11356-020-08637-z

Brudler, S., Rygaard, M., Arnbjerg-Nielsen, K., Hauschild, M. Z., Ammitsøe, C., & Vezzaro, L. (2019). Pollution levels of stormwater discharges and resulting environmental impacts. *Science of the Total Environment*, *663*, 754–763. https://doi.org/10.1016/j.scitotenv.2019.01.388

Burton, F., Tchobanoglous, G., Stensel, H. D., Metcalf & Eddy, Tsuchihashi, R., Abu-Orf, M., Bowden, G., & Pfrang, W. (2013). *Wastewater engineering : treatment and resource recovery* (5th ed.). McGraw-Hill Education - Europe.

Camatini, M., Crosta, G. F., Dolukhanyan, T., Sung, C., Giuliani, G. P., Corbetta, G. M., Cencetti, S., & Regazzoni, C. (2001). Microcharacterization and identification of tire debris in heterogeneous laboratory and environmental specimens. *Materials Characterization*, *46*(4). https://doi.org/10.1016/S1044-5803(00)00098-X

Center for Watershed Protection. (n.d.). Performance Criteria: Stormwater Ponds. https://www.stormwatercenter.net/Manual_Builder/Performance%20Criteria/Stormwater%20ponds.htm

Cho, Y., Shim, W. J., Ha, S. Y., Han, G. M., Jang, M., & Hong, S. H. (2023). Microplastic emission characteristics of stormwater runoff in an urban area: Intra-event variability and influencing factors. *Science of the Total Environment*, *866*. https://doi.org/10.1016/j.scitotenv.2022.161318

Davis, M. L. (2020). *Water and Wastewater Engineering: Design Principles and Practice* (2nd ed.). McGraw-Hill Education.

Dröge, R., & Tromp, P. (2019). *CEDR call 2016: environmentally sustainable roads: surface- and groundwater quality* (tech. rep.). CEDR Conference of European Directors of Roads.

EBS. (2011, January). Total Suspended Solids (TSS) & Volatile Suspended Solids (VSS). https://www.ebsbiowizard.com/articles/total-suspended-solids-tss-volatile-suspended-solids-vss/

EEA. (n.d.). EPER pollution register glossary. https://www.eea.europa.eu/help/glossary/eper-pollution-register-glossary

Egemose, S., Sønderup, M. J., Grudinina, A., Hansen, A. S., & Flindt, M. R. (2015). Heavy metal composition in stormwater and retention in ponds dependent on pond age, design and catchment type. *Environmental Technology (United Kingdom)*, *36*(8), 959–969. https://doi.org/10.1080/09593330.2014.970584

Eisakhani, M., Abdullah, M. P., Karim, O. A., & Malakahmad, A. (2012). Validation of MIKE 11 Model Simulated Data for Biochemical and Chemical Oxygen Demands Transport. *American Journal of Applied Sciences*, *9*(3), 382–387.

Ejhed, H., Hansson, K., Olshammar, M., Lind, E., Nguyen, M., Hållén, J., Allard, A.-S., Stadmark, J., Jutterström, S., Löfgren, S., & Hellgren, S. (2018). Belastning och påverkan från dagvatten. *Smed*, (12). https://www.naturvardsverket.se/contentassets/34e231a6ea91468ba0168816d8e3abd1/belastning-och-paverkan-fran-dagvatten-smed-underlagsrapport.pdf

EMEP/EEA. (2016). EMEP/EEA air pollutant emission inventory guidebook - 2016 — European Environment Agency. *EEA Reports*, (21).

EPA. (2023, April). *Where the Rubber Meets the Road: Opportunities to Address Tire Wear Particles In Waterways* (tech. rep.). Office of Wetlands, Oceans and Watersheds. http://www.ustires.org/innovation.

EPA. (2024, October). Storm Water Management Model (SWMM). https://www.epa.gov/water-research/storm-water-management-model-swmm

EPA. (2025, February). Urbanization - Stormwater Runoff. https://www.epa.gov/caddis/urbanization-stormwater-runoff

EPA & Hayter, E. J. (2006). *Evaluation of the State-of-the-Art Contaminated Sediment Transport and Fate Modeling System* (tech. rep.). Ecosystems Research Division, National Exposure Research Laboratory. Athen.

Erickson, A. J., Weiss, P. T., & Gulliver, J. S. (2013). *Optimizing Stormwater Treatment Practices* (1st ed.). Springer New York. https://doi.org/10.1007/978-1-4614-4624-8

European Commission. (2023). *EU action against microplastics*. Publications Office of the European Union. https://doi.org/10.2779/917472

European Union. (2000). Directive 2000/60/EC of the European Parliament and of the Council of 23 October 2000 establishing a framework for Community action in the field of water policy. *Official Journal of the European Communities*, *43*.

Ferguson, B. K. (1998, February). *Introduction to stormwater: concept, purpose, design*. Wiley, cop. 1998. https://doi.org/10.5860/CHOICE.35-6248

Fletcher, T. D., Andrieu, H., & Hamel, P. (2013). Understanding, management and modelling of urban hydrology and its consequences for receiving waters: A state of the art. *Advances in Water Resources*, *51*, 261–279. https://doi.org/10.1016/j.advwatres.2012.09.001

Gaggini, E. L., Polukarova, M., Bondelind, M., Rødland, E., Strömvall, A. M., Andersson-Sköld, Y., & Sokolova, E. (2024). Assessment of fine and coarse tyre wear particles along a highway stormwater system and in receiving waters: Occurrence and transport. *Journal of Environmental Management*, *367*. https://doi.org/10.1016/j.jenvman.2024.121989

Gao, L., & Li, D. (2014, December). A review of hydrological/water-quality models. https://doi.org/10.15302/J-FASE-2014041

German, J., Jansons, K., Svensson, G., Karlsson, D., & Gustafsson, L. G. (2005). Modelling of different measures for improving removal in a stormwater pond. *Water Science and Technology*, *52*(5). https://doi.org/10.2166/wst.2005.0120

GESAMP. (2015). Sources, fate and effects of microplastics in the marine environment: a global assessment. *Rep. Stud. GESAMP*, *No. 90*(IMO/FAO/UNESCO-IOC/UNIDO/WMO/IAEA/UN/UNEP/UNDP Joint Group of Experts on the Scientific Aspects of Marine Environmental Protection), 96. www.imo.org

Gillis, C. J. (2017, January). *The flow pattern, solids settling, and characteristics of a Saskatoon, Saskatchewan stormwater management pond* [Doctoral dissertation, University of Saskatchewan].

Göteborgs Stad. (n.d.). Snöröjning och halkbekämpning. https://goteborg.se/wps/portal/start/trafik-och-resor/renhallning-och-snorojning/sno-och-halka/snorojning-och-halkbekampning

Göteborgs stad. (2020). *Riktlinjer och riktvärden för utsläpp av förorenat vatten till dagvattennät och recipient (R2020:13)* (tech. rep.). Miljöförvaltningen, Göteborgs Stad. https://goteborg.se/wps/portal/start/foretag-och-organisationer/tillstand-och-regler/hantera-vatten-och-avlopp/riktvarden-for-utslapp-av-fororenat-vatten

Gunawardana, C., Goonetilleke, A., Egodawatta, P., Dawes, L., & Kokot, S. (2012). Source characterisation of road dust based on chemical and mineralogical composition. *Chemosphere*, *87*(2). https://doi.org/10.1016/j.chemosphere.2011.12.012

Hwang, H. M., Fiala, M. J., Park, D., & Wade, T. L. (2016, September). Review of pollutants in urban road dust and stormwater runoff: part 1. Heavy metals released from vehicles. https://doi.org/10.1080/12265934.2016.1193041

IPCC. (2021, July). *Climate Change 2021: The Physical Science Basis* (V. Masson-Delmotte, P. Zhai, A. Pirani, S. Connors, C. Péan, S. Berger, N. Caud, Y. Chen, L. Goldfarb, M. Gomis, M. Huang, K. Leitzell, E. Lonnoy, J. Matthews, T. Maycock, T. Waterfield, O. Yelekçi, R. Yu, & B. Zhou, Eds.). Cambridge University Press. https://doi.org/10.1017/9781009157896

Jaeger, A., Monaghan, J., Tomlin, H., Atkinson, J., Gill, C. G., & Krogh, E. T. (2024). Intensive Spatiotemporal Characterization of the Tire Wear Toxin 6PPD Quinone

in Urban Waters. *ACS ES and T Water*. https://doi.org/10.1021/acsestwater.4c00614

Jan Kole, P., Löhr, A. J., Van Belleghem, F. G., & Ragas, A. M. (2017, October). Wear and tear of tyres: A stealthy source of microplastics in the environment. https://doi.org/10.3390/ijerph14101265

Järlskog, I., Jaramillo-Vogel, D., Rausch, J., Gustafsson, M., Strömvall, A. M., & Andersson-Sköld, Y. (2022). Concentrations of tire wear microplastics and other traffic-derived non-exhaust particles in the road environment. *Environment International*, *170*. https://doi.org/10.1016/j.envint.2022.107618

Järlskog, I., Nyberg, E., Fager, H., Gustafsson, M., & Blomqvist, G. (2024). *Microplastic emissions from wear of road markings-overview and assessment for Swedish conditions (VTI rapport 1207A)* (tech. rep.). Swedish National Road and Transport Research Institute (VTI). https://vti.diva-portal.org/smash/record.jsf?pid=diva2%3A1851997&dswid=5004

Järlskog, I., Strömvall, A. M., Magnusson, K., Galfi, H., Björklund, K., Polukarova, M., Garção, R., Markiewicz, A., Aronsson, M., Gustafsson, M., Norin, M., Blom, L., & Andersson-Sköld, Y. (2021). Traffic-related microplastic particles, metals, and organic pollutants in an urban area under reconstruction. *Science of the Total Environment*, *774*. https://doi.org/10.1016/j.scitotenv.2021.145503

Järlskog, I., Strömvall, A. M., Magnusson, K., Gustafsson, M., Polukarova, M., Galfi, H., Aronsson, M., & Andersson-Sköld, Y. (2020). Occurrence of tire and bitumen wear microplastics on urban streets and in sweepsand and washwater. *Science of the Total Environment*, *729*. https://doi.org/10.1016/j.scitotenv.2020.138950

Joshi, U. M., & Balasubramanian, R. (2010). Characteristics and environmental mobility of trace elements in urban runoff. *Chemosphere*, *80*(3), 310–318. https://doi.org/10.1016/j.chemosphere.2010.03.059

Kadlec, R. H., & Wallace, S. D. (2009). *Treatment wetlands (2nd ed.)* CRC Press.

Kirshen, P. H. (1972, September). *Mathematical Model for Screening Storm Water Control Alternatives* (tech. rep.). Massachusetts Institute of Technology.

Klöckner, P., Reemtsma, T., Eisentraut, P., Braun, U., Ruhl, A. S., & Wagner, S. (2019). Tire and road wear particles in road environment – Quantification and assessment of particle dynamics by Zn determination after density separation. *Chemosphere*, *222*, 714–721. https://doi.org/10.1016/j.chemosphere.2019.01.176

Klöckner, P., Seiwert, B., Eisentraut, P., Braun, U., Reemtsma, T., & Wagner, S. (2020). Characterization of tire and road wear particles from road runoff indicates highly dynamic particle properties. *Water Research*, *185*, 116262. https://doi.org/10.1016/j.watres.2020.116262

Knight, L. J., Parker-Jurd, F. N., Al-Sid-Cheikh, M., & Thompson, R. C. (2020). Tyre wear particles: an abundant yet widely unreported microplastic? *Environmental Science and Pollution Research*, *27*(15), 18345–18354. https://doi.org/10.1007/s11356-020-08187-4

Kooi, M., Van Nes, E. H., Scheffer, M., & Koelmans, A. A. (2017). Ups and Downs in the Ocean: Effects of Biofouling on Vertical Transport of Microplastics. *Environmental Science and Technology*, *51*(14), 7963–7971. https://doi.org/10.1021/acs.est.6b04702

Koutnik, V. S., Leonard, J., Glasman, J. B., Brar, J., Koydemir, H. C., Novoselov, A., Bertel, R., Tseng, D., Ozcan, A., Ravi, S., & Mohanty, S. K. (2022). Microplas-

tics retained in stormwater control measures: Where do they come from and where do they go? *Water Research*, *210*. https://doi.org/10.1016/j.watres.2021.118008

Kovochich, M., Liong, M., Parker, J. A., Oh, S. C., Lee, J. P., Xi, L., Kreider, M. L., & Unice, K. M. (2021). Chemical mapping of tire and road wear particles for single particle analysis. *Science of the Total Environment*, *757*. https://doi.org/10.1016/j.scitotenv.2020.144085

Li, K., Yu, J., Chen, X., Kong, D., Peng, Y., Xiu, X., Su, H., & Yan, L. (2022). Effects of tire wear particles with and without photoaging on anaerobic biofilm sulfide production in sewers and related mechanisms. *Chemosphere*, *308*. https://doi.org/10.1016/j.chemosphere.2022.136185

Li, P., Zhu, D. Z., Krywiak, D., & Yue, D. (2019). Flow characteristics and energy dissipation of an offset jet in a rectangular stormwater pond. *Canadian Water Resources Journal*, *44*(3), 307–318. https://doi.org/10.1080/07011784.2019.1623078

Liu, F., Olesen, K. B., Borregaard, A. R., & Vollertsen, J. (2019). Microplastics in urban and highway stormwater retention ponds. *Science of the Total Environment*, *671*, 992–1000. https://doi.org/10.1016/j.scitotenv.2019.03.416

Liu, J., Feng, Q., Yang, H., Fan, X., Jiang, Y., & Wu, T. (2023). Acute toxicity of tire wear particles and leachate to Daphnia magna. *Comparative Biochemistry and Physiology Part - C: Toxicology and Pharmacology*, *272*. https://doi.org/10.1016/j.cbpc.2023.109713

Lundy, L., Blecken, G., Österlund, H., & Viklander, M. (2021). *Systematic review of urban stormwater research in Sweden (2012-2021)* (tech. rep.). Luleå University of Technology. Luleå, Luleå University of Technology. https://www.diva-portal.org/smash/get/diva2:1645888/FULLTEXT01.pdf

Lusk, M. G., Bean, E. Z., Iannone, B. V., & Reisinger, A. J. (2025, February). Stormwater ponds: Unaccounted environmental challenges of a widely-adopted best management practice in urban landscapes. https://doi.org/10.1016/j.jenvman.2025.124170

Magnusson, K., Eliasson, K., Fråne, A., Haikonen, K., Hultén, J., Olshammar, M., Stadmark, J., & Voisin, A. (2016). *Swedish sources and pathways for microplastics to the marine environment A review of existing data* (tech. rep.). www.ivl.se

Maniquiz-Redillas, M., Robles, M. E., Cruz, G., Reyes, N. J., & Kim, L. H. (2022, April). First Flush Stormwater Runoff in Urban Catchments: A Bibliometric and Comprehensive Review. https://doi.org/10.3390/hydrology9040063

McKetta Jr, J. J. (1998). *Encyclopedia of Chemical Processing and Design* (Vol. 1). CRC Press Inc.

MIKE. (2017). *Flow Model FM - Particle Tracking Module* (tech. rep.). DHI. Hørsholm. www.mikepoweredbydhi.com

MIKE. (2019). *MIKE 3 Flow Model FM - Hydrodynamic and Transport Module - Scientific Documentation* (tech. rep.). DHI. https://manuals.mikepoweredbydhi.help/2019/Coast_and_Sea/MIKE_3_Flow_FM_Scientific_Doc.pdf

MIKE. (2025a). MIKE 21 and MIKE 3: Supercharge your marine water modelling projects. https://www.dhigroup.com/technologies/mikepoweredbydhi/mike-21-3

MIKE. (2025b). *MIKE ECO Lab: Numerical Lab for Ecological and Agent Based Modelling - User Guide* (tech. rep.). DHI.

MOE. (1994). *Stormwater management practices planning and design manual*. Queen's Printer for Ontario.

Moharir, R. V., Khairnar, K., & Paunikar, W. N. (2014). MIKE 3 as a modeling tool for flow characterization: A review of applications on water bodies. *International Journal of Advanced Studies in Computer Science & Engineering IJASCSE*, *3*. www.ijascse.org

Molazadeh, M., Liu, F., Simon-Sánchez, L., & Vollersten, J. (2023). Buoyant microplastics in freshwater sediments – How do they get there? *Science of the Total Environment*, *860*. https://doi.org/10.1016/j.scitotenv.2022.160489

Nayeb Yazdi, M., Scott, D., Sample, D. J., & Wang, X. (2021). Efficacy of a retention pond in treating stormwater nutrients and sediment. *Journal of Cleaner Production*, *290*. https://doi.org/10.1016/j.jclepro.2021.125787

Nihart, A. J., Garcia, M. A., El Hayek, E., Liu, R., Olewine, M., Kingston, J. D., Castillo, E. F., Gullapalli, R. R., Howard, T., Bleske, B., Scott, J., Gonzalez-Estrella, J., Gross, J. M., Spilde, M., Adolphi, N. L., Gallego, D. F., Jarrell, H. S., Dvorscak, G., Zuluaga-Ruiz, M. E., … Campen, M. J. (2025). Bioaccumulation of microplastics in decedent human brains. *Nature Medicine*. https://doi.org/10.1038/s41591-024-03453-1

Öborn, L., Österlund, H., Lorenz, C., Vianello, A., Lykkemark, J., Vollertsen, J., & Viklander, M. (2024). Composition and concentrations of microplastics including tyre wear particles in stormwater retention pond sediments. *Water Science and Technology*, *90*(10), 2857–2869. https://doi.org/10.2166/wst.2024.368

Overton, D. E., & Meadows, M. E. (1976). *Stormwater Modeling*. Elsevier. https://doi.org/10.1016/C2013-0-11266-4

Pettersson, T. J. R. (1999). *Stormwater Ponds for Pollution Reduction* [Doctoral dissertation, Chalmers University of Technology]. https://research.chalmers.se/en/publication/821

Rama, L. A. (2023). *Design criteria for forebays in wet stormwater ponds* (tech. rep.). Chalmers University of Technology. Gothenburg. www.chalmers.se

Rasmussen, L. A., Liu, F., Klemmensen, N. D. R., Lykkemark, J., & Vollertsen, J. (2024). Retention of microplastics and tyre wear particles in stormwater ponds. *Water Research*, *248*. https://doi.org/10.1016/j.watres.2023.120835

Rødland, E. S., Lind, O. C., Reid, M., Heier, L. S., Skogsberg, E., Snilsberg, B., Gryteselv, D., & Meland, S. (2022). Characterization of tire and road wear microplastic particle contamination in a road tunnel: From surface to release. *Journal of Hazardous Materials*, *435*. https://doi.org/10.1016/j.jhazmat.2022.129032

Rossman, L. A. (2010). *Storm Water Management Model User's Manual Version 5.0* (tech. rep.). National Risk Management Research Laboratory, Cincinnati.

Rugendo, M. K., Gichimu, B. M., Mugwe, J. N., Mucheru-Muna, M., & Mugendi, D. N. (2023). Surface runoff and soil erosion from Nitisols and Ferralsols as influenced by different soil organic carbon levels under simulated rainfall conditions. *Heliyon*, *9*(7). https://doi.org/10.1016/j.heliyon.2023.e17684

Scholz, M. (2023). *Wetlands for Water Pollution Control* (3rd ed.). Elsevier. https://doi.org/10.1016/C2022-0-02985-8

Seitzinger, S. P., Sanders, R. W., & Styles, R. (2002). Bioavailability of DON from natural and anthropogenic sources to estuarine plankton. *Limnology and Oceanography*, *47*(2), 353–366. https://doi.org/10.4319/lo.2002.47.2.0353

Sewwandi, M., Kumar, A., Pallewatta, S., & Vithanage, M. (2024, September). Microplastics in urban stormwater sediments and runoff: An essential component in the microplastic cycle. https://doi.org/10.1016/j.trac.2024.117824

Shafi, M., Lodh, A., Khajuria, M., Ranjan, V. P., Gani, K. M., Chowdhury, S., & Goel, S. (2024). Are we underestimating stormwater? Stormwater as a significant source of microplastics in surface waters. *Journal of Hazardous Materials*, *465*, 133445. https://doi.org/10.1016/j.jhazmat.2024.133445

Shahidzadehasadi, M., Linhoss, A., Cook, M., Moore, D., Reichley, S., Mickle, P., & Lawrence, M. (2024). Sensitivity analysis and calibration of a Lagrangian particle tracking using GPS-tagged drifters. *Estuarine, Coastal and Shelf Science*, *303*. https://doi.org/10.1016/j.ecss.2024.108793

SMHI. (2024, December). Dataserier med normalvärden för perioden 1991-2020. https://www.smhi.se/data/temperatur-och-vind/temperatur/dataserier-med-normalvarden-for-perioden-1991-2020

SMHI. (2025, February). Extreme precipitation. https://www.smhi.se/en/climate/tools-and-inspiration/climate-indicators/extreme-precipitation

Sommer, F., Dietze, V., Baum, A., Sauer, J., Gilge, S., Maschowski, C., & Gieré, R. (2018). Tire abrasion as a major source of microplastics in the environment. *Aerosol and Air Quality Research*, *18*(8), 2014–2028. https://doi.org/10.4209/aaqr.2018.03.0099

Sønderup, M. J., Egemose, S., Hansen, A. S., Grudinina, A., Madsen, M. H., & Flindt, M. R. (2016). Factors affecting retention of nutrients and organic matter in stormwater ponds. *Ecohydrology*, *9*(5), 796–806. https://doi.org/10.1002/eco.1683

Sörensen, J., & Rana, A. (2013). Comparative Analysis of Flooding in Gothenburg, Sweden and Mumbai, India: A Review. *Exeter*, (Paper presented at International Conference on Flood Resilience).

Svensson, N., & Andersson-Sköld, Y. (2021). *Dispersion and fate models for microplastics from tyre and road wear* (tech. rep.). Swedish National Road and Transport Research Institute (VTI).

Thompson, R. C., Courtene-Jones, W., Boucher, J., Pahl, S., Raubenheimer, K., & Koelmans, A. A. (2024, October). Twenty years of microplastic pollution research-what have we learned? https://doi.org/10.1126/science.adl2746

Tian, Z., Gonzalez, M., Rideout, C. A., Zhao, H. N., Hu, X., Wetzel, J., Mudrock, E., James, C. A., McIntyre, J. K., & Kolodziej, E. P. (2022). 6PPD-Quinone: Revised Toxicity Assessment and Quantification with a Commercial Standard. *Environmental Science and Technology Letters*, *9*(2), 140–146. https://doi.org/10.1021/acs.estlett.1c00910

United Nations. (2015). *Transforming our world: the 2030 Agenda for Sustainable Development* (tech. rep.). United Nations. New York. https://sdgs.un.org/2030agenda

USEPA. (2004). Stormwater Best Management Practice Design Guide Volume 2 Vegetative Biofilters.

Vogelsang, C., Lusher, A. L., Dadkhah, M. E., Sundvor, I., Umar, M., Ranneklev, S. B., Eidsvoll, D., & Meland, S. (2020). Microplastics in road dust - characteristics, pathways and measures.

Vorne, V., & Waara, S. (2021). *REPORT ON WATER QUALITY RESULTS.* (tech. rep.). https://www.researchgate.net/publication/366237369

Wang, C., O'Connor, D., Wang, L., Wu, W. M., Luo, J., & Hou, D. (2022). Microplastics in urban runoff: Global occurrence and fate. *Water Research*, *225*. https://doi.org/10.1016/j.watres.2022.119129

Wu, G. (2017). The Mechanisms of Rubber Abrasion. *Materials Science*. https://api.semanticscholar.org/CorpusID:139337229

Wu, J., & Malmström, M. E. (2015). Nutrient loadings from urban catchments under climate change scenarios: Case studies in Stockholm, Sweden. *Science of The Total Environment*, *518-519*, 393–406. https://doi.org/10.1016/j.scitotenv.2015.02.041

Yan, H., Lipeme Kouyi, G., Gonzalez-Merchan, C., Becouze-Lareure, C., Sebastian, C., Barraud, S., & Bertrand-Krajewski, J. L. (2014). Computational fluid dynamics modelling of flow and particulate contaminants sedimentation in an urban stormwater detention and settling basin. *Environmental Science and Pollution Research*, *21*(8), 5347–5356. https://doi.org/10.1007/s11356-013-2455-6

Yang, Y., Zhu, D. Z., Loewen, M. R., Ahmed, S. S., Zhang, W., Yan, H., van Duin, B., & Mahmood, K. (2023). Evaluation of pollutant removal efficiency of urban stormwater wet ponds and the application of machine learning algorithms. *Science of the Total Environment*, *905*. https://doi.org/10.1016/j.scitotenv.2023.167119

Zahari, N. M., Zawawi, M. H., Sidek, L. M., Mohamad, D., Itam, Z., Ramli, M. Z., Syamsir, A., Abas, A., & Rashid, M. (2018). Introduction of discrete phase model (DPM) in fluid flow: A review, 020234. https://doi.org/10.1063/1.5066875

Zhong, C., Sun, J., Zhang, J., Liu, Z., Fang, T., Liang, X., Yin, J., Peng, J., Wu, L., Zhang, Q., & Mao, H. (2024). Characteristics of Vehicle Tire and Road Wear Particles' Size Distribution and Influencing Factors Examined via Laboratory Test. *Atmosphere*, *15*(4). https://doi.org/10.3390/atmos15040423

Zhu, X., Chatain, V., Gautier, M., Blanc-Biscarat, D., Delolme, C., Dumont, N., Aubin, J. B., & Lipeme Kouyi, G. (2020). Combination of Lagrangian Discrete Phase Model and sediment physico-chemical characteristics for the prediction of the distribution of trace metal contamination in a stormwater detention basin. *Science of the Total Environment*, *698*. https://doi.org/10.1016/j.scitotenv.2019.134263

A Appendix

A.1 DXF to XYZ Conversion Code

Code that we created to converse a DXF to XYZ-file:

```
!pip install ezdxf
import ezdxf

def dxf_to_xyz(dxf_file, xyz_file):
    # Load DXF file
    doc = ezdxf.readfile(dxf_file)
    msp = doc.modelspace()
    with open(xyz_file, "w") as f:
        for entity in msp:
            # Check if the entity is a 3D POLYLINE
            if entity.dxftype() == "POLYLINE" and entity.is_3d_polyline:
                for vertex in entity.vertices:
                    x, y, z = vertex.dxf.location
                    f.write(f"{x} {y} {z}\n")

            # Check if the entity is an LWPOLYLINE (2D)
            elif entity.dxftype() == "LWPOLYLINE":
                for point in entity.get_points():
                    x, y = point[0], point[1]
                    z = 0.0
                    f.write(f"{x} {y} {z}\n")

print(f"XYZ file saved: {xyz_file}")

# Call the function with your DXF file
dxf_to_xyz("Kryddv gen_rev1.dxf", "output.xyz")
```

A.2 Timeseries Wind

Table A2.1: Wind time series used for Scenario 4 in 3D hydrodynamic modeling

Date & Time	Wind Speed [m/s]	Wind Direction [°]
5/2/2025 7:00	3.61	225
5/2/2025 7:00	3.61	270
5/2/2025 7:30	3.06	225
5/2/2025 8:00	4.72	270
5/2/2025 8:30	4.17	225
5/2/2025 9:00	5.56	225
5/2/2025 9:30	6.67	270
5/2/2025 10:00	8.33	270
5/2/2025 10:30	7.78	270
5/2/2025 11:00	9.72	270
5/2/2025 11:30	8.33	270
5/2/2025 12:00	8.89	270
5/2/2025 12:30	9.72	270
5/2/2025 13:00	9.17	270
5/2/2025 13:30	9.70	270
5/2/2025 14:00	8.33	225
5/2/2025 14:30	7.50	270
5/2/2025 15:00	6.67	270
5/2/2025 15:30	6.94	270
5/2/2025 16:00	6.00	270
5/2/2025 16:30	5.55	225
5/2/2025 17:00	4.44	225
5/2/2025 17:30	3.89	270
5/2/2025 18:00	4.72	225
5/2/2025 18:30	3.61	270

Table A2.2: Wind time series used for Scenario 5 in 3D hydrodynamic modeling

Date & Time	Wind Speed [m/s]	Wind Direction [°]
5/22/2025 3:00	5.00	45
5/22/2025 3:00	6.00	45
5/22/2025 4:00	6.00	45
5/22/2025 5:00	7.00	45
5/22/2025 6:00	6.00	45
5/22/2025 7:00	6.00	22.5
5/22/2025 8:00	6.00	22.5
5/22/2025 9:00	5.00	22.5
5/22/2025 10:00	5.00	22.5
5/22/2025 11:00	5.00	22.5
5/22/2025 12:00	5.00	22.5
5/22/2025 13:00	5.00	22.5
5/22/2025 14:00	5.00	22.5
5/22/2025 15:00	4.00	22.5
5/22/2025 16:00	4.00	0
5/22/2025 17:00	3.00	0
5/22/2025 18:00	3.00	0
5/22/2025 19:00	2.00	337.5
5/22/2025 20:00	2.00	315
5/22/2025 21:00	1.00	292.5
5/22/2025 22:00	1.00	270

Table A2.3: Wind time series used for Scenario 6 in 3D hydrodynamic modeling

Date & Time	Wind Speed [m/s]	Wind Direction [°]
5/22/2025 3:00	5.00	45
5/22/2025 3:00	6.00	45
5/22/2025 4:00	6.00	45
5/22/2025 5:00	7.00	45
5/22/2025 6:00	6.00	45
5/22/2025 7:00	6.00	22.5
5/22/2025 8:00	6.00	22.5
5/22/2025 9:00	5.00	22.5
5/22/2025 10:00	5.00	22.5
5/22/2025 11:00	5.00	22.5
5/22/2025 12:00	5.00	22.5
5/22/2025 13:00	5.00	22.5
5/22/2025 14:00	5.00	22.5
5/22/2025 15:00	4.00	22.5
5/22/2025 16:00	4.00	0
5/22/2025 17:00	3.00	0
5/22/2025 18:00	3.00	0
5/22/2025 19:00	2.00	337.5
5/22/2025 20:00	2.00	315
5/22/2025 21:00	1.00	292.5
5/22/2025 22:00	1.00	270

B Appendix

B.1 Particle Tracking - Scenario 1

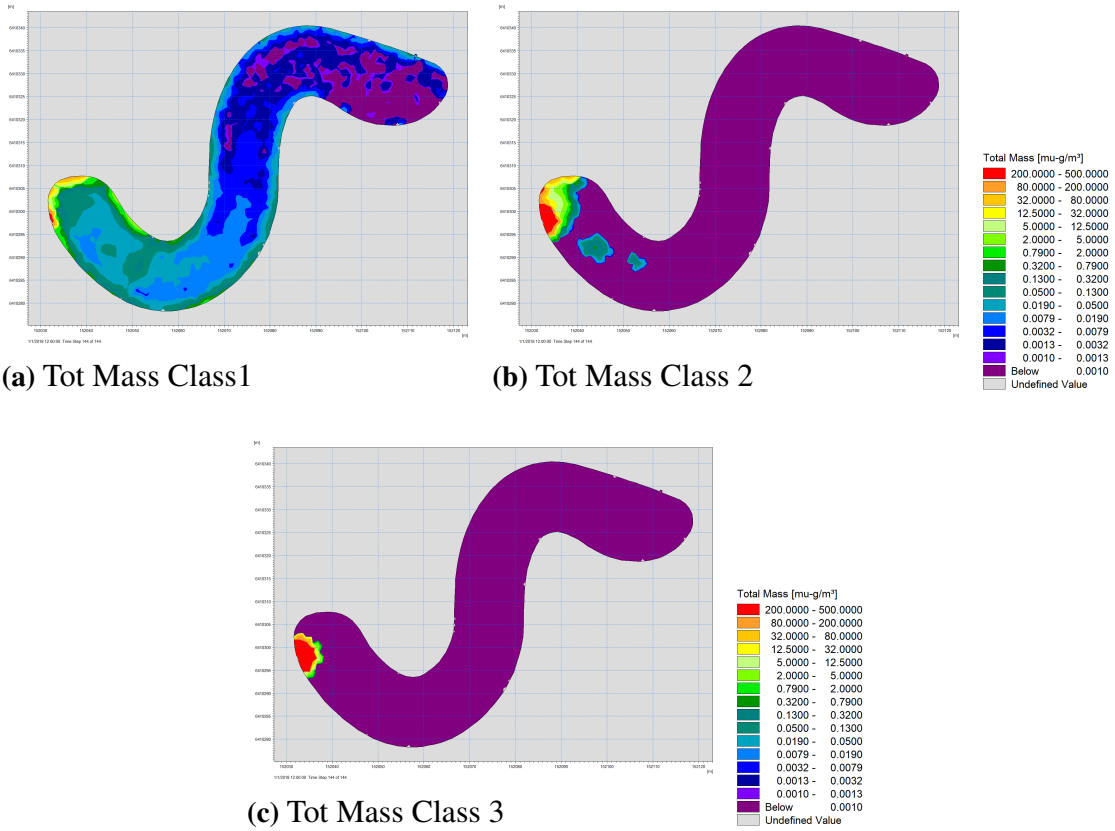

(a) Tot Mass Class1 **(b)** Tot Mass Class 2

(c) Tot Mass Class 3

Figure B1.1: Distribution of total particle mass in $\mu g/m^3$ of particles of class 1 (a), 2 (b) and 3 (c) in Scenario 1.

Table B1.1: Mass distribution by size and state for Scenario 1

Class	Size [μm]	Type	Total Mass [mg]
1	10	Total	0.096562
		Suspended	0.000143
		Sedimented	0.096419
2	50	Total	16.670286
		Suspended	0.000000
		Sedimented	16.670246
3	100	Total	134.498382
		Suspended	0.000000
		Sedimented	134.498073

Table B1.2: Mass balance comparison for Scenario 1

Class	Input Mass [mg]	Final Mass [mg]	Mass Loss [%]
1	0.9948	0.0966	90.3
2	124.3547	16.6703	86.6
3	994.8377	134.4984	86.5

B.2 Particle Tracking - Scenario 4

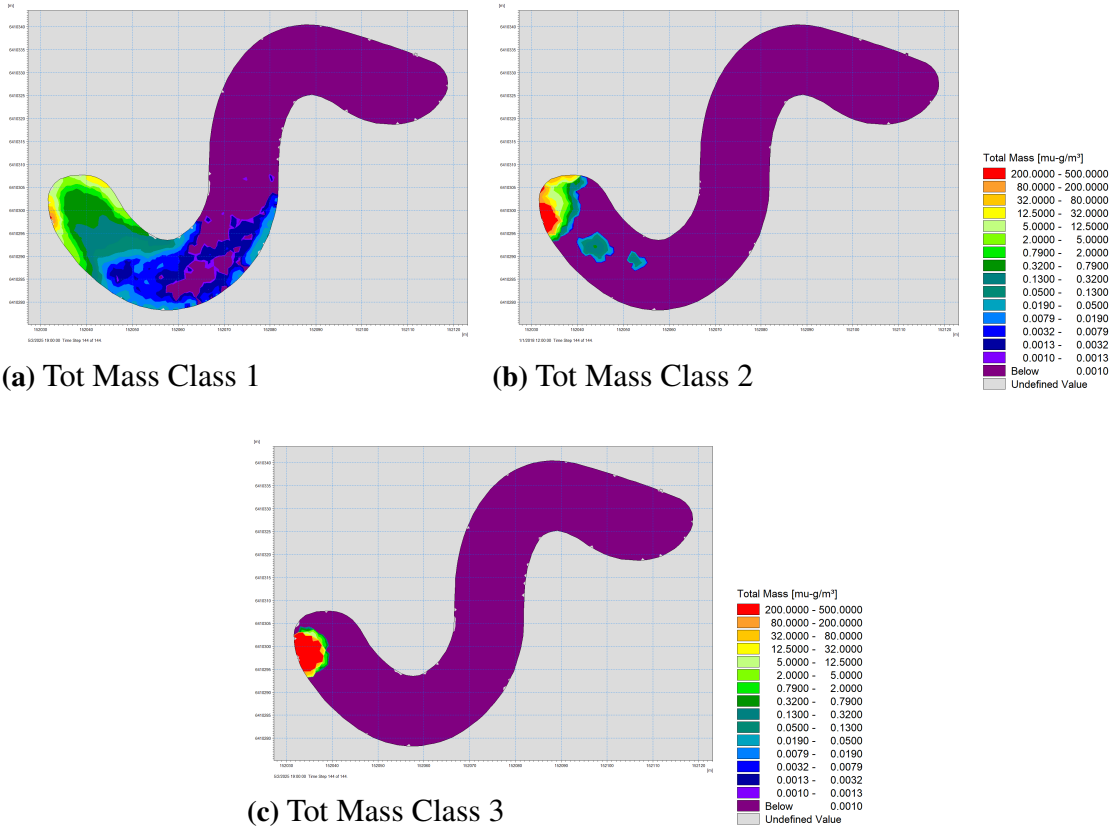

(a) Tot Mass Class 1 **(b)** Tot Mass Class 2

(c) Tot Mass Class 3

Figure B2.2: Distribution of total particle mass in μg/m^3 of particles of class 1 (a), 2 (b) and 3 (c) in Scenario 4.

Table B2.3: Mass distribution by size and state for Scenario 4

Class	Size [μm]	Type	Total Mass [mg]
1	10	Total	0.133430
		Suspended	0.000000
		Sedimented	0.133430
2	50	Total	97.520556
		Suspended	0.000000
		Sedimented	97.520402
3	100	Total	874.224010
		Suspended	0.000000
		Sedimented	874.223364

Table B2.4: Mass balance comparison for Scenario 4 and 5

Class	Input Mass [mg]	Final Mass [mg]	Mass Loss [%]
1	0.9948	0.1334	86.6
2	124.3547	97.5206	21.6
3	994.8377	874.2240	12.1

B.3 Particle Tracking - Scenario 5

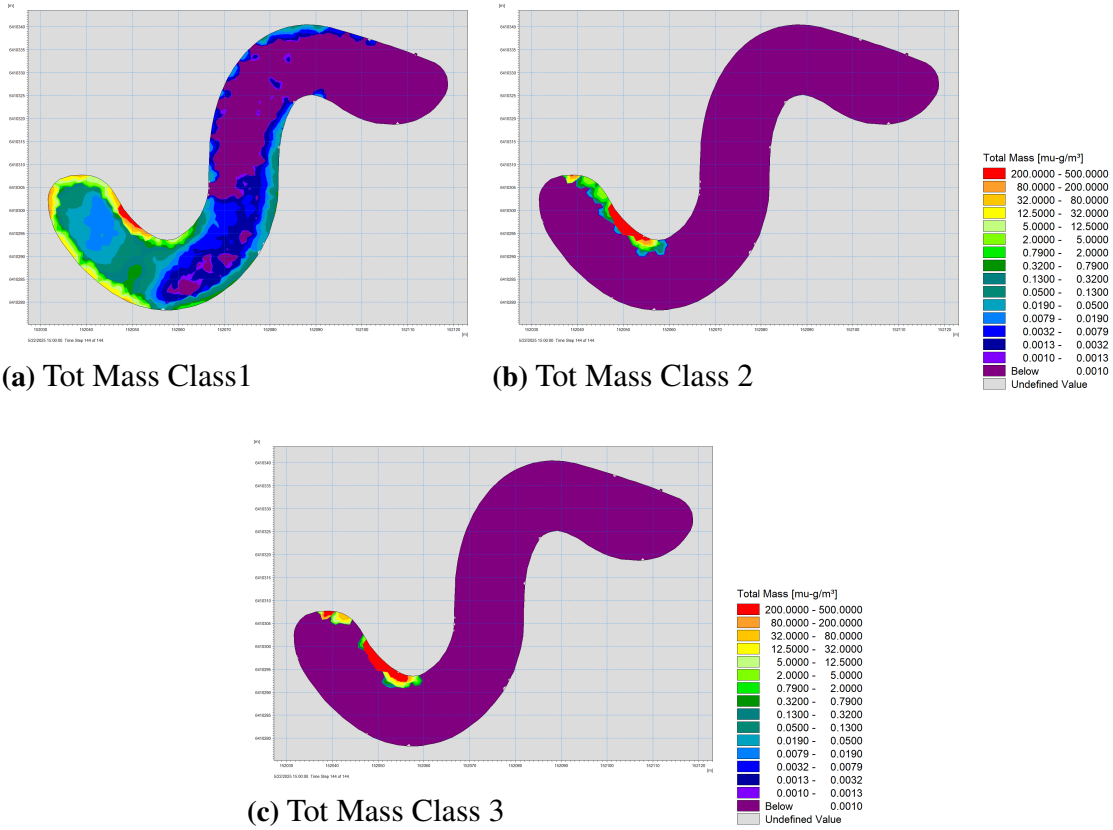

(a) Tot Mass Class1 **(b)** Tot Mass Class 2

(c) Tot Mass Class 3

Figure B3.3: Distribution of total particle mass in μg/m^3 of particles of class 1 (a), 2 (b) and 3 (c) in Scenario 5.

Table B3.5: Mass distribution by size and state for Scenario 5 at last time step

Class	Size [μm]	Type	Total Mass [mg]
1	10	Total Suspended Sedimented	0.133430 0.000000 0.133430
2	50	Total Suspended Sedimented	97.520556 0.000000 97.520402
3	100	Total Suspended Sedimented	874.224010 0.000000 874.223364

DEPARTMENT OF ARCHITECTURE AND
CIVIL ENGINEERING
CHALMERS UNIVERSITY OF TECHNOLOGY
Gothenburg, Sweden 2025
www.chalmers.se

CHALMERS
UNIVERSITY OF TECHNOLOGY